SARS CORONAVIRUS ANTAGONIZES INNATE IMMUNE SIGNALING INITIATED BY RIG-I BUT IS RECOGNIZED BY TLR SIGNALING VIA THE ADAPTOR MOLECULE TRIF

Allison Totura

A dissertation submitted to the faculty at the University of North Carolina at Chapel Hill in partial fulfillment of the requirements for the degree of Doctor of Philosophy in the Department Microbiology & Immunology of The School of Medicine.

Chapel Hill
2014

Approved By:

Ralph Baric

Mark Heise

Nathaniel Moorman

Raymond Pickles

Jason Whitmire

ABSTRACT

Allison Totura: SARS Coronavirus Antagonizes Innate Immune Signaling Initiated by RIG-I but is Recognized by TLR Signaling via the Adaptor Molecule TRIF
(Under the Direction of Ralph S. Baric and Mark T. Heise)

The recent emergence of highly pathogenic coronaviruses Severe Acute Respiratory Syndrome coronavirus (SARS-CoV) and Middle East Respiratory Syndrome coronavirus (MERS-CoV) is a concern for global public health, as there is a lack of efficacious vaccine platforms and antiviral therapeutic strategies. Pathogen Recognition Receptors (PRRs) are cellular sensors that enable hosts to differentiate between "self" vs. "non-self" and initiate innate immune responses against invading pathogens, like coronaviruses. Agonists and antagonists of PRRs have proposed utility as vaccine adjuvants or antiviral compounds, and highly pathogenic coronaviruses encode multiple strategies to modulate host cell intrinsic immune responses to viral infection so it is imperative to discern the function of PRRs in the pathogenesis of highly pathogenic coronaviruses. The role of PRRs including Toll-like Receptors (TLRs) and RIG-I-like receptors (RLRs) in the pathogenesis of SARS-CoV is the focus of this dissertation.

We demonstrate that mice deficient in the TLR3/TLR4 adaptor TRIF are highly susceptible to SARS-CoV infection, showing increased SARS-related disease signs and mortality; $TLR3^{-/-}$ and $TLR4^{-/-}$ mice are more susceptible to SARS-CoV than wild type mice, but experience only mild disease with no mortality in response to infection. Aberrant cellular signaling programs were observed following infection of $TRIF^{-/-}$ mice, similarly to those seen in

human patients with poor disease outcome following SARS-CoV or MERS-CoV infection. These findings highlight the importance of TLR signaling in generating a balanced protective innate immune response to highly pathogenic coronavirus infections, and should inform the design and use of TLR agonists and antagonists in coronavirus-specific vaccine and antiviral strategies.

In addition, we demonstrate modulation of a host PRR by the SARS-CoV nonstructural protein 7 (nsp7) to subvert host innate immune responses. Nsp7, a replicase protein required for coronavirus viability, antagonizes interferon responses via the RIG-I signaling pathway. IFN antagonism activity is mapped to critical residues in the N-terminal 20 amino acids of SARS-CoV nsp7. The nsp7 protein from other mammalian coronaviruses, including nsp7 from coronaviruses of bats, interacts with RIG-I to block IFN expression in a conserved manner. This suggests that the nsp7 proteins of zoonotic coronaviruses are pre-positioned to antagonize human sensing machinery, perhaps contributing to cross-species transmission and pathogenic potential in alternative hosts. In sum, these studies contribute to our understanding of host detection of highly pathogenic coronaviruses and viral antagonism of the host innate immune response.

DEDICATION

For my parents and grandparents, who always supported my dream of becoming a virologist.

ACKNOWLEDGEMENTS

I would like to thank my mentors Ralph Baric and Mark Heise for the opportunity to work on these studies. They fostered a well-funded, stable work environment where I could explore projects of interest to me, which is no easy task during the tumultuous times that academic science is experiencing. During my tenure in the lab, SARS-CoV became a Select Agent, and Amy Sims had a huge part in easing this transition for everyone in the lab, which allowed us to keep projects up and running, for which I am very grateful. Matt Frieman and I made some of the initial observations on my nsp7 story together when he was training me in molecular techniques, and I learned a lot from his nonspecific enthusiasm for all things virology related. Lisa Gralinski had a very important role in helping train me in mouse handling in particular, which was critically important for all of the studies described in this dissertation. I'd like to thank all of the members of the Baric Lab: past, present, and recent. I've learned something from all of you (yes, all of you), whether it was about life or science.

I would like to thank all of the wonderful friends I made at UNC-Chapel Hill for helping me through, even if they didn't realize they were doing it. There are too many people to name and it wouldn't feel right to put them in any order, but I hope that you know who you are. In particular though, I would like to thank Damon Shattuck, my future and forever partner in crime, for all of his support and doing his very best to bring out the best in me. I would like to thank my family for all of their support, both literal and figurative; I could not have done this without you.

TABLE OF CONTENTS

LIST OF ABBREVIATIONS

ACE2: angiotensin converting enzyme 2

ARDS: acute respiratory distress syndrome

BCoV: bovine coronavirus

BtCoV: bat coronavirus

CCL(x): chemokine (CC motif) ligand

CD(x): cluster of differentiation

CoV: coronavirus

CXCL(x): chemokine (CXC motif) ligand

DAD: diffuse alveolar damage

DCs: dendritic cells

DMV: double membrane vesicles

DPP4: dipeptidyl peptidase 4

E: Envelope protein

HAE: human airway epithelium

HCoV: human coronavirus

IAV: Influenza A virus

IBV: (avian) infectious bronchitis virus

IFIT: interferon induced protein with tetratricopeptide repeats

IFITM: interferon induced transmembrane protein

IFN: interferon

IFNAR1: interferon alpha beta receptor 1

IKK: I kappa b kinase

IL(x): interleukin

IRF(x): interferon regulatory factor

ISG: interferon stimulated gene

JAK: janus kinase

LGP2: laboratory of genetics and physiology 2

M: Membrane protein

MA15: mouse adapted by 15 serial passages

MAL: MyD88 adaptor like

MAVS: mitochondrial antiviral signaling protein

MDA5: melanoma differentiation associated protein 5

MERS: Middle East Respiratory Syndrome

MHV: mouse hepatitis virus

MxA: mxyovirus resistance gene A

MyD88: myeloid differentiation primary response 88

N: Nucleocapsid protein

NF-κB: nuclear factor light chain enhancer of activated B cells

Nsp: nonstructural protein

OAS1: 2'-5'-oligoadenylate synthetase 1

ORF: open reading frame

PAMP: pathogen associated molecular pattern

PBMC: peripheral blood mononuclear cells

PEDV: porsine epidemic diarrhea virus

pI:C: polyinosinic-polycytidylic acid

PKR: protein kinase R

PLP: papain like protease

PRR: pathogen recognition receptor

RAG1: recombination activating gene 1

RdRp: RNA-dependent RNA-polymerase

RIG-I: retinoic acid inducible gene 1

RLR: RIG-I-like receptor

RSAD2: radical S-adenosyl methionine domain containing 2

RSV: respiratory syncytial virus

S: Spike glycoprotein

SARS: Severe Acute Respiratory Syndrome

SeV: Sendai virus

STAT: signal transducer and activators of transcription

TBK1: TANK binding kinase 1

TCoV: turkey coronavirus

TGEV: transmissible gastroenteritis coronavirus

TLR: toll-like receptor

TNF: tumor necrosis factor

TRAM: TRIF related adaptor molecule

TRIF: TIR-domain containing adaptor producing interferon-β

TRIM(x): tripartite motif protein

TRS: transcriptional regulatory sequences

TYK2: tyrosine kinase 2

VRP: viral replicon particle

WNV: West Nile virus

LIST OF TABLES

LIST OF FIGURES

CHAPTER 1: SARS-COV AND INNATE IMMUNITY[1]

SARS-COV: THE FIRST VIRAL PANDEMIC OF THE NEW MILLENIUM

In 2002 the first major viral pandemic of the new millennium emerged from the Guangdong province in Southern China. Severe Acute Respiratory Syndrome (SARS) presented as initial "flu-like" symptoms (cough, sore throat, and fever) that could progress to atypical pneumonia in patients with severe SARS disease (1, 2). An unprecedented rapid response from scientists identified a novel coronavirus as the causative agent of SARS, named SARS coronavirus (SARS-CoV) and angiotensin converting enzyme 2 (ACE2) as the viral receptor (3). Despite identification of the virus, the disease spread from China to other Southeast Asia countries eventually becoming a global threat, with significant outbreaks reported in Singapore, Hong Kong, Taiwan, and Canada (4). At the end of the epidemic 774 of the 8096 confirmed cases resulted in death yielding a mortality rate of 9.6% (5). By July of 2003 the virus was eventually controlled by public health measures, but no vaccines or antivirals are currently approved for the treatment of SARS-CoV should the virus re-emerge (6).

SARS disease in patients with poor outcome was marked by the progression to Acute Respiratory Distress Syndrome (ARDS), the most severe form of Acute Lung Injury. The acute phase of ARDS is characterized by pulmonary edema, severe hypoxia, and the accumulation of inflammatory cells in the lungs, which can progress to late ARDS phase fibrosis, organizing pneumonia, systemic inflammation responses, and multiple organ failure (7). Histologically,

[1] This Chapter originally appeared as Totura, A.L. and R.S. Baric, *SARS coronavirus pathogenesis: host innate immune responses and viral antagonism of interferon*. Current Opinion in Virology, 2012. **2**(3):p. 264-275, but has been adapted to reflect current information

post-mortem lungs from SARS patients showed diffuse alveolar damage (DAD) featuring hyaline membranes and organizing pneumonia patterns of fibrosis, both hallmarks of ARDS (8). Consistent with ARDS progression, the primary targets of SARS-CoV infection are ciliated cells of the airway epithelium and alveolar type II pneumocytes (9, 10). Progression to ARDS was noted in approximately 30% of SARS-CoV infected patients, and these cases were more likely to result in death from SARS disease, with ARDS-associated death rate exceeding 50% (11). Additionally, elderly patients were more susceptible to SARS than younger patients, with a mortality rate of 50% in patients 65 year of age or older (12). ARDS is also associated with the induction of inflammatory cytokines including IL-1, IL-6, IL-8, CXCL10, and TNFα, many of which are highly expressed in the lungs of SARS patients (13, 14). In many viral infections interferon (IFN) is a cytokine of critical antiviral importance not only in controlling viral infections, but also in programming the adaptive immune response to promote viral clearance. However, in patients with severe SARS disease, aberrant IFN, interferon stimulated genes (ISGs), and cytokine responses were observed compared to healthy individuals providing evidence that SARS is an innate immune regulated disease (15, 16).

MERS-CoV AND OTHER CORONAVIRUSES OF HUMANS AND MAMMALS

In 2012 a similar respiratory syndrome to SARS was identified in several patients from the Arabian Peninsula, and was confirmed to be caused by a novel coronavirus initially termed HCoV-EMC, but later the syndrome and virus were officially named Middle East Respiratory Syndrome (MERS) and MERS-CoV (17, 18). As of November 2014, there have been 940 laboratory confirmed cases with 376 deaths attributed to MERS-CoV, a 40% mortality rate since the virus emerged in late 2012 (19). The majority of cases reported have been concentrated on the Arabian Peninsula in the Kingdom of Saudi Arabia and the United Arab Emirates, but several incidents of traveler associated infections outside of Arabia have been reported in North America

and Europe (20, 21). Similarly to SARS-CoV, there appears to be an age-related component to MERS-CoV susceptibility, with elderly patients more likely to succumb to the disease (22). Also like SARS-CoV, patients with severe MERS disease have aberrant cytokine, chemokine, and ISG responses, and the efficacy of interferon or ribavirin as potential therapeutics for the amelioration of MERS has yet to be proven (23, 24). MERS-CoV utilizes the receptor DPP4 to enter host cells (25). Although MERS-CoV has caused sporadic outbreaks with relatively few total cases, the high case-fatality rate associated with MERS and lack of efficacious therapies highlights the importance of continuing studies of coronaviruses with emergent potential.

While SARS-CoV and MERS-CoV are highly pathogenic coronaviruses of humans, other coronaviruses associated with infections of humans include HCoV-HKU1, HCoV-OC43, HCoV-229E, and HCoV-NL63, which also cause respiratory disease but are generally much less severe than SARS or MERS (26). Coronaviruses are also important pathogens of livestock in cattle (bovine coronavirus, BCoV), swine (porsine epidemic diarrhea virus, PEDV; transmissible gastroenteritis virus, TGEV), and poulty (turkey coronavirus, TCoV; avian infectious bronchitis virus, IBV). Spillover events from livestock populations into humans have been hypothesized for viral emergence of HCoV-OC43 into human populations from BCoV precursor strains less than 150 years ago (27). However, coronaviruses infecting animals are also a significant threat to the economic stability of agriculture: highly virulent strains of PEDV first detected in China in 2004 arrived in the United States in 2012, causing epidemics of disease with >95% mortality in piglets, resulting in losses for the United States hog industry (28)

Like other members of the viral family *Coronaviridae*, SARS-CoV has a positive-sense, single-stranded RNA genome that is amenable to manipulation using reverse genetic techniques (29). In SARS-CoV, the first open reading frame (ORF) encodes the 16 nonstructual proteins that make up the viral replicase, while the ensuing ORFs encode structural proteins that compose

the virion, as well as eight accessory proteins (Figure 1.1). The SARS-CoV accessory proteins share no homology to the accessory proteins of other human coronaviruses, and while dispensable for replication *in vitro*, encode functions that likely impact viral pathogenesis *in vivo* (30). The typical coronavirus genome size is quite large in comparison to many other positive-sense RNA viruses; within the SARS-CoV genome of 29.7 kB at least ten genes with potential functions that modulate innate immunity have been characterized (Figure 1.1 and Table 1.1).

MAMMALIAN CORONAVIRUS EMERGENCE FROM BATS

The emergence of SARS-CoV likely originated from animal markets in Guangdong Province of China, and during the epidemic SARS-CoV was detected in a variety of animals typical of these markets, including masked palm civets and raccoon dogs. SARS-like-CoVs from civets are closely related to human isolates from the outbreak, leading to the hypothesis that civets acted as an intermediate host species prior to human infection (31). Similarly, MERS-CoV has been detected in dromedary camels, a common beast of burden in the Arabian Peninsula where the majority of MERS cases have been reported (32). While intermediate host species such as camels in the MERS outbreak and civets in the SARS outbreak are likely to be common sources of coronavirus infections of humans due to proximity, bat species are hypothesized to be the reservoir hosts for coronavirus infection of intermediate hosts.

Surveillance of the virome of bats suggests that bat populations contain diverse pools of antigenically distinct coronaviruses likely to be the source of coronavirus emergence (33). In 2005, a SARS-like-CoV was identified in the Chinese horseshoe bat populations outside of Hong Kong (34, 35). Recent reports of coronaviruses in bats capable of using ACE2 as a receptor for viral entry indicates that potentially emergent coronaviruses similar to the virus that caused the SARS outbreak of 2002-2004 continue to circulate in bat populations (36). A bat coronavirus (BtCoV) similar to MERS-CoV can utilize similar host receptors for viral entry, but

preferentially enters via bat receptors compared to the homologous human receptors, indicating that at least at the step of viral entry, some host adaptation must occur for productive infection of human cells (37). Discovery of BtCoVs within coronavirus genogroups with known human pathogens includes BtCoV species similar to group 1b, HCoV-NL63-like coronaviruses including Appalachian Ridge Coronavirus (BtCoV-AR) and group 2c MERS-like coronaviruses including BtCoV-HKU4 and BtCoV-HKU5 (38-40). While the pathogenic potential of the majority of BtCoVs in human or other mammalian systems is unknown, mouse adaptation of BtCoV-HKU5 demonstrates that coronaviruses of bats can gain virulence in mammalian infection models (41). The discovery of BtCoVs similar to highly pathogenic human coronaviruses SARS-CoV and MERS-CoV has the potential to be used for novel studies into how the evolution of viruses from zoonotic reservoirs to intermediate species to humans affects viral modulation of innate immune factors.

MODELS OF CORONAVIRUS INFECTION FOR ELUCIDATION OF VIRAL PATHOGENESIS

Cell Culture Models of SARS-CoV Infection

Initial models of SARS-CoV innate immune pathogenesis were viral infection of cell lines including Vero E6 cells, Caco-2, and Huh-7 cells, but these cells may not yield relevant biological information consistent with SARS-CoV infection of pneumocytes, because they are not derived from lung tissues (42). Human PBMCs have been used to model cytokine responses from SARS-CoV infection, but are not thought to be the primary target cell of SARS-CoV in the lungs (43, 44). Human Airway Epithelial Cultures (HAEs) are differentiated primary cell lines of pseudostratified mucocilliary epithelium that replicate the morphological and physiological characteristics of human airways. HAEs can be infected with SARS, are derived directly from normal lung tissues, contain the relevant epithelial cell types within human airways for SARS-CoV infection, and have intact cell signaling pathways; however, these cells are difficult to

procure and are highly heterogeneous, due to being derived from human donors (10, 45). Another line of human lung cells, Calu-3 cells also support SARS-CoV replication and form differentiated pseudostratified columnar epithelia (46). However, relatively low expression of the SARS-CoV receptor ACE2 on Calu-3 cells can reduce efficient infection and viral growth (47). Recently, the 2B4 cell line derived from a clonally selected population of Calu-3 cells was developed that has the benefits of Calu-3 cells, in addition to high expression of the ACE2 receptor for increased permissibility to SARS-CoV infection. These 2B4 cells have shown utility in providing data on innate immune responses within a biologically relevant *in vitro* system (47).

Mouse Models of SARS-CoV

Small animal models of SARS-CoV infection have benefits into the elucidation of innate immune pathogenesis beyond cell culture systems due to their ability to model the interaction of lung epithelium and immune cell types within an infected organism. Mice, hamsters, and ferrets have all been considered for use as small animal models of SARS-CoV infection (48-50). In general, a robust mouse model has been more vigorously pursued, because of the relative ease of genetic manipulation of the host, as well as greater availability of immunological reagents. SARS-CoV epidemic isolates from humans replicate in young mice but do not cause clinical disease, limiting the use of these models for pathogenesis studies (51, 52). Approaches to generate mouse models of SARS-CoV infection with human SARS-CoV strains have included (i) the use of immunodeficient mice, (ii) mice expressing the hACE2 transgene (the SARS-CoV receptor), and (iii) the use of aged mice (52-57). RAG1 $^{-/-}$ mice, CD1$^{-/-}$ mice and beige mice did not develop clinical illness, and lack of particular immune cell populations limits the use of immunodeficient models (52). Transgenic mice expressing the hACE2 transgene developed clinical disease, but the brain becomes a major target organ of infection, a phenotype rarely seen

in human SARS cases (54, 55). Aged mice (12 months) exhibit minor clinical illness upon infection with SARS-CoV, but do not address pathogenic mechanisms associated with SARS disease in non-senescent populations (57). Infections using the mouse coronavirus MHV-1 have also been proposed as models for SARS-CoV infection (58).

More recently, mouse adapted SARS coronaviruses (MA-SARS-CoV) have been developed by serial passage through the lungs of BALB/c mice yielding several different MA-SARS-CoV strains (59, 60). Infection of 6-10 week old mice with SARS-CoV adapted by 15 serial passages (MA15-SARS-CoV) causes morbidity and mortality, viral replication in the lungs, and lung pathology associated with SARS disease (59, 60). In addition, age-related phenotypes have been observed in MA-SARS-CoV infections of 12 month old mice which exhibit exacerbated SARS disease that mimics the age-dependent phenotype of SARS in humans (61, 62). Another approach incorporating the Spike glycoproteins of a zoonotic variant of SARS-CoV that had been found in civets during the SARS epidemic showed increased lung pathology and lethality in aged mice(63). Currently, studies are underway to determine the response of recombinant inbred lines of mice (known as the Collaborative Cross) to MA15-SARS-CoV infection, utilizing Genome Wide Associate Studies to map quantitative trait loci that contribute to *in vivo* phenotypes (e.g. weight loss or lung pathology) (64). These studies offer an unbiased approach to determining the contributions of many different genes to the complex trait of SARS-CoV disease, and could provide novel data on innate immune factors involved in SARS-CoV pathogenesis.

Nonhuman Primate Models of SARS-CoV

Currently there are no proven efficacious treatments or vaccines to protect against the re-emergence of SARS-CoV (6, 65). While the use of primate models is typically limited due to ethical concerns and expense, infection of primates with SARS-CoV can test drug treatments and

vaccines in a more relevant model to humans than rodent models. SARS-CoV replicates in the lungs of nonhuman primate species, including African green monkeys, cynomolgus macaques, and rhesus macaques (66). Infection of cynomolgus macaques with SARS-CoV replicates aspects of the human disease, including lung pathology of diffuse alveolar damage (DAD) found in humans (67). Additionally, a comparison of SARS-CoV infection of young adult cynomolgus macaques to aged cynomolgus macaques found age-dependent susceptibility to severe SARS disease resembling the same trend in humans (68). More recently, it has been shown that SARS-CoV causes increased severity of disease in African green monkeys compared to cynomolgus macaques, and that the increased lung injury is associated with differential innate immune signaling (69).

Models of MERS-CoV Infection

MERS-CoV can infect cell lines including human primary cells such as HAEs, highlighting the potential for spread via the respiratory route in humans (70). Attempts to generate a small animal or rodent model of MERS-CoV by similar methods to the generation of mouse adapted SARS-CoV viruses have been unsuccessful likely due to limitations of MERS-CoV Spike interactions with the rodent DPP4 receptor molecule (71). Recently, the first mouse model of MERS has been described, using the approach of adenovirus vectored hDPP4 expressed in the mice to allow for better virus/receptor interaction, but this model requires the absence of type I IFN or TLR signaling to replicate severe MERS disease (72). Currently, efforts are ongoing to make refinements to such an approach to generate a small rodent model of MERS-CoV infection. Nonhuman primate models of MERS-CoV infection of rhesus macaques and marmosets have been described in the literature, where macaques develop a mild, transient illness but marmosets develop lethal MERS disease (73).

HOST ANTIVIRAL INNATE IMMUNE DETECTION AND RESPONSE TO SARS-COV INFECTION

Innate immune signaling is the earliest detection of "non-self" pathogens from "self" cellular molecules that alerts the host cells to the presence of invading viruses. Pattern Recognition Receptors (PRRs), such as the RIG-I-like Receptors (RLRs) and Toll-like Receptors (TLRs) recognize Pathogen Associated Molecular Patterns (PAMPs) from viral components or replication intermediates, resulting in a signaling cascade that initiates an antiviral state in cells as a result of infection (74, 75) . PRRs are located on plasma membranes, endosomal membranes, and within the cytosol of host cells to ensure maximal detection of viral motifs. The PAMPs that are recognized as "non-self" by these receptors can include nucleic acid motifs, carbohydrate moieties, glycoproteins, lipoproteins or other small molecules present within the viral life cycle, but absent from normal cellular components.

RIG-I-Like Receptor Signaling

The family of RIG-I-like Receptors (RLRs, Figure 1.2) contains three cytosolic RNA helicases that recognize non-self RNA species resulting from viral replication (76). The two detection molecules within the RLR family are retinoic acid-inducible gene I (RIG-I) and melanoma differentiation associated factor 5 (MDA5). The third RLR, laboratory of genetics and physiology 2 (LGP2), facilitates recognition of viral PAMPs by RIG-I and MDA5, but is dispensable for their signaling (77). RIG-I recognizes primarily 5'ppp-RNA molecules with secondary motifs of dsRNA or ssRNA of short length (78, 79). MDA5 recognizes longer dsRNA motifs than RIG-I (80). While RLRs are expressed in a wide range of cell types, typically at low levels, both RIG-I and MDA5 are interferon stimulated genes (ISGs) that are transcribed during SARS-CoV infection *in vitro* (47). MHV, another coronavirus, is recognized by MDA5 in brain macrophages and microglial cells, and by RIG-I and MDA5 in oligodendrocyte cells (9, 81). Currently it is not known whether SARS-CoV is recognized by

RIG-I or MDA5, however since MHV and SARS-CoV are likely to have similar replication intermediates (which would serve as RLR ligands), it is likely that SARS-CoV could be detected by RLRs.

Following binding of viral RNAs, RIG-I and MDA5 interact with the adaptor molecule MAVS to transduce the signal(82). MAVS is located on the mitochondrial membrane, and cleavage of MAVS from the mitochondria results in ablation of the signal (83). MAVS acts as a central adaptor for complexes of kinases: the IKKε/TBK1 complex and the IKKα/IKKβ/IKKγ complex (84, 85). The IKKε/TBK1 kinases phosphorylate the transcription factors IRF3 and IRF7, which then form homodimers or heterodimers. Upon dimerization, the transcription factors enter the nucleus to initiate transcription of Type I IFNs (IFNα and IFNβ). While IRF3 is nearly ubiquitously expressed in cells, IRF7 is an ISG typically expressed at low levels, so it is thought that IRF3 mediates transcription of the majority of early IFN expression. The IKKα/IKKβ/IKKγ kinases phosphorylate IκBα, targeting this repressor protein of NF-κB for degradation. Activation of NF-κB leads to transcription of proinflammatory cytokines, and NF-kB mediated transcription has also been linked to the pathogenesis of ARDS (86). *In vitro* SARS-CoV infections have demonstrated that the expression of NF-κB generated transcripts, such as IL-6 and IL-8, happens as early as 12 hours post infection, while IRF3/IRF7 transcription of Type I IFNs is delayed until 48 hours post infection (47). Similar observations have been made *in vivo* in the macaque model of age-dependent SARS-CoV pathogenesis. NF-κB induced genes are more highly expressed in aged macaques that have significantly increased lung injury compared to young adult macaques where higher expression of IFNs was observed (68). While severe SARS-CoV disease can be correlated with different transcriptional regimes, the key to finding determinants of severe disease associated with SARS-CoV may be how innate immune sensing

mechanisms initiate transcription at critical junctures during infection, and which types of innate immune sensing are protective.

Toll-Like Receptor Signaling

In addition to RLRs, the TLR family of receptors also recognizes viral PAMPs, although no TLR has been directly implicated in the recognition of SARS-CoV. Unlike RLRs, TLRs are membrane bound sensors expressed either on the plasma membrane (Figure 1.3) or within endosomes (Figure 1.4). TLR4 can recognize viral proteins, as has been demonstrated with RSV, is expressed on the surface of lung epithelium, and has been implicated as a potential entry co-factor for respiratory viruses (87, 88). TLR4 has also been identified as a protective host factor against MHV-1 in the respiratory model of infection used to simulate SARS-CoV disease (89). TLR2/6 heterodimers help to activate the innate immune response to RSV, though the viral PAMP recognized has not been determined (90) TLR1/2 heterodimers have been shown to recognize viral glycoproteins, though their potential role in respiratory virus infection has not been determined (91). In the endosomal compartment, TLRs recognize viral nucleic acid PAMPs: TLR3 recognizes dsRNAs, TLR7/8 recognizes ssRNAs, and TLR9 recognizes CpG DNA motifs. While it is not known which TLRs can detect SARS-CoV, it has been shown in mice that transcription of TLRs is upregulated two days post infection, suggesting that TLRs are more highly expressed in SARS-CoV infected cells (92). Similar results in human dendritic cells showed that TLR1, TLR2 and TLR7 are induced as early as 3 hours following infection with SARS-CoV(93). Additionally, the activation of TLR3 with pI:C ligand has protective effects in a mouse model of SARS-CoV infection (94).

While there are many TLRs that recognize viral PAMPs, they signal through common adaptor molecules. MyD88 is an adaptor molecule for all of the TLRs with the exception of TLR3, which uses the adaptor TRIF. To test the hypothesis that TLRs could detect SARS-CoV

in mice, MyD88$^{-/-}$ mice were infected with MA15-SARS-CoV, and a protective role for MyD88 in SARS-CoV infection was established (95). While wild type mice experienced transient weight loss, from which they recovered after 7 days, MyD88 $^{-/-}$ mice lost significantly more weight, and all of the MyD88 $^{-/-}$ mice died by day 6 post-infection(95). Additionally, higher viral loads, more severe lung pathology and differences in cytokines and chemokines were observed in MyD88$^{-/-}$ mice compared to wild type mice(95). Studies that address the roles of other TLR adaptor proteins (TRIF and TRAM) in SARS-CoV infections, as well as what TLR(s) contribute to these responses are the subjects of Chapters 2 and 3. MyD88 and the other TLR adaptor molecules signal through the IKKε/TBK1 complex and the IKKα/IKKβ/IKKγ complex similarly to RLRs, but can also recruit an IRAK-1/IRAK4/TRAF6 complex capable of activating the transcription factors IRF3, IRF7 and NF-κB. Due to the considerable crosstalk between TLR and RLR signaling, it is difficult to discriminate between transcriptional products generated by the two sensor families, but it is likely that both play an important role in the innate immune response to SARS-CoV infection.

INNATE IMMUNE SIGNALING EFFECTOR MOLECULES AND SARS-COV PATHOGENESIS

Interferon

Following detection of virus by the host cells, the production of cytokines, chemokines, ISGs and other effector molecules continues the innate immune response to viral infection. Interferons are potent cytokines of critical importance in controlling viral infections. Robust expression of Type I and Type II IFN was detected in patients during the acute phase of SARS-CoV infection (16). In the 2B4 cell culture model of SARS-CoV infection, early expression of Type III IFN was detected 24 hours earlier than Type I IFN transcripts, demonstrating a delay in Type I IFN signaling and a potentially protective role of Type III IFN (47). Several studies of antiviral treatments tested against SARS-CoV replication show administration of Type I IFN

inhibits SARS-CoV growth in cell culture (96-98). Treatment with rIFNα2b was an effective prophylactic against severe SARS-CoV disease in cynomolgus macaques, decreasing viral titer and diffuse alveolar damage normally observed during the course of infection (67). Additionally, IFNβ treatment of aged macaques was shown to have anti-inflammatory effects and ameliorate age-dependent disease (68). IFN treatment through adenovirus vectored IFN expression, induction via dsRNA, or direct IFN injection decreases SARS-CoV replication in mouse models (99, 100). Typically, mice deficient in IFN receptor genes are highly susceptible to viral infections; surprisingly, despite the potential importance of IFNs in controlling SARS-CoV replication, infection of mice deficient in Type I, II, or III IFN receptors showed minimal phenotypic difference in weight loss, viral titer, lung pathology, and mortality from wild type 129 mice in the MA15-SARS-CoV model (101). Transcriptional analysis from these studies showed that ISGs were induced even in the absence of IFNAR1, demonstrating that there may be compensatory mechanisms through other innate immune signaling to protect against severe SARS-CoV disease in the absence of IFN (92). Additional studies by Mordstein *et al*. also showed that mice deficient in Type I, Type III, or Type I and Type III IFN receptors had slightly higher levels of viral replication in the lungs using the SARS-CoV model of mouse infection, in which viral replication occurs in the absence of any other disease phenotypes (102). While IFNs continue to be an attractive potential antiviral strategy if SARS were to re-emerge, their role as a protective component of the innate immune response during SARS-CoV infection still needs additional investigation, particularly into protective innate immune mechanisms that occur in the absence of IFN signaling.

STAT1

The secretion of IFNα and IFNβ molecules from an infected cell leads to an autocrine and paracrine signaling through the IFNαβ Receptor (composed of the IFNAR1 and IFNAR2

subunits) resulting in the activation of the JAK-STAT pathway (Figure 1.5). The JAK/TYK2 kinases phosphorylate the transcription factors STAT1 and STAT2, which form heterodimers complexed with IRF9. The STAT complex translocates to the nucleus leading to the transcription of interferon stimulated genes (ISGs) that establish an antiviral state in the cell. Because neighboring cells can receive IFN stimulation prior to infection, it is a crucial pathway to preventing viral spread in the host. Mice deficient in STAT1 showed an increased susceptibility to SARS-CoV infection (103). Although there were no differences in mice deficient in IFN receptors, $STAT1^{-/-}$ mice showed increased weight loss, viral titer, and lung pathology compared to wild type over the course of MA15-SARS-CoV infection, demonstrating that STAT has important IFN-independent role in SARS-CoV infection (104). Severe lung pathology in $STAT1^{-/-}$ mice infected with MA15-SARS-CoV was associated with the infiltration of immune cells and fibrotic lung response. The $STAT1^{-/-}$ dependent prolonged expression of inflammatory cytokines (IL-1, IL-6, IL-10, IL-12, and TNFα) and chemokines (CCL2, CCL3, CCL4, CCL7, and CCL20), could be a transcriptional regime responsible for fibrotic phenotypes within the lungs. Additionally, ISG responses were significantly lower in $STAT1^{-/-}$ mice compared to wild type or $IFNAR^{-/-}$ mice, leading to the conclusion that STAT1-dependent, IFNAR1-independent ISG expression was protective in these mice(104). It remains unclear how STAT1 controls ISGs independent of IFNAR expression, or which ISGs have important potential roles in SARS-CoV pathogenesis.

Cytokines, Chemokines, and ISGs

The initiation of innate immune signaling culminates in the production of effector molecules such as cytokines, chemokines, and ISGs. Cytokines are secreted molecules that modulate the host immune response, and are typically categorized into proinflammatory and anti-inflammatory categories. The induction of proinflammatory cytokines may be necessary for

mounting an initial immune response to pathogens, but prolonged expression is associated with exacerbated immune responses leading to immunopathology such as ARDS (105). Chemokines are a subclass of cytokines with chemotactic properties to recruit immune cells to the site of infection. The role of chemokines in attracting cells that perpetuate the inflammatory response has also been linked to the pathogenesis of ARDS (86). Interferon stimulated genes (ISGs) can include cytokines and chemokines, as well as other innate immune effector molecules with antiviral functions (106). While several ISGs such as MxA, OAS1, RNaseL, PKR, IFIT, RSAD2, and TRIM5α have described functions, these are only a subset of this large family of molecules, most of which have antiviral properties that are not yet well understood.

Differences in patterns of innate immune effector molecule expression following SARS-CoV infection may be a determinant of disease outcome. Cameron *et al*. found that innate immune responses such as IFN (Type I and Type II IFN), chemokines (CXCL10 and CCL2), and ISGs (RSAD2, MxA, IFITM1, IFIT3) were similarly upregulated in SARS patients during the acute phase of illness, regardless of the following disease outcome (16). While resolution of IFN, ISG, and chemokine expression to levels similar to uninfected controls was associated with recovery from SARS, a continued hyperimmune response of the same effector molecules persisted in SARS-CoV patients with severe hypoxemia (including patients that eventually succumbed to SARS) (16). *In vitro* studies found that SARS-CoV infection initiates an early proinflammatory cytokine response early (24 hours post infection), but that IFNs and ISGs are delayed in expression until 48 hours post infection(47). Studies comparing the innate immune response in mice found elevated levels of proinflammatory cytokines (TNFα, IL-6, and IL-1β) were highly expressed early during SARS-CoV infection of susceptible aged mice (53, 56). The chemokine receptors CCR1, CCR2 and CCR5 all have potentially protective roles during MA15-SARS-CoV infection in the mouse model as well as SARS-CoV infection of human DCs,

indicating the importance of chemokine signaling in controlling SARS-CoV infections (93, 95). The role of ISGs in SARS-CoV infection is less described than cytokines and chemokines. Different transcriptional profiles of ISGs associated with increased SARS-CoV disease have been described in several different model systems, but which ISGs are protective against SARS-CoV infection has not been well studied. Recently, it was shown that members of the IFITM family of ISGs including IFITM1, IFITM2, and IFITM3 could restrict SARS-CoV entry into host cells (107). The antiviral functions of other ISGs induced by SARS-CoV infection are still not well described. Currently, it is unknown if ISGs are differentially induced by SARS-CoV or zoonotic precursor SARS-like-CoV isolated from bats. Additional studies are required to determine (i) what ISGs are induced in reservoir hosts compared to epidemic hosts, (ii) the contribution of ISGs to limiting cross-species transmission, (iii) the crucial ISGs that control SARS-CoV infection or potentially contribute to severe disease, and (iv) potential functions of ISGs that could be exploited for the development of antiviral therapies. Extant reagents to study the over-expression of ISGs singly and in combination could determine which are effective at initiating an antiviral state against SARS-CoV infection (108).

MODULATION OF INNATE IMMUNE RESPONSE BY SARS-COV: EVASION OF INNATE IMMUNE DETECTION

SARS-CoV has evolved two general mechanisms to avoid detection by the host cell it infects: segregating the viral PAMPs from cellular receptors and masking the viral PAMPs from the receptors that recognize them. For SARS-CoV, the segregation of viral nucleic acids during replication may occur due to the biology of where replication takes place: on Double Membrane Vesicles (DMVs) of endoplasmic reticulum origin (109). The interior of DMVs where SARS-CoV replication is predicted to take place does not appear to connect to the cytoplasm and that viral dsRNAs were located in the interior of the vesicles (110). If the majority of the viral

nucleic acids are shielded from the cytosol by DMVs, it could potentially prevent recognition of these viral PAMPs by the RLR cytosolic family of receptors. It is less clear whether small viral ssRNA or dsRNA degradation products are also sequestered within DMVs or are more readily available for recognition by PRRs.

In addition to segregating viral factors from host receptors, viruses also attempt to mask viral nucleic acids to mimic those of the host cell. The lack of a 5'cap on ssRNAs in the cytoplasm distinguishes viral mRNAs from other eukaryotic mRNAs, and many viruses (including SARS-CoV) have evolved mechanisms to mimic host capping machinery. SARS-CoV nsp14 has been identified as a guanine-N7-methyltransferase, a critical component in RNA capping machinery (111). SARS-CoV nsp14 methyltransferase activity is the initial step to building an RNA cap that is structurally similar to the RNA cap used by the host, making it more difficult for the host to discriminate viral non-self RNAs from self mRNAs (112). Additionally, nsp16 of SARS-CoV has been identified as a 2'-O-methlytransferase, which modifies the cap of viralRNAs (112). In vitro capping of SARS-CoV RNAs requires nsp14 and an nsp16/nsp10 complex, where nsp10 acts as an activator or stabilizer for nsp16 (112, 113). The 2'-O-methylation of nsp16 seems to be of particular import in evading recognition by host PRRs such as MDA5 (114), as well as host ISGs such as IFIT family members IFIT1 and IFIT2 (115).

STRATEGY OF ANTAGONISM OF INNATE IMMUNE MOLECULES BY SARS-COV: BLOCK IFN

Transcription and subsequent signaling of interferon is vital for activating the antiviral response in host cells. Because of this, many viruses (including SARS-CoV) encode proteins that antagonize the IFN response to viral infection. The SARS-CoV genome encodes for 16 nonstructural proteins (nsp1-nsp16), four structural proteins (Spike, Envelope, Membrane, and Nucleocapsid), and eight accessory proteins (ORF 3a, ORF3b, ORF 6, ORF7a, ORF7b, ORF8a, ORF8b, and ORF9b). Of these viral proteins, eight have been identified as interferon

antagonists. SARS-CoV proteins nsp1, PLP (Papain Like Protease, or PLpro), nsp7, nsp15, N, and ORF6 were identified as IFN antagonists using a Venezuelan Equine Encephalitis Virus Replicon system to screen for antagonism of IFN expression in cell culture (116). Deletion of the nonstructural proteins or structural proteins that encode the IFN antagonists leads to replication incompetent SARS-CoV, while SARS-CoVΔORF6 and SARS-CoVΔORF3 are capable of growing in tissue culture (117).

SARS-CoV Nonstructural Proteins

Within the first open reading frame, SARS-CoV encodes sixteen nonstructural proteins that make up the viral replicase. The first nonstructural protein, SARS-CoV nsp1 antagonizes Type I IFN by three mechanisms: inactivation of host translational machinery, degradation of host mRNAs, and inhibition of phosphorylation of STAT1 (118-120). SARS-CoV nsp1 binds to the 40s ribosome subunit, inactivating host translational machinery (119). In addition to blocking translation of host cell genes, including those associated with the Type I IFN response, this binding also initiates cleavage of host mRNAs, leading to their degradation (121). While nsp1 mediates host mRNA degradation, SARS-CoV mRNAs are not susceptible to the cleavage or subsequent degradation (120). Recently it has been shown that IFN antagonism activity of nsp1 is conserved in SARS-like-CoV derived from bats and the human coronaviruses 229E and NL63 (122, 123). Additionally, nsp1 inhibits STAT1 phosphorylation, but not the phosphorylation of STAT2, indicating a level of specificity for antagonism of STAT1 signaling (118).

Part of the third nonstructural protein, SARS-CoV PLP is a papain like protease that is required for viral replication and contains a Ubiquitin like domain as well as de-ubiquitinase activity. Initial reports of IFN antagonism indicated that PLP antagonized IRF3 by blocking phosphorylation of the protein, and that this likely occurred due to a direct interaction between

IRF3 and PLP (124). This report also found that mutations within the catalytic site of the protease did not affect IFN antagonism activity. However, additional studies by Frieman *et al.* found that PLP blocked IRF3 phosphorylation in cell culture, but that this did not occur with purified components of the signaling pathway, indicating that a direct interaction between PLP and IRF3 did not take place (116). Additionally, mutations within the catalytic site of the protease were capable of decreasing the IFN antagonism. The Ubiquitin like domain of PLP was determined to be necessary, but not sufficient for IFN antagonism activity of PLP. PLP from NL63 but not MHV had similar IFN antagonism function. In contrast with the earlier study, Frieman *et al*. also found that PLP blocked NF-kB signaling in addition to IRF3 signaling. The exact mechanism by which PLP blocks IRF3 phosphorylation remains to be determined.

In addition to SARS-CoV nsp1 and PLP, SARS-CoV nsp7 and nsp15 have both been identified as potential IFN antagonists (116). SARS-CoV nsp7 antagonizes IFN transcription induced by RIG-I signaling, and the antagonism activity is well conserved in coronaviruses MHV and NL63, but less efficiently from coronaviruses derived from bats (as described in Chapter 4). The mechanism of nsp15 antagonism of IFN has not been deduced, but nsp15 has been reported to block MAVS mediated apoptosis, which may interfere with the downstream signaling of RLR family detectors (125). The majority of the SARS-CoV nonstructural proteins are required for replication, including those that have been identified as IFN antagonists. Their essential functions in viral replication may be due at least in part to their innate immune modulatory functions.

Structural Proteins

The structural proteins S, E, M, and N are all essential elements that make up the SARS-CoV virion. In addition to this function, at least two of these proteins modulate innate immune signaling by antagonizing IFN. The Nucleocapsid (N) protein of SARS Co-V forms helices of

protein encircled by the viral genomic RNAs within the SARS-CoV virion (126). SARS-CoV N is capable of blocking dimerization and nuclear translocation of the transcription factor IRF3 when induced by Sendai virus or pI:C (104, 127). However, Nucleocapsid does not block IFNβ transcription when induced by upstream mediators of IFNβ such as RIG-I, MDA5, MAVS, IKKε, TBK1 or TRIF, meaning that N exerts its effects prior to these signaling mediators, possibly at the point of binding of RLR ligands (128). Nullifying the hypothesis that interaction with the PRRs RIG-I or MDA5 might enable nucleocapsid antagonism of IFNβ, Lu *et. al* determined that N does not co-immunoprecipitate with either RIG-I or MDA-5 (127). Analyses of the N terminal domain of the Nucleocapsid proteins of SARS-CoV and MHV have revealed a conserved RNA-protein binding interface, with the interaction of the MHV N protein and the Transcriptional Regulatory Sequence (TRS) of viral RNAs (1, 129). Additional studies using MHV Nucleocapsid identified IFN antagonism activity through RNaseL mediated host translation shutoff, but this has yet to be shown with SARS-CoV N (130). While the mechanism of SARS-CoV nucleocapsid inhibition of IFNβ antagonism resulting from pI:C stimulation or SeV infection has not been directly determined, it could potentially be mediated by the interaction of RLR ligands with RNA binding sites or through similar mechanism as MHV nucleocapsid.

The SARS-CoV Membrane (M) protein is a structural component of the virion that blocks transcription of IFNβ luciferase message when stimulated by dsRNA (131). SARS-CoV M was able to block IFNβ/Luciferase message induced by the components of the RIG-I signaling pathway including RIG-I, MAVS, IKKε, and TBK1, but not the transcription factor IRF3, suggesting that the block in signaling was prior to IRF3 initiating transcription (131). SARS-CoV M also co-immunoprecipitated with RIG-I, IKKε, and TBK1, suggesting that SARS-CoV

M interacts with a complex formed by these proteins as a mechanism for disrupting IFNβ transcription. SARS-CoV M was not identified as an IFN antagonist by the Venezuelan Equine Encephalitis Virus Replicon screen, demonstrating the need for multiple approaches to identify all of the IFN antagonist proteins within the SARS-CoV genome (132). Structural components of the SARS-CoV virion act as antagonists of IFN, which may be important for blocking IFN induction immediately upon introduction of the virion into the cell, because these components are present within the cell prior to viral replication. However, the temporal nature of antagonism of IFN signaling by SARS-CoV is not yet well understood.

Accessory Proteins

SARS-CoV encodes eight accessory proteins that share no homology with proteins from other human coronaviruses and are dispensable for viral replication (133). SARS-CoV Accessory protein ORF3b is initially expressed within the nucleus, but then redistributes to the mitochondrial outer membrane (134). ORF3b is involved with G0/G1 cell cycle arrest, as well as the induction of apoptosis and necrosis (135, 136). ORF3b was identified as an antagonist of Type I IFN capable of inhibiting IFNβ expression and IRF3 phosphorylation when induced by IFNβ and Sendai virus (104). ORF3b inhibits RIG-I and MAVS mediated induction of IFNβ by the transcription factors IRF3 and NF-κB (134). However, ORF3b does not inhibit TNFα mediated activation of NF-κB transcription, leading to speculation that the disruption of NF-κB signaling is specific for induction by the RLRs (134). While the mechanism of antagonism of IFN is unknown, it seems likely that MAVS is involved, due to the location of ORF3b on the mitochondria. While ORF3b from SARS-like CoVs found in Chinese bats have a close similarity to human epidemic strains of SARS CoV (114aa protein with 91.2% identity and 93% similarity), ORF3b from SARS-like-CoVs found in European bats are strikingly dissimilar from human epidemic strains of SARS CoV (115aa protein with 44.3% identity and 57.4% similarity)

or are not present at all (137). Recently, it has been shown that ORF3b from at least one SARS-like-CoV retains IFN antagonism, while others no longer function as IFN antagonists (138). This highlights differences in innate immune modulation that may occur during infections with SARS-like-CoVs derived from bats, and potential mechanisms for increased pathogenesis that may have evolved during cross-species transmission of SARS-CoV.

Another accessory protein, SARS-CoV ORF6, has dual functions in pathogenesis of SARS-CoV associated with viral growth and IFN antagonism (104, 117, 139). ORF6 protein was identified as a potential virulence factor of SARS-CoV when increased morbidity and mortality was observed in mouse infection studies where the ORF6 protein of SARS-CoV was expressed in an attenuated MHV background (140). The addition of ORF6 to MHV increased viral RNA and viral protein synthesis of the recombinant virus *in vitro* (139). The N-terminal domain (amino acids 1-41) of the ORF6 protein is associated with the viral growth enhancement phenotype, and is capable of inducing membrane formations similar to DMVs when overexpressed(141, 142). It has also been demonstrated that ORF6 interacts with nsp8, a primase that forms a secondary RdRp in complex with nsp7, but whether this interaction impacts the increase in viral growth is not clear (143-145). In addition to its role in viral replication, ORF6 is also an antagonist of Type I IFN (104, 132, 146). In the presence of SARS-CoV ORF6 the translocation of the transcription factor STAT1 into the nucleus is inhibited, preventing signaling of the JAK/STAT pathway downstream of the IFN$\alpha\beta$ receptor (104). STAT1 is still phosphorylated in the presence of ORF6, indicating that factors upstream of STAT1 are not affected by ORF6 (104). ORF6 binds to karyopherin-α2, and tethers karyopherin-β1 on internal membranes, disrupting formation of the complex of proteins associated with the nuclear import of STAT1 (146). The C-terminus of ORF6 interferes with proteins with NLS-signals, disrupting the classical nuclear import pathway (147, 148). The IFN antagonist effects of the C-terminal

protein appear to function independently of the increase in viral replication. Because the disruption of nuclear transport is not specific to STAT1, but to a particular nuclear import pathway, there are potentially many other transcription factors that modulate innate immunity that could be affected by SARS-CoV ORF6.

SARS-CoV encodes at least eight proteins that directly modulate the induction of IFN, as well as two others that mediate an RNA capping mechanism that disguise viral RNAs from the host. Many of these factors have been identified in systems using overexpression of only one viral component in cell culture based systems. These models may not accurately reflect innate immune signaling that occurs in the target cells of SARS-CoV *in vivo*, so additional studies need to be done to determine IFN antagonism by these proteins in the context of infection. Additionally, it has been established that SARS-CoV proteins interact and can form large complexes during viral infection, and the role of these complexes in potentially modulating innate immune responses has not been established. Because of the complicated replication scheme utilized by coronaviruses like SARS-CoV, some viral proteins may be expressed at different levels during viral infection or compartmentalized in different areas of the cell, which are factors that still need to be investigated in the context of how viral proteins affect innate immune signaling (149).

SARS-CoV Pathogenesis: Innate Immune Factors Still at Large

SARS-CoV is a highly pathogenic respiratory virus where the mechanisms of severe disease are largely mediated by innate immune pathways. There currently exist several models for studying SARS-CoV pathogenesis that replicate findings from the SARS outbreak in humans: HAE and 2B4 cell lines for studying *in vitro* responses in human lung epithelial cell cultures, mouse models of fibrosis and GWAS mapping of traits, as well as primate models of comparative species infection and age-dependent phenotypes. Due to the development of these

models, SARS-CoV is uniquely suited for a systems biology based platform to compare respiratory virus infection in multiple relevant model systems as an unbiased approach to identify novel host modulators of innate immunity in the context of viral infections. SARS-CoV encodes many proteins that antagonize the host's interferon response, but little is known about the timing of when these antagonists exert their effects during viral infection, the effects of these proteins in intermediate and reservoir host species, or the function of these proteins in SARS-like-CoVs identified in bats. Of the currently well-described innate immune signaling pathways, there is evidence to support that RLR and TLR innate immune receptors detect and respond to SARS-CoV infection, but no mechanism or SARS-CoV ligand for these receptors has been determined. Unique gene transcription signatures associated with defined temporal expression of proinflammatory cytokines and Interferon stimulated genes in models of severe SARS-CoV disease have been described, but few of these genes have been evaluated for their role in SARS pathogenesis or the host antiviral response to SARS-CoV, which could help identify novel innate immunomodulatory therapies in the event of SARS-CoV re-emergence. In future studies, SARS could be particularly useful as a comparative model for Influenza A viruses or RSV infection to evaluate common targets for antiviral strategies as well as unique mechanisms of innate immune pathogenesis across multiple virus families with similar tropisms.

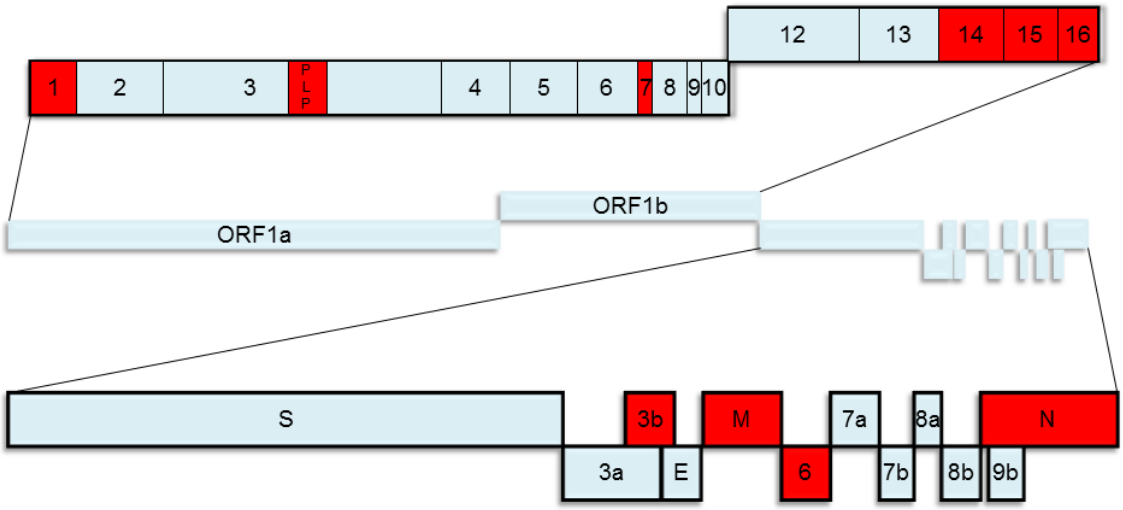

Figure 1.1 The SARS-CoV Genome

The typical coronavirus genome size is quite large in comparison to many other positive-sense RNA viruses; within the SARS-CoV genome of 29.7 kB at least ten genes with potential functions that modulate innate immunity have been characterized (highlighted here in red). Like other members of the viral family *Coronaviridae*, SARS-CoV has a positive-sense, single-stranded RNA genome that is amenable to manipulation using reverse genetic techniques. In SARS-CoV the first open reading frame (ORF) encodes the 16 nonstructual proteins that make up the viral replicase, while the ensuing ORFs encode structural proteins that compose the virion, as well as eight accessory proteins. The SARS-CoV accessory proteins share no homology to the accessory proteins of other human coronaviruses, and while dispensable for replication *in vitro*, encode functions that likely impact viral pathogenesis *in vivo.*

SARS-CoV Protein	Innate Immune Function	References
nsp1	Antagonizes IFN; inactivates host translation; degrades host mRNA; blocks phosphorylation of STAT1	[118-123]
PLP	Antagonizes IFN; interacts with STING; blocks IRF Phosphorylation; blocks NF-κB signaling	[116]
nsp7	Antagonizes IFN by undescribed mechanism	[116]
nsp14	Guanine-N7-methyltransferase activity part of viral RNA capping machinery for evading host detection	[112]
nsp15	Antagonizes IFN by undescribed mechanism	[116]
nsp16	2'-O-methlytransferase activity modifies the cap of viral RNAs for evading host detection	[112]
ORF3b	Antagonizes IFN signaling induced by MAVS/RIG-I	[104, 134]
Membrane	Antagonizes IFN signaling through kinases TBK1/IKKε	[131]
ORF6	Antagonizes IFN by blocking nuclear import of STAT1	[104, 132, 146]
Nucleocapsid	Antagonizes IFN by unknown mechanism	[127,128]

Table 1.1 Functions of SARS-CoV Innate Immune Antagonists.

Transcription and subsequent signaling of interferon is vital for activating the antiviral response in host cells. Because of this, many viruses (including SARS-CoV) encode proteins that antagonize the IFN response to viral infection. SARS-CoV encodes at least eight proteins that directly modulate the induction of IFN, as well as two others that mediate an RNA capping mechanism that disguises viral RNAs from the host. Many of these factors have been identified in systems using overexpression of only one viral component in cell culture based systems. These models may not accurately reflect innate immune signaling the occurs in the target cells of SARS-CoV *in vivo*, so additional studies need to be done to determine IFN antagonism by these proteins in the context of infection. Additionally, it has been established that SARS-CoV

proteins interact and can form large complexes during viral infection, and the role of these complexes in potentially modulating innate immune responses has not been established. Because of the complicated replication scheme utilized by coronaviruses like SARS-CoV, some viral proteins may be expressed at different levels during viral infection or compartmentalized in different areas of the cell, which are factors that still need to be investigated in the context of how viral proteins affect innate immune signaling.

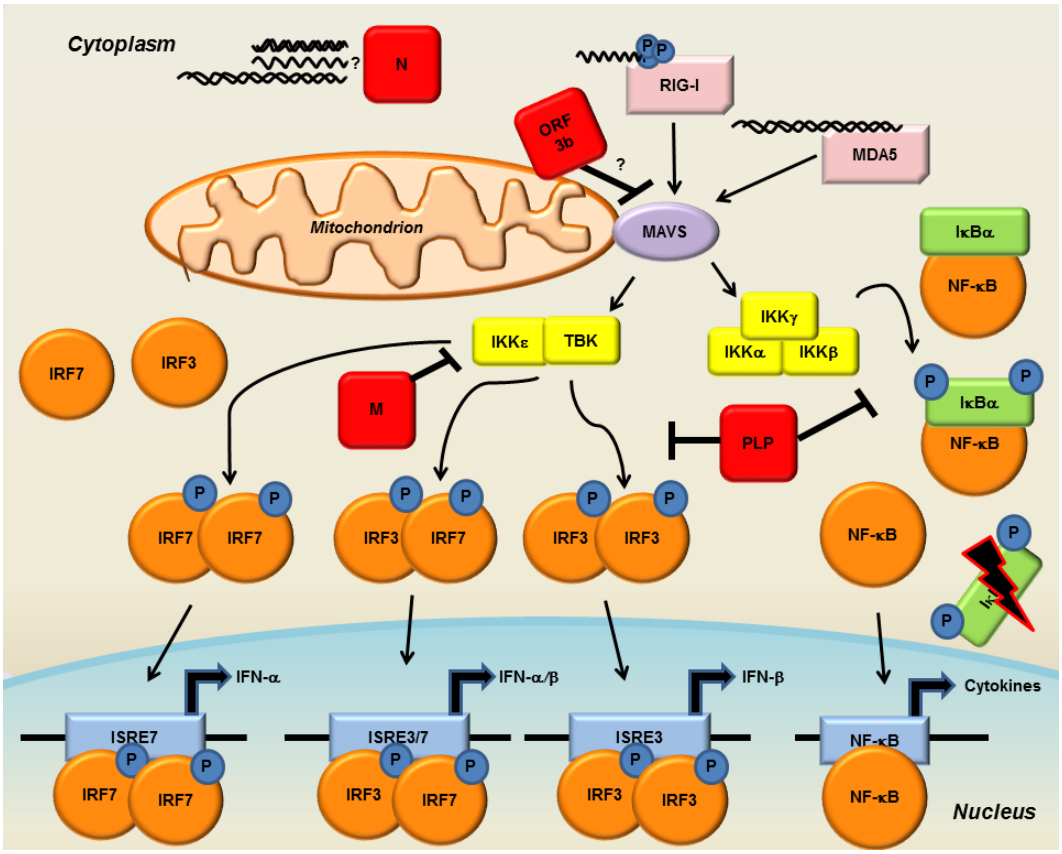

Figure 1.2 RLR Family of Innate Immune Receptors Induce Type I Interferon

The family of RIG-I-like Receptors (RLRs) circulate within the cytoplasm of host cells to detect nucleic acid PAMPs. Following detection of PAMPs, RLRs initiate a signaling cascade that leads to the activation of IFNs, producing an antiviral state in the infected cell. SARS-CoV encodes proteins that antagonize RLR family signaling, shown here in red.

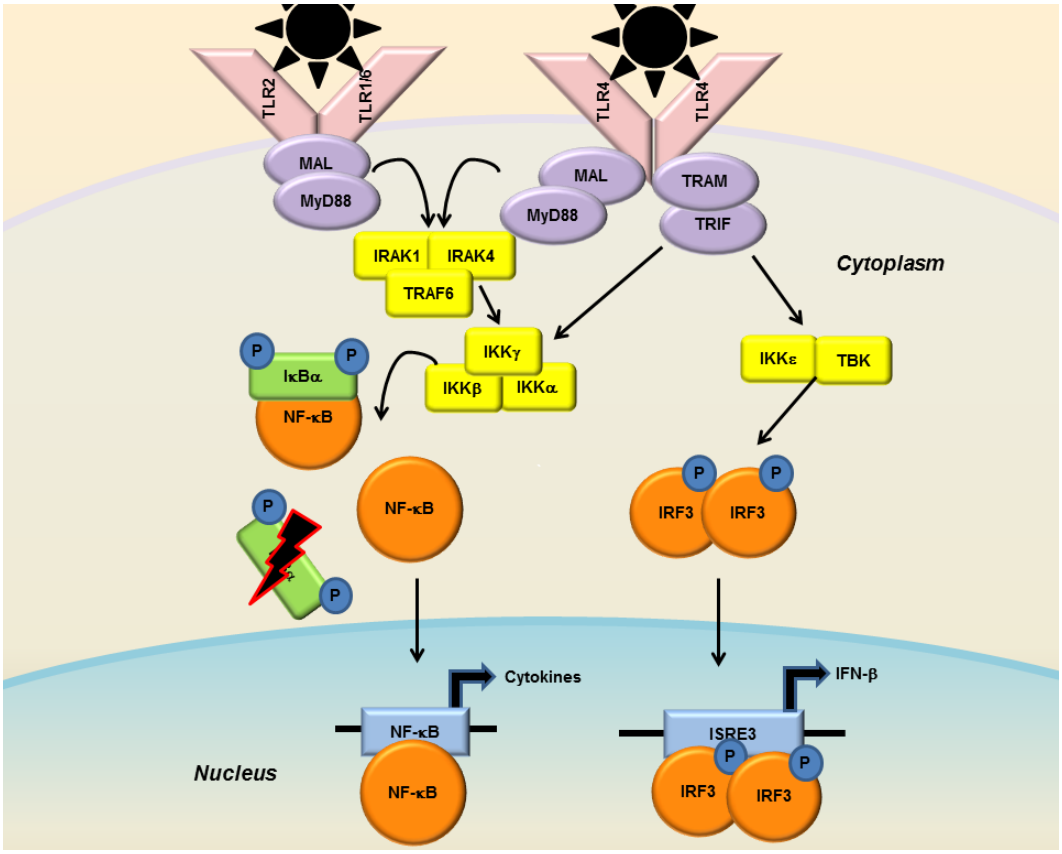

Figure 1.3 Pathogen Associated Molecular Pattern Sensing by Toll-Like Receptors: Plasma Membrane.

On the surface of cells, TLR2 and TLR4 are known to recognize viral glycoproteins. TLR2/6 heterodimers help to activate the innate immune response to RSV, though the viral PAMP recognized has not been determined (90) TLR1/2 heterodimers have been shown to recognize viral glycoproteins, though their potential role in respiratory virus infection has not been determined (91). TLR4 utilizes the sorting adaptors MAL and TRAM to differentiate between MyD88-dependent signaling and TRIF-dependent signaling. Signaling downstream of MyD88 and TRIF leads to the activation of innate immune signaling programs including cytokines and IFNs.

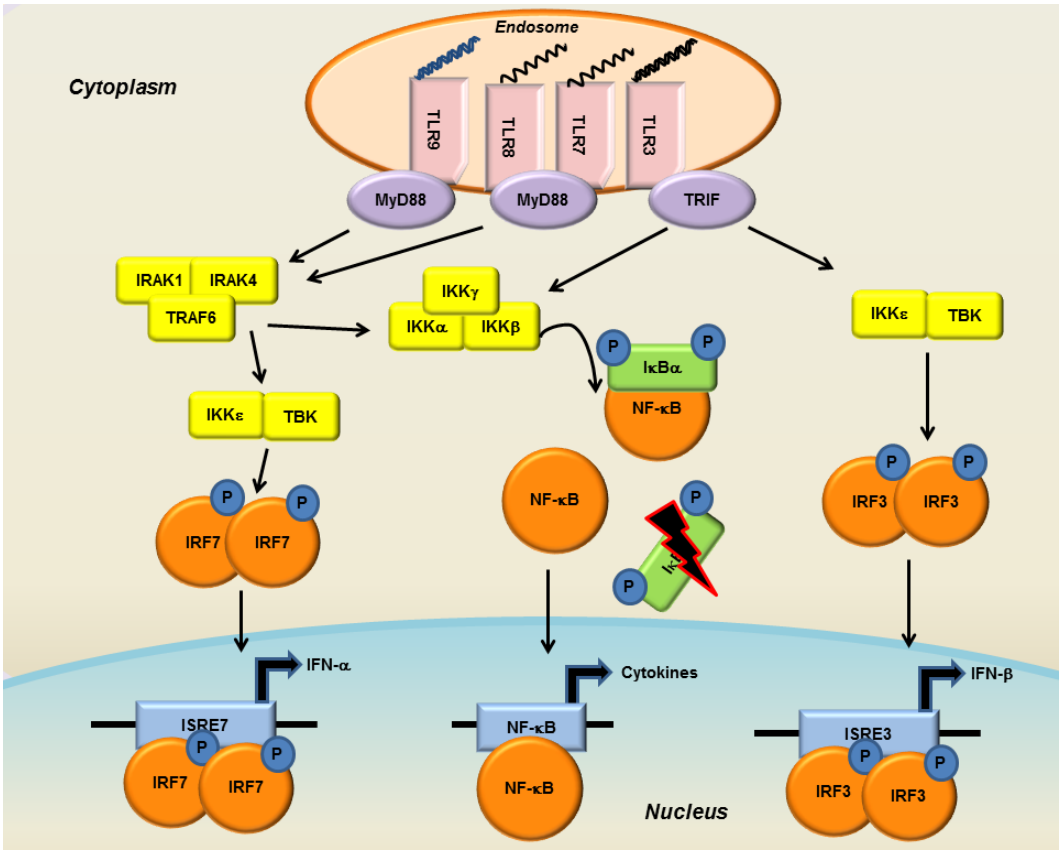

Figure 1.4 Pathogen Associated Molecular Pattern Sensing by Toll-Like Receptors: Endosome.

In the endosomal compartment, TLRs recognize viral nucleic acid PAMPs: TLR3 recognizes dsRNAs, TLR7/8 recognizes ssRNAs, and TLR9 recognizes CpG DNA motifs. While there are many TLRs that recognize viral PAMPs, they signal through common adaptor molecules. MyD88 is an adaptor molecule for all of the TLRs with the exception of TLR3, which uses the adaptor TRIF. The TLR adaptor molecules signal through the IKKε/TBK1 complex and the IKKα/IKKβ/IKKγ complex similarly to RLRs, but can also recruit an IRAK-1/IRAK4/TRAF6 complex capable of activating the transcription factors IRF3, IRF7, and NF-κB. Activation of these transcription factors leads to the transcription of Type I IFNs and other cytokines

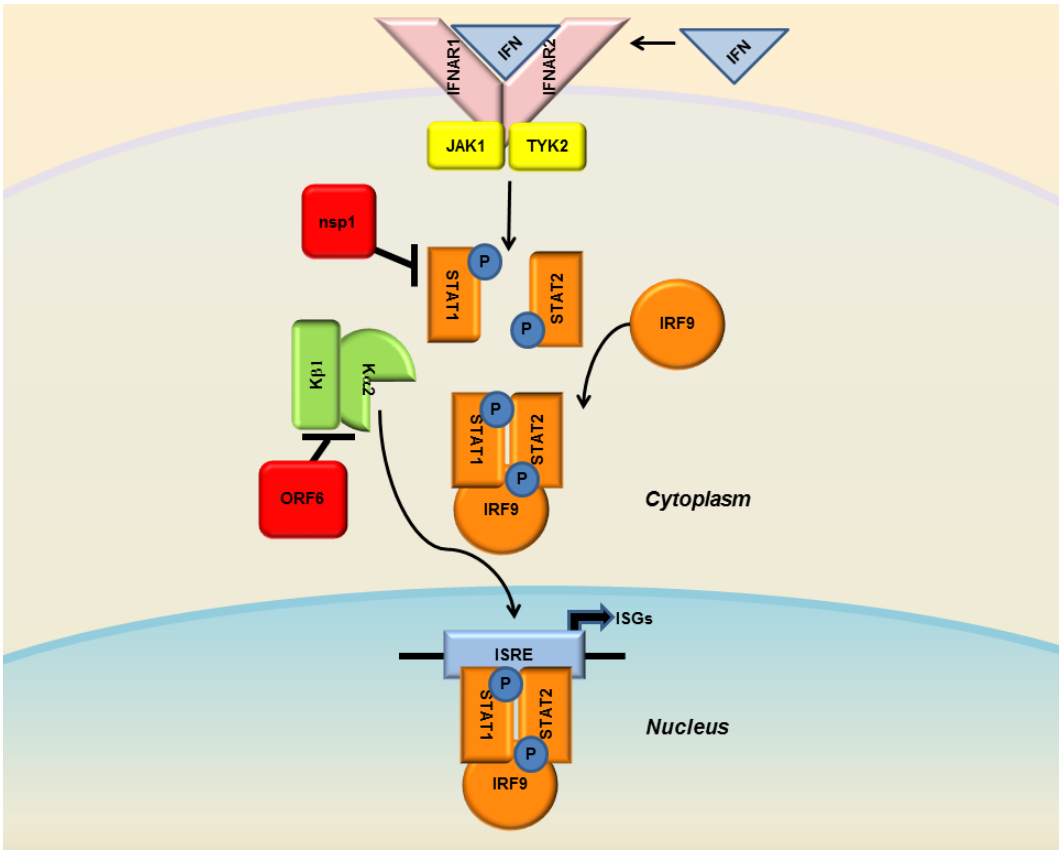

Figure 1.5 Interferon Signals through the JAK/STAT Pathway to Induce Interferon Stimulated Genes.

The secretion of IFNα and IFNβ molecules from an infected cell leads to an autocrine and paracrine signaling through the IFNαβ Receptor (composed of the IFNAR1 and IFNAR2 subunits) resulting in the activation of the JAK-STAT pathway. The JAK/TYK2 kinases phosphorylate the transcription factors STAT1 and STAT2, which form heterodimers complexed with IRF9. The STAT complex translocates to the nucleus leading to the transcription of interferon stimulated genes (ISGs) that establish an antiviral state in the cell. Because neighboring cells can receive IFN stimulation prior to infection, it is a crucial pathway to preventing viral spread in the host. SARS-CoV also encodes proteins that antagonize the JAK-STAT pathway, shown here in red.

CHAPTER 2: TLR3 SIGNALING VIA TRIF CONTRIBUTES TO A PROTECTIVE INNATE IMMUNE RESPONSE TO SARS CORONAVIRUS INFECTION[2]

INTRODUCTION

The recent emergence of highly pathogenic Severe Acute Respiratory Syndrome (SARS, pandemic in 2002-2004), Middle East Respiratory Syndrome (MERS, Arabian Peninsula epidemic in 2012-present), and Porcine Epidemic Diarrhea (PEDV, United States porcine epidemic in 2013-present) coronavirus (CoV) infections is indicative of a reoccurring global public health vulnerability (1, 2, 5, 17, 28, 150). At the end of the SARS-CoV pandemic, 774 patients died from SARS of the 8096 cases confirmed by the WHO, a mortality rate of slightly less than 10% (5). Ten years later, the emergence of a novel human coronavirus Middle East Respiratory Syndrome Coronavirus (MERS-CoV) has been confirmed in 940 patients of which 376 have died, a mortality rate of approximately 40%, highlighting the need for continued surveillance for emergent human coronaviruses with the potential to cause severe disease (150). Particularly troubling, is the relative ease with which these pathogens have been spread outside of the original geographic origins by global travelers (21). Furthermore, recent surveys of bat populations, a known reservoir host of zoonotic coronaviruses, have observed that bats harbor myriad novel and potentially emergent coronaviruses with unknown pathogenic potential, indicating that coronavirus spillover into human and livestock populations may continue (33). Despite the importance of SARS and MERS as public health threat, there are currently no available antivirals against these pathogens, with current evidence suggesting that the antiviral

drugs ribavirin and interferon are not efficacious in ameliorating SARS or MERS, although MERS-CoV appears more sensitive *in vitro* (6, 24, 151). While research on MERS-CoV is still in the nascent stages, efforts to develop a vaccine against SARS-CoV have been hindered by the challenges of vaccine induced immune pathology as well as the likely need for cross-protection against highly variable and antigenically distinct coronaviruses with unknown emergent potential (36, 65, 152).

SARS-CoV and MERS-CoV are phylogenetically and antigenically distinct members of the *Coronaviridae* family but use similar replication strategies to generate progeny viruses (1, 17). Pathogen associated molecular patterns (PAMPs) that differentiate between viral and host molecules are likely to exist in similar locations within coronavirus infected host cells and thus potentially be detected by similar classes of cellular sensors. Innate immune sensors function in host cells to recognize PAMPs specific to viruses and other invading pathogens, triggering transcriptional changes in host cell signaling programs to establish and antiviral state the suppresses viral replication efficiency. Respiratory virus infections are potentially devastating global health concerns as evidenced by emerging highly pathogenic Influenza A H5N1 and H7N9 viruses (IAV), as well as the SARS-CoV and MERS-CoV epidemics (153). The human lung has critical functions in gas exchange and represents a large and complex, but highly vulnerable mucosal surface that interfaces with multiple microorganisms in the environment. Lung cells including type II pneumocytes and ciliated cells of the airway epithelium are the primary targets of SARS-CoV and IAV infection in the lung (9, 153). When these cells are exposed to pathogens, innate immune signaling cascades are initiated by pattern recognition receptors (PRRs), which include multiple classes of cellular sensors distributed at cellular

---

[2] This chapter is currently in submission to a peer-reviewed journal as: Totura AL, Whitmore A, Agnihothram S, Schäfer A, Katze MG, Heise MT, and RS Baric. *TLR3 signaling via TRIF contributes to a protective response to SARS coronavirus infection*.

membranes and within the cytosol to ensure maximal detection of viruses at multiple stages of the replication cycle, including viral entry and genome replication (154).

Toll-like Receptors (TLRs) are membrane bound PRRs that detect molecular patterns from viruses, bacteria, and fungi at the plasma membrane and within endosomes. TLR3 has been implicated in the detection of many RNA viruses and in altering the pathogenesis of airway disease resulting from respiratory virus infections such as Influenza A virus, respiratory syncytial virus, and rhinovirus (155-157). Basal levels of TLR3 expression are detectable in lung tissues such as in human alveolar cells and bronchial epithelial cells, as well as various immune cell populations (158). In cells, TLR3 is anchored to the membrane of endosomes, where it recognizes dsRNA motifs from invading pathogens (159). After binding the dsRNA motif, TLR3 dimerizes and recruits the adaptor protein TRIF (160, 161). TRIF recruitment to the endosome results in signaling to activate transcription factors including IRF3 and NF-κB (162). In addition to TLR3 specific signaling, TRIF has also been described as an adaptor for TLR4 signaling and signaling by DDX 1/21/36 complexes(163). TLR3 signaling via TRIF leads to the activation of type I interferons (IFNβ, IFNα), proinflammatory cytokines (IL-6, TNF, IFNγ, CCL5), and interferon stimulated genes (RSAD2, IFIT1, CXCL10) (158, 161). These effector molecules have defined importance in the context of ARDS and respiratory virus infections (153, 164).

TLR agonists and antagonists have been proposed as compounds with broad-spectrum therapeutic potential against a number of respiratory infections in the context of antiviral drugs and vaccine adjuvants (165-168). There is a need to understand how TLR signaling and effector networks may regulate coronavirus pathogenesis, given the diverse pool of zoonotic precursors with potential for spillover into human and livestock populations. Previous data from our lab had described a protective role for the TLR adaptor protein MyD88, which facilitates

downstream signaling through a large number of TLRs, in our mouse model of SARS-CoV disease (95). Here, we present evidence that MyD88-independent signaling through TLR3 and its adaptor protein TRIF exerts a powerful protective cell intrinsic defense network in response to SARS-CoV infection and disease.

MATERIALS & METHODS

Viruses, cells, and plaque assay.

A mouse model of recombinant mouse adapted SARS-CoV-rMA15 virus used in this study has been previously described (60, 95). As previously described, virus stocks were propagated on Vero E6 cells (60). Plaque assays to quantify virus in viral stocks and to enumerate the number of viruses in the lower left lobe of lungs from mice were performed in Vero E6 cells, with a limit of detection of 100 PFU (152). Experiments with SARS-CoV-rMA15 were performed in a certified biosafety level 3 laboratory, using class II biological safety cabinet. Lab workers were equipped with high-efficiency particulate air (HEPA)-filtered powered air-purifying respirators (PAPRs), Tyvek suits, hoods, aprons, booties, and personal protective equipment.

Animals.

All animal housing and care was conducted according to University of North Carolina - Chapel Hill (Animal Welfare Assurance #A3410-01) Institutional Animal Care and Use Committee (IACUC) approved protocols. Animals were maintained in HEPA-filtered Sealsafe cages (Techniplast) during experiments with SARS-CoV-rMA15. Age matched female mice were obtained from Jackson labs: C57B/6NJ (stock no. 005304), $TLR3^{-/-}$ (stock no. 009675), C57BL/6J (stock no. 000664), and $TRIF^{-/-}$ (stock no. 005307). At ten weeks of age, mice were anesthetized with a mixture of ketamine/xylazine and inoculated intranasally with 50uL of either phosphate buffered saline (PBS, for mock inoculated controls) or 10^5 PFU of MA15-SARS-CoV

in PBS. Animals were weighed daily, and lung tissues from days 2, 4, and 7 postinfection (C57BL/6NJ and TLR3$^{-/-}$ mice) or days 2, 4, and 6 postinfection (C57BL/6J and TRIF$^{-/-}$ mice) were collected for downstream analyses by plaque assay, histology and RNA analysis.

Flow Cytometry.

On days 4 and 6 postinfection, whole lungs were harvested in groups of 3-4 mock treated wild type and TRIF$^{-/-}$ mice and 4-5 SARS-CoV infected wild type and TRIF$^{-/-}$ mice. Whole lungs were prepared for flow cytometry analysis by collagenase digestion and tissue disruption into cell suspensions as previously described (65). Antibody staining panels of anti-Ly6C/FITC (Becton-Dickinson), anti-SigLecF/PE (Becton-Dickinson), anti-CD11c/PETR (Molecular Probes), anti-B220/PerCP (Biolegend), anti-Gr-1/PE-Cy7 (eBioscience), anti-CD11b/eF450 (eBioscience), anti-LCA/APC (eBioscience), and anti-MHC-II/APC-eF780 (eBioscience) for monocyte derived cell staining or anti-CD94/FITC (eBioscience), anti-CD3ε/PE (eBioscience), anti-CD4/PETR (Molecular Probes), anti-CD8α/PerCP (Becton-Dickinson), anti-CD94b/PE-Cy7 (eBioscience), anti-LCA/eF450 (eBioscience), anti-CD19/AF647 (Biolegend), and anti-B220/APC-eF780 (eBioscience) for lymphocyte derived cell staining were used to stain cell preparations. Analysis was performed with Summit software (Beckman-Coulter) to sort into defined subpopulations: viable lymphoid and myeloid cells (LCA^{pos}), eosinophils (LCA^{pos}, CD11c^{low}, SigLecF^{pos}, GR-1^{low}, CD11b^{pos}), alveolar macrophages (LCA^{pos}, CD11c^{pos}, SigLecF^{pos}, CD11b^{pos}, GR-1^{low}), plasmacytoid dendritic cells (B220^{pos}, MHCII^{neg} after gating out GR-I^{high} and SigLecF^{pos} cell populations), neutrophils (LCA^{pos}, SigLecF^{neg}, GR-1^{high}, CD11b^{pos}), monocytes (LCA^{pos}, CD11c^{neg}, CD11b^{pos}), Ly6C^{high} monocytes (Ly6C^{high}, GR-1^{pos}), Ly6C^{low} monocytes (Ly6C^{low}, GR-1^{neg}), monocyte derived dendritic cells (LCA^{pos}, CD11c^{pos}, SigLecF^{neg}, CD11b^{pos}, MHCII^{neg}), CD11b^{high} dendritic cells (LCA^{pos}, CD11c^{pos}, SigLecF^{neg}, CD11b^{pos}, MHCII^{pos}), viable lymphocytes (LCA^{pos}, CD11b^{neg}, CD11c^{neg}), T cells (LCA^{pos}, CD11b^{neg},

CD11c^{neg}, CD3^{pos}), CD4 T cells (LCA^{pos}, CD11b^{neg}, CD11c^{neg}, CD3^{pos}, CD4^{pos}), CD8 T cells (LCA^{pos}, CD11c^{neg}, CD3^{pos}, CD8^{pos}), and B cells (LCA^{pos}, CD11b^{neg}, CD11c^{neg}, CD3^{neg}, CD19^{pos}, B220^{pos}).

Hemorrhage scores, histological analysis, and immunohistochemistry.

Scores for gross hemorrhage were recorded by observation of the lung during necropsy using a scale where a value of zero indicates no hemorrhage to a value of 4, indicating severe hemorrhage in all lobes of the lung as has been previously described (169). For histological analysis, the entire right lobe of lungs from infected or mock treated wild type and knockout mice was fixed in 10% formalin, embedded in paraffin, and prepared in 5uM sections for hematoxylin & eosin (H&E) staining by the UNC histopathoglogy core facility. For immunohistochemistry (IHC), formalin-fixed and paraffin-embedded histology samples from C57BL/6J and TRIF$^{-/-}$ mice were sectioned (5uM) and stained for viral antigen using a commercially available polyclonal SARS-CoV anti-nucleocapsid antibody (Imgenex) following the manufacturer's protocols (41). Slides for IHC and H&E histology were scored in a blinded manner (n=4-5 mice per group) for metrics of inflammation and images were captured using Olympus BX41 microscope with an Olympus DP71 camera**.**

Whole body plethysmography.

Lung function was measured by unrestrained whole body plethysmography using IACUC approved protocols as has been previously described (170). Briefly, animals were introduced into randomized individual plethysmography chambers following calibration according to manufacturer protocols (Buxco). After a 30 min acclimation period, data on lung function parameters was collected for 5 min measurement period. Data were analyzed by Finepoint software (Buxco) for established metrics of airway hyperresponsiveness and virus infection associated airway obstruction, including Enchanced Pause (P_{ENH}), Tidal Midexpiratory Flow

(EF_{50}), and Ratio of T_{PEF}:T_E (R_{PEF}). P_{ENH} is an empirical measure calculated by $\frac{Te-Tr}{Tr} * \frac{PEF}{PIF}$ where PEF is the peak expiratory flow, PIF is the peak inspiratory flow, T_E represents the time of expiration, and T_R represents the relaxation time to 35%, of the peak expiration pressure (171). P_{ENH} has been controversially linked to airway hyperresponsiveness, obstruction, and bronchoconstriction, but has been used in several viral models of airway infection, where increases in the P_{ENH} value correlate with increased lung pathology following respiratory viral infection (170-174). EF_{50} indicates the flow rate at 50% of the tidal volume. R_{PEF} is calculated by $\frac{Tpef}{Te}$ where T_{PEF} is the time to peak expiratory flow and T_E is the time of expiration, and the ratio may be interpreted as an indication of the shape of breath during exhalation.

Real-Time qPCR Analysis.

The upper left lobe of SARS-CoV-rMA15 infected mice was stored in RNALater solution (Life Technologies) for 48 hours at 4C, and then stored at -80C. Lung sections were thawed and then homogenized in TRIzol (Life Technologies) for 60 seconds at 6000 rpm using a MagNa Lyzer Instrument (Roche). Following chloroform/isopropanol extraction of RNA from TRIzol homogenates, cDNA was generated by RT-PCR using SuperScript III First Strand Synthesis kit (Life Technologies). Quantative PCR was performed using TaqMan Gene Expression Assays (Life Technologies) for cytokines or chemokines normalized to 18s expression. For each cytokine or chemokine, expression from groups of 4 SARS-CoV-rMA15 infected mice were normalized to PBS mock inoculated mice of either wildtype or knockout mice. Normalized fold change was calculated using the $\Delta\Delta^{CT}$ method as has been previously described (65).

ELISA.

Levels of IFNβ were quantified using the VeriKine Mouse IFN Beta ELISA kit (RD Systems) according to manufacturer protocols. The lower left lobe of lungs from $TRIF^{-/-}$ or

C57Bl/6J mice from mock inoculated or SARS-CoV infected group (n=4 each group) was homogenized in 1mL of PBS using a MagNa Lyzer Instrument (Roche). 100uL of cleared homogenate was used for the ELISA assay sample. A seven point standard curve was prepared using manufacturer's protocol, and interferon titers in the samples were determined by plotting the standards using a 4-parameter fit. Optical densities were read at an absorbance of 450nm.

Differentially expressed gene identification.

Differentially expressed gene targets were selected from data collected in a study previously described with transcriptomics data banked at NCBI Gene Expression Omnibus #GSE33266 (169). Briefly, this study performed microarray analysis on RNA from lungs of 20 week old female C57BL/6J mice infected with 10^2, 10^3, 10^4, or 10^5 PFU doses of mouse adapted SARS-CoV to identify differentially expressed genes compared to mock (PBS) inoculated mice. A linear fit model was used to determine differential expression (DE) for each transcript, requiring an absolute $\log_2$(fold change) >1.5 as well as a false discovery rate (FDR) adjusted *p* value of <0.05. In a separate study, $TLR3^{-/-}$ lung homogenates in TRIzol were analyzed by microarray and full data set are available at Omics-lhv-discovery.wisc.edu in the pathway folder for Systems Virology Data/SARS/SM036.

RESULTS

Toll -like Receptor Pathways are key regulators of SARS-CoV pathogenesis

Using a network integration approach to identify key regulators of SARS-CoV pathogenesis, a previous study that assayed host mRNA responses in C57BL/6J mice infected with 10^2, 10^3, 10^4, or 10^5 PFU doses of SARS-CoV yielded a highly prioritized list of candidate genes involved in the host response to SARS-CoV (169, 175). From these microarray data derived from the host mRNAs in the lung, network analyses identified host pathways regulating SARS-CoV pathogenesis that were both previously uncharacterized (wound repair pathways,

(169)) as well as pathways that have a well-established foothold in the literature in respect to SARS-CoV pathogenesis (innate immune pathways) (175). Toll-like Receptors (TLRs) play a critical role in the recognition of pathogens and induction of the innate immune response to many viruses, but TLR recognition of SARS-CoV is not well characterized. Two TLR related genes that were highly ranked on the prioritized list are differentially expressed in response to SARS-CoV infection compared to mock inoculated mice: MyD88 and TLR3 (Figure 2.1a, 2.1b).

MyD88 transcripts were significantly upregulated at the doses of 10^3, 10^4, and 10^5 at day 2 postinfection, and met the fold change threshold to be categorized as a differentially expressed gene at this timepoint, but not at days 1, 4, or 7 postinfection (Figure 2.1a). MyD88 was previously identified as a protective component of the innate immune response to SARS-CoV infection in a mouse model (95). SARS-CoV infected mice had a similar RNA expression profile for TLR3 as MyD88: it is differentially expressed at day 2 postinfection with SARS-CoV at the doses of 10^3, 10^4, and 10^5PFU of SARS-CoV (Figure 2.1b). Based on the similarities in gene expression of MyD88 and TLR3 and ranking of the genes by network integration analyses, we hypothesized that TLR3 signaling may also be involved in the protective innate immune response to SARS-CoV infection. TLR3 signaling occurs in a MyD88-independent manner via the adaptor protein TRIF, so these data indicate that at least two discrete TLR signaling pathways are involved in the host response to SARS-CoV infection (Figure 2.1e).

To test the hypothesis that TLR3 has a protective role in SARS-CoV infection of mice, 10-week old female TLR3$^{-/-}$ mice and wild type C57BL/6NJ mice were infected intranasally with 10^5 PFU of MA15-SARS-CoV to observe differences in the pathogenesis of SARS-CoV disease. Wild type mice infected with SARS-CoV experienced transient weight loss that peaked on day 3 postinfection, but all of the wild type mice began to recover from weight loss on day 4 postinfection and recovered fully from weight loss by 6-7 dpi (Figure 2.1c). TLR3$^{-/-}$ mice lost a

greater average percentage of their starting weight with statistically significant differences in TLR3$^{-/-}$ weight loss compared to wild type mice on day 2-7 post infection (Figure 2.1c, $^{**}p<0.01$, $^{***}p<0.005$). About 4 fold higher titers were observed in the lungs of TLR3$^{-/-}$ mice infected with SARS-CoV compared to wild type mice at days 2 and about 20 fold higher titers were observed in the lungs of TLR3$^{-/-}$ mice infected with SARS-CoV compared to wild type mice at 4 postinfection (Figure 2.1d, $^{***}p<0.005$). On day 7 postinfection, one TLR3$^{-/-}$ mouse had detectable virus in the lungs, while the rest of the TLR3$^{-/-}$ mice and all of the C57BL/6NJ mice had no detectable virus in the lungs (Figure 2.1d).

To determine if there were differences in lung function associated with the increased viral titer and weight loss observed in TLR3$^{-/-}$ vs. wild type mice infected with SARS-CoV, whole body plethysmography was used to measure parameters indicative of airway hyper-responsiveness and obstruction in SARS-CoV infected mice (Figure 2.2a-c) (174, 176). A rise to similar peak levels of P_{ENH}, a measure indicative of airway resistance and obstruction, was seen in both groups of SARS-CoV infected mice by day 2 postinfection (Figure 2.2a). However, while wild type mice infected with SARS-CoV returned to basal levels of P_{ENH} by day 4 postinfection, TLR3$^{-/-}$ mice infected with SARS-CoV retain significantly higher levels of P_{ENH} on days three through seven postinfection ($^{*}p<0.05$, $^{***}p<0.005$). The midtidal expiratory flow (EF_{50}) is significantly higher in the TLR3$^{-/-}$ mice on days 4 thru 7 postinfection (Figure 2.2b, $p<0.005$), an indicator of disease consistent with previous data in SARS-CoV infection models and studies of hypoxic conditions (170, 177). TLR3$^{-/-}$ mice maintained a lower ratio of T_{PEF}:T_E (R_{PEF}) measurement at days 4-7 postinfection while wild type mice resolved to mock levels (Figure 2.2b). Evaluation of H&E stained lung tissue samples of TLR3$^{-/-}$ and wild type mice infected with SARS-CoV at day 7 postinfection revealed no statistically significant differences in inflammation surrounding the large airways (Figure 2.2e), vasculature (Figure 2.2f), or alveoli

(Figure 2.2g, 2.2h). However, significantly more exudative fluids and debris were present in the alveolar spaces of TLR3$^{-/-}$ mice infected with SARS-CoV than in wild type mice (Figure 2.2d, 2.2i), indicating that alveolar fluid may be causing airway obstruction, resulting in detrimental lung function parameters in the TLR3$^{-/-}$ mice even after the mice have begun to recover from weight loss due to SARS-CoV infection.

TLR3 regulates downstream responses of several key proinflammatory cytokines and TLR3 can also regulate the induction of type I interferon and downstream signaling by interferon stimulated genes (ISGs). Surprisingly, microarray analysis of host gene expression showed few alterations in gene expression downstream of TLR3 when TLR3$^{-/-}$ mice were compared to wild type mice (Figure 2.3). There was no change in the levels of IL-6 or TNF, two proinflammatory cytokines downstream of TLR3 signaling (Figure 2.3a, 2.3b). CCL5 and IFNγ were differentially expressed in TLR3$^{-/-}$ mice compared to wild type mice, with higher gene expression in the wildtype mice compared to TLR3$^{-/-}$ mice greater than a 1.5 fold change difference on day 4 postinfection (Figure 2.3c, 2.3d, *>1.5 fold change). No differences were observed in IFNβ, a type I interferon (Figure 2.3e), or RSAD2 (Figure 2.3f), CXCL10 (Figure 2.3g), and IFIT1 (Figure 2.3h), three ISGs.

Toll-like Receptor adaptor TRIF has a protective role in the host response to SARS-CoV

Because TLR3$^{-/-}$ utilizes the adaptor TRIF for downstream signaling programs we infected TRIF$^{-/-}$ mice and wild type C57BL/6J mice intranasally with 10^5 PFU of SARS-CoV-rMA15 to determine the role of TRIF in SARS-CoV pathogenesis. TRIF$^{-/-}$ mice experienced typical early weight loss, and then continued to lose weight on days 4 through 6 post infection, when wild type mice were recovering from weight loss (Figure 2.4a). All of the TRIF$^{-/-}$ mice approached 70% of their starting weight on day 6 post infection, when the experiment was ended according to our humane endpoint animal protocols. At days 2 and 4 post infection, significantly

higher viral loads were observed in the lungs of TRIF$^{-/-}$ mice compared to wild type mice (Figure 2.4b, $p<0.001$). By day 6 postinfection wild type mice have cleared virus below the limit of detection of the plaque assay, but there is still detectable virus in the lungs of TRIF$^{-/-}$ mice (Figure 2.4b, $p<0.001$). Additionally, at 6 days postinfection, the lungs of TRIF$^{-/-}$ mice infected with SARS-CoV had severe hemorrhage encompassing the entire lung tissue, while little if any hemorrhage was observed in the lungs of wild type mice (Figure 2.4c, $p<0.001$). Based on these observations, TRIF$^{-/-}$ mice had more severe SARS-CoV clinical disease signs compared to TLR3 $^{-/-}$ mice (Figure 2.1, Figure 2.4).

To determine if the increased susceptibility of TRIF$^{-/-}$ mice to SARS-CoV infection affects lung function, whole body plethysmography was used to measure changes in lung function over the course of the SARS-CoV infection in TRIF$^{-/-}$ mice compared to wild type mice (Figure 2.4d, 2.4e, 2.4f). TRIF$^{-/-}$ mice had significantly higher levels of Enhanced Pause (P_{ENH}) on day 2-6 postinfection (Figure 2.4d, $*p<0.05$, $***p<0.001$) indicative of airway hyper-responsiveness and infection associated airway obstruction. Lower values of the R_{PEF} in TRIF$^{-/-}$ mice persisted throughout SARS-CoV infection, while wild type mice R_{PEF} values recovered to basal levels by day 4 postinfection (Figure 2.4e, $***p<0.001$). The Midtidal Expiratory Flow (EF_{50}) is significantly higher in TRIF$^{-/-}$ mice compared to wild type mice on days 1-6 postinfection with SARS-CoV (Figure 2.4f, $*p<0.05$, $**p<0.01$). These measures indicate that major changes in lung function occur in the TRIF$^{-/-}$ mice infected with SARS-CoV potentially due to changes in large airway debris and denudation indicated by histological analysis.

To determine if differences in viral titer in TRIF$^{-/-}$ mice infected with SARS-CoV compared to wild type mice resulted in increased viral spread or were associated with infection of different cell types, we evaluated lung sections stained by immunohistochemistry specific for the SARS-CoV nucleocapsid protein (Figure 2.5). Significantly more viral antigen was present

in the lungs of TRIF$^{-/-}$ mice compared to wild type mice at day 2 postinfection, confirming the higher viral loads quantified by plaque assay (Figure 2.5f, *p<0.05). In the large airways of TRIF$^{-/-}$ mice infected with SARS-CoV, no difference in the amount of viral antigen present was observed (Figure 2.5b, 2.5e), but cells infected in both the C57BL/6J and TRIF$^{-/-}$ mice were morphologically consistent with ciliated airway epithelial cells, a primary target of SARS-CoV in humans. Interestingly, significantly more viral antigen staining was observed in the parenchyma of the lungs of TRIF$^{-/-}$ mice compared to C57BL/6J mice infected with SARS-CoV (Figure 2.5a, 2.5e, **p<0.01). Alveolar spaces show the presence of viral antigen in cells morphologically consistent with type ii pnuemocytes, another primary target cell of SARS-CoV (Figure 2.5c, last two panels). Observation of the immunohistochemistry did not reveal any evidence that SARS-CoV infection of TRIF$^{-/-}$ mice occurs in alternate cell types than in C57BL/6J mice.

Because TRIF$^{-/-}$ mice infected with SARS-CoV showed signs of severe lung dysfunction by whole body plethysmography (Figure 2.4d-f), H&E stained lung sections from TRIF$^{-/-}$ and C57BL6/J mice were scored for signs of SARS-CoV disease on day 6 postinfection (Figure 2.6). Although mock inoculated wild type and TRIF$^{-/-}$ mice show no signs of abnormal pathology (Figure 2.6a-d, left panels), wild type and TRIF$^{-/-}$ mice infected with SARS-CoV displayed hallmarks of SARS-CoV disease, including airway inflammation (Figure 2.6c, 2.6e), perivascular cuffing (Figure 2.6b, 2.6f), and alveolar inflammation (Figure 2.6d, 2.6g-i). TRIF$^{-/-}$ mice infected with SARS-CoV had significantly more accumulation of inflammatory cells surrounding the large airways than wild type mice (Figure 2.6a, 2.6c, right panels; Figure 2.6e, *p<0.05). Similar observations that increased infiltrating cells surrounded the vasculature in the lungs of TRIF$^{-/-}$ mice infected with SARS-CoV compared to wild type mice (Figure 2.6c; 2.6f, *p<0.05). In the alveolar spaces of TRIF$^{-/-}$ mice, increased thickening of the septa between

alveoli (Figure 2.6d; 2.6g, *p<0.05) was observed in addition to more infiltrating cells (Figure 2.6d; 2.6h, *p<0.05). Similarly to TLR3$^{-/-}$ mice (Figure 2.2d, 2.2i), the presence of alveolar exudates was observed in significantly more TRIF$^{-/-}$ mice infected with SARS-CoV compared to wild type mice (Figure 2.6d; 2.6h, **p<0.01). These increased alveolar exudates in TLR3$^{-/-}$ mice that correlated with differences in whole body plethysmography measures of P_{ENH}, R_{PEF}, and EF_{50} were also observed in TRIF$^{-/-}$ mice infected with SARS-CoV and correlated with the same whole body plethysmography measures.

Aberrant cellular responses in TRIF$^{-/-}$ mice following SARS-CoV infection

Because TRIF acts as a TLR adaptor protein that leads to activation of transcription factors that transcribe cytokines and chemokines, we hypothesized that differences in chemokines downstream of TRIF$^{-/-}$ signaling would be altered in TRIF$^{-/-}$ mice compared to wild type mice. Measurements of proinflammatory cytokines IL-6, TNF, IFNγ and chemokines CCL2, CCL3, CCL5, CCL7, CCL8 showed reduced expression of all these genes at day 2 postinfection in TRIF$^{-/-}$ mice, while these transcripts are highly induced in wild type mice infected with SARS-CoV (Figure 2.7 a-h). At day 4 postinfection, significantly more expression of IL-6, TNF, CCL5, and IFNγ was observed in TRIF$^{-/-}$ mice, while expression was diminished in wild type animals infected with SARS-CoV (Figures 2.7a-d). On day 4 postinfection there was no significant difference in the levels of chemokines CCL2, CCL3, CCL7, or CCL8 in the TRIF and wild type mice infected with SARS-CoV (Figure 2.7e-h). In contrast, increased protein levels of IFNβ were observed in TRIF$^{-/-}$ mice on day 2 and day 4 postinfection compared to wild type mice infected with SARS-CoV (Figure 2.8a, 2.8b, *p<0.05) which is probably due to the increased viral loads in the lungs of TRIF$^{-/-}$ mice at these timepoints. Interferon stimulated genes RSAD2, CXCL10, and IFIT1 were greatly reduced in TRIF$^{-/-}$ mice infected with SARS-CoV on day 2 postinfection compared to wild type mice (Figure 2.8c-e) but were induced to very

high levels in the TRIF$^{-/-}$ mice infected with SARS-CoV on day 4 postinfection while the ISG response was waning in wild type mice.

Because differences in inflammation were observed in H&E stained lung sections of TRIF$^{-/-}$ mice, and differences in chemokines that recruit inflammatory cells were observed in TRIF$^{-/-}$ mice compared to wild type mice, we hypothesized that differences in infiltrating immune cell populations would be observed TRIF$^{-/-}$ mice compared to wild type mice infected with SARS-CoV. Both wild type and TRIF$^{-/-}$ lungs from mice infected with SARS-CoV had larger numbers of cells due to infiltrating cells populations compared to mock inoculated mice, but there were no significant differences in the overall number of infiltrating cells of TRIF$^{-/-}$ lungs on days 4 or 6 postinfection compared to lungs from wild type mice infected with SARS-CoV (Figure 2.9a, 2.9c). There were significantly more neutrophils in the lungs of TRIF$^{-/-}$ mice infected with SARS-CoV compared to lungs of wild type mice on day 4 postinfection (Figure 2.9b, $p<0.05$), however by day 6 postinfection there were no longer significant differences in neutrophils (Figure 2.9d). The chemokines that are chemotactic for neutrophil recruitment CXCL1, CXCL2, and CXCL3 were significantly lower on day 2 postinfection in TRIF$^{-/-}$ mice infected with SARS-CoV, but were higher in TRIF$^{-/-}$ mice on day 4 postinfection, coinciding with the increased recruitment of neutrophils in the TRIF$^{-/-}$ mice infected with SARS-CoV (Figures 2.9e-g).

While there were no significant differences in the number of total monocytes between TRIF$^{-/-}$ and wild type mice infected with SARS-CoV on day 4 or day 6 postinfection (Figure 2.10a, 2.10f), differences in monocytic subpopulations were observed. There were significantly more Ly6C^{high} inflammatory monocytes in the TRIF$^{-/-}$ mice infected with SARS-CoV on day 4 postinfection (Figure 2.10c, $p<0.05$), but there was no difference between TRIF$^{-/-}$ and wild type mice infected with SARS-CoV on day 6 post infection (Figure 2.10h). Conversely, there was no

difference between wild type and TRIF$^{-/-}$ mice in the Ly6C^{low} population of monocytes on day 4 postinfection (Figure 2.10b), but wild type mice infected with SARS-CoV had significantly more Ly6C^{low} regulatory monocytes on day 6 postinfection (Figure 2.10g, $p<0.05$). On day 4 postinfection there was no significant difference in the number of alveolar macrophages or plasmacytoid dendritic cells (pDCs) between the lungs TRIF$^{-/-}$ and wild type mice infected with SARS-CoV (Figure 2.10d, 2.10e), but at day 6 postinfection there were significantly more alveolar macrophages and pDCs in the lungs of TRIF$^{-/-}$ mice infected with SARS-CoV compared to wild type mice (Figure 2.10i, 2.10j). No statistically significant differences were observed in populations of eosinophils, monocyte derived DCs, or CD11b^{pos} DC populations between TRIF$^{-/-}$ mice and wild type mice infected with SARS-CoV (data not shown).

The total number of lymphocytes was not significantly different between TRIF$^{-/-}$ mice and wild type mice at day 4 of day 6 postinfection (Figure 2.11a, 2.11e). There were no differences in the number of T cells in the lungs of TRIF$^{-/-}$ mice and wild type mice infected with SARS-CoV on day 4 postinfection (Figure 2.11b), but on day 6 postinfection there were significantly more T cells in the lungs of wild type mice infected with SARS-CoV compared to wild type mice (Figure 2.11f, $p<0.05$). There were no significant differences in the number of CD4+ T cells on day 4 or day 6 postinfection (Figure 2.11c, 2.11g), of CD8+ T cells on day 4 postinfection (Figure 2.11d) but there were significantly more CD8+ T cells observed in wild type mice at day 6 postinfection, compared to TRIF$^{-/-}$ mice (Figure 2.11h). Aberrant SARS-CoV disease responses were observed in the TRIF$^{-/-}$ mice including increased weight loss, lack of viral clearance, alterations in lung function and pathology, changes in infiltrating cell populations and aberrant cellular signaling programs, all indicating that TRIF is a master regulator in the protective innate immune response to SARS-CoV disease.

DISCUSSION

The critical importance of TLR signaling programs is demonstrated by the key regulation of host immune responses by the TLR adaptor proteins MyD88 and TRIF in controlling respiratory virus infections. In SARS-CoV infected $TRIF^{-/-}$ mice, there is significantly increased mortality, weight loss, and viral titers (Figure 2.4a, 2.4b) leading to expression of cytokines, chemokines and ISGs (Figure 2.7, Figure 2.8) consistent with aberrant cellular signaling programs seen in patients that succumbed to SARS or MERS disease (16, 23). Although $MyD88^{-/-}$ mice infected with SARS-CoV have comparable mortality, weight loss, and viral loads to $TRIF^{-/-}$ mice infected with SARS-CoV, the outcomes in downstream cellular signaling programs were very different (95). In $MyD88^{-/-}$ mice infected with SARS-CoV there was an absence of induction of cytokine and chemokine signaling at days 2, 4, and 6 postinfection compared to wild type mice; in contrast, $TRIF^{-/-}$ mice infected with SARS-CoV had a similar lack of cytokine and chemokine signaling on day 2, but an increased amount of IFNβ, followed by a marked increase in proinflammatory cytokine and ISG signaling on day 4 post infection. Consistent with these data, $TRIF^{-/-}$ mice infected intranasally with Herpes Simplex virus (HSV-1) have increased mortality rate, significantly greater viral titers in the brain, and increased production of type I IFN (178). In contrast, $TRIF^{-/-}$ mice infected with Influenza A virus were not significantly different from wild type mice in mortality, but one study found $MyD88^{-/-}$ mice were more susceptible than wild type mice, while another found there was no difference between $MyD88^{-/-}$ mice and wild type mice infected with Influenza A virus (155, 179). These data indicate that although both TLR adaptors MyD88 and TRIF are vitally important to a protective immune response to SARS-CoV, differences exist between the cellular signaling programs induced by highly pathogenic respiratory infections caused by coronaviruses and influenza viruses that should be considered prior to the administration of therapeutic regimes (180).

The differences in viral pathogenesis between MyD88$^{-/-}$ and TRIF$^{-/-}$ mice also include major differences in infiltrating cell populations resulting from SARS-CoV infection. MyD88$^{-/-}$ mice had significantly fewer inflammatory monocytes and macrophages at day 2 postinfection compared to wild type mice infected with SARS-CoV, but no cellular populations measured were significantly different at day 4 postinfection (95). In addition, despite similarities in infiltrating cell populations in MyD88$^{-/-}$ and wild type mice infected with SARS-CoV on day 4 postinfection, a lack of cytokine and chemokine signaling persisted, indicating a likely deficiency in the activation of signaling programs of these cells. However, in TRIF$^{-/-}$ mice many differences in infiltrating cell populations were observed at day 4 and day 6 postinfection, but the increase in transcription of proinflammatory cytokines indicates that a lack of TRIF does not inhibit cell signaling programs by these cell populations. Rather, the large induction of IFNβ on day 2 postinfection and the presence of significantly more viral antigen at early times postinfection likely drive the increased stimulation of infiltrating cell types in TRIF$^{-/-}$ mice contributing to aberrant cellular responses.

The influx of inflammatory cells is a hallmark of highly pathogenic respiratory virus infections. The accumulation of neutrophils in TRIF$^{-/-}$ mice on day 4 postinfection with SARS-CoV correlates with increased amount of neutrophil recruitment chemokines CXCL1 and CXCL2 (IL-8 rodent homologs) and increased levels of proinflammatory cytokines like TNF and IL-6, mirroring the neutrophil infiltration and cellular responses of ARDS patients (reviewed in (181)). Similarly indicative of lethal pathogenesis of respiratory viruses, infection of mice with highly pathogenic strains of influenza including 1918 H1N1 and H5N1 Influenza viruses had significantly more recruitment of neutrophils (similarly to levels seen in TRIF$^{-/-}$ mice infected with SARS-CoV) than was observed following infection with low pathogenic seasonal influenza strains (182). There is evidence that neutrophils infiltrating the pulmonary compartment

produce robust amounts of CXCL10 contributing to the pathogenesis of ARDS from influenza virus infection, and the induction of large levels of CXCL10 was observed in TRIF$^{-/-}$ mice infected with SARS-CoV on day 4 postinfection, coinciding with the influx of neutrophils (164). In influenza virus infection, infiltrating Ly6C^{hi} monocytes resulting from IFN induction contributes to resistance of influenza virus infection, while in our model significantly more Ly6C^{hi} monocytes were observed in the more susceptible TRIF$^{-/-}$ mice on day 4 postinfection (183). This inflammatory monocyte population can differentiate into macrophage and pDC subsets, which are observed in significantly higher numbers in TRIF$^{-/-}$ mice infected with SARS-CoV on day 6 postinfection (Figure 2.10i, 2.10j; reviewed in (184)).

Because TLR3 senses double stranded RNAs, an intermediate nucleic acid species present during acute viral infections, it could be predicted that loss of TLR3 signaling would negatively impact the host and alter cellular signaling programs in response to highly pathogenic respiratory virus infections as is observed with SARS-CoV. Although TLR3$^{-/-}$ mice infected with SARS-CoV experience greater weight loss, higher viral titers, and more significant alterations in lung function over the course of infection (Figure 2.1c, 2.1d, and 2.2a-c), relatively few changes in downstream cellular signaling programs result from absence of TLR3 (Figure 2.3a-h) indicating that additional pathways may compensate for the absence of TLR3 in SARS-CoV infection. In contrast to our results with SARS-CoV, TLR3$^{-/-}$ mice are less susceptible to H3N2 and H5N1 Influenza viruses with a decreased mortality rate compared to lethal infection of wild type mice, but there is no difference in survival of TLR3$^{-/-}$ mice compared to wild type mice infected with a lethal dose of p2009 H1N1 infected mice (155, 185). The phenotype of TLR3$^{-/-}$ mice in West Nile virus (WNV) mouse models is somewhat controversial, with one group showing modest increase in WNV induced mortality with no differences in type I IFN

levels in TLR3$^{-/-}$ mice, while another group showed TLR3$^{-/-}$ mice have less susceptibility to WNV and reduced proinflammatory cytokine responses compared to wild type mice (186, 187).

Despite the varying outcomes in host survival and morbidity in SARS-CoV, WNV, influenza virus infection models, the commonality is that TLR3$^{-/-}$ mice have increased viral loads in the infected tissues, demonstrating that the initial recognition of viral PAMPs by TLR3 is necessary for controlling viral replication, and that the increased presence of viral antigen could partially drive downstream phenotypes in these systems (Figure 2.1d) (155, 186, 187). Neither MyD88$^{-/-}$ nor TRIF$^{-/-}$ mice infected with SARS-CoV efficiently clear the virus by day 6 postinfection, but both show increased signs of disease ultimately leading to death of the TLR adaptor knockout mice from SARS-CoV infection. Our observations confirm previous findings that signaling through TRIF is critical CD8+ T cell priming and expansion, a key component of adaptive immunity for viral clearance (188, 189). In contrast to the TLR adaptor knockout mice, RAG1$^{-/-}$ mice with no mature T cells fail to clear SARS-CoV, but show no signs of increased disease, as defined by weight loss, indicating that the lack of clearance of virus is not responsible alone for the disease phenotypes seen in the TRIF$^{-/-}$ and MyD88$^{-/-}$ mice (95). In generating a protective immune response to highly pathogenic coronavirus infections, our findings indicate that not only is the activation of adaptive response required for viral clearance, but also the proper activation of a balanced innate immune response through both adaptor arms of TLR mediated signaling.

TLR agonists have been proposed for usage as respiratory vaccine adjuvants, while TLR agonists and antagonists have been proposed as having utility in protection against respiratory virus induced disease or immunopathology (165-168). There is evidence that adjuvant approaches which stimulate TLR pathways through both MyD88 as well as TRIF generate synergistic effects and our findings indicate the both MyD88 and TRIF-dependent signaling are

critical components to the host response to SARS-CoV. Our data shown here confirm that innate immune responses important for antiviral state of cells, immune cell recruitment, and priming of adaptive immune responses. Comparison of these data to other models of highly pathogenic respiratory virus infection (particularly influenza) indicates that although these viruses may be detected by similar pathways, the result of that sensing can lead to differences in disease outcome, which should be considered in the design and administration of vaccine and antiviral therapeutics.

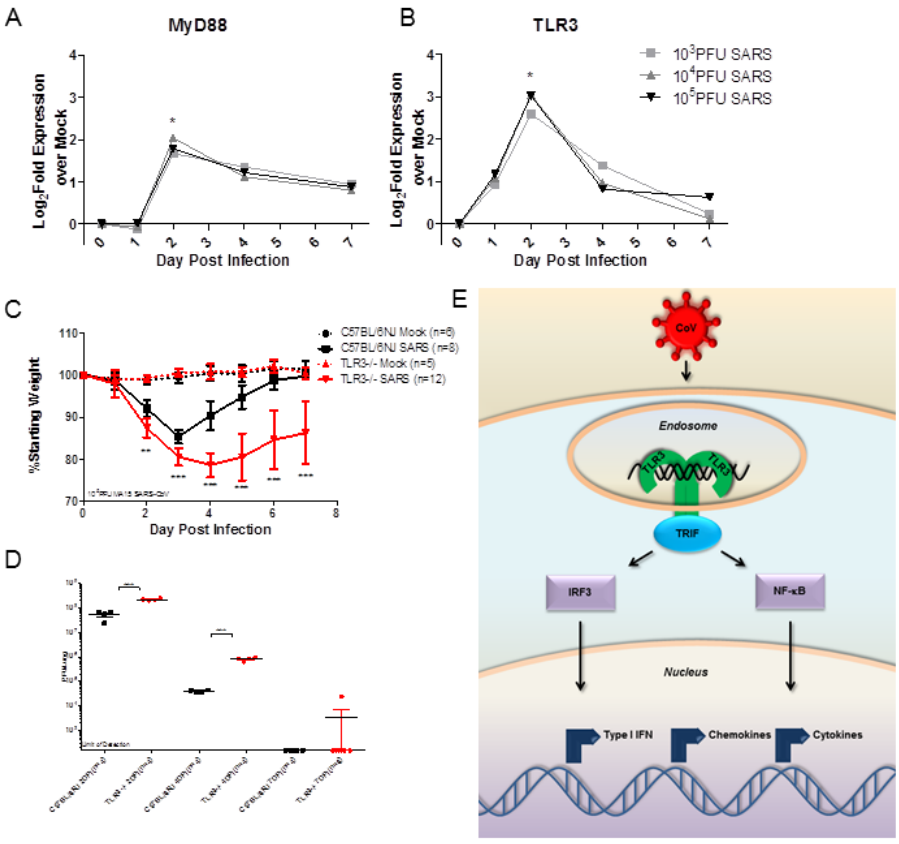

Figure 2.1 Two Discrete TLR Pathways Regulate SARS-CoV Pathogenesis.

Profiles from microarray analysis of MyD88 (a) and TLR3 (b) RNA expression in 20 week C57BL/6J infected with 10^3, 10^4, 10^5 PFU of SARS-CoV indicate that differential gene expression occurs at day 2 postinfection (* indicates differential expression determined by >1.5Log_2 fold expression over mock and $p<0.05$). Infection of $TLR3^{-/-}$ and C57BL/6NJ mice with SARS-CoV shows significantly greater weight loss in $TLR3^{-/-}$ mice compared to wild type (c, $^{**}p<0.01$, $^{***}p<0.001$, by non-parametric Mann-Whitney test, where values indicate the mean percent starting weight, error bars indicate standard deviation) and viral titers (d, $^{***}p<0.001$, by student's unpaired *t*-test) were significantly higher in the $TLR3^{-/-}$ mice compared to wild type mice. TLR3 signaling through the adaptor protein TRIF activate innate immune antiviral signaling programs in a MyD88-independent manner, indicating that at least two discrete TLR signaling pathways are involved in SARS-CoV pathogenesis (e).

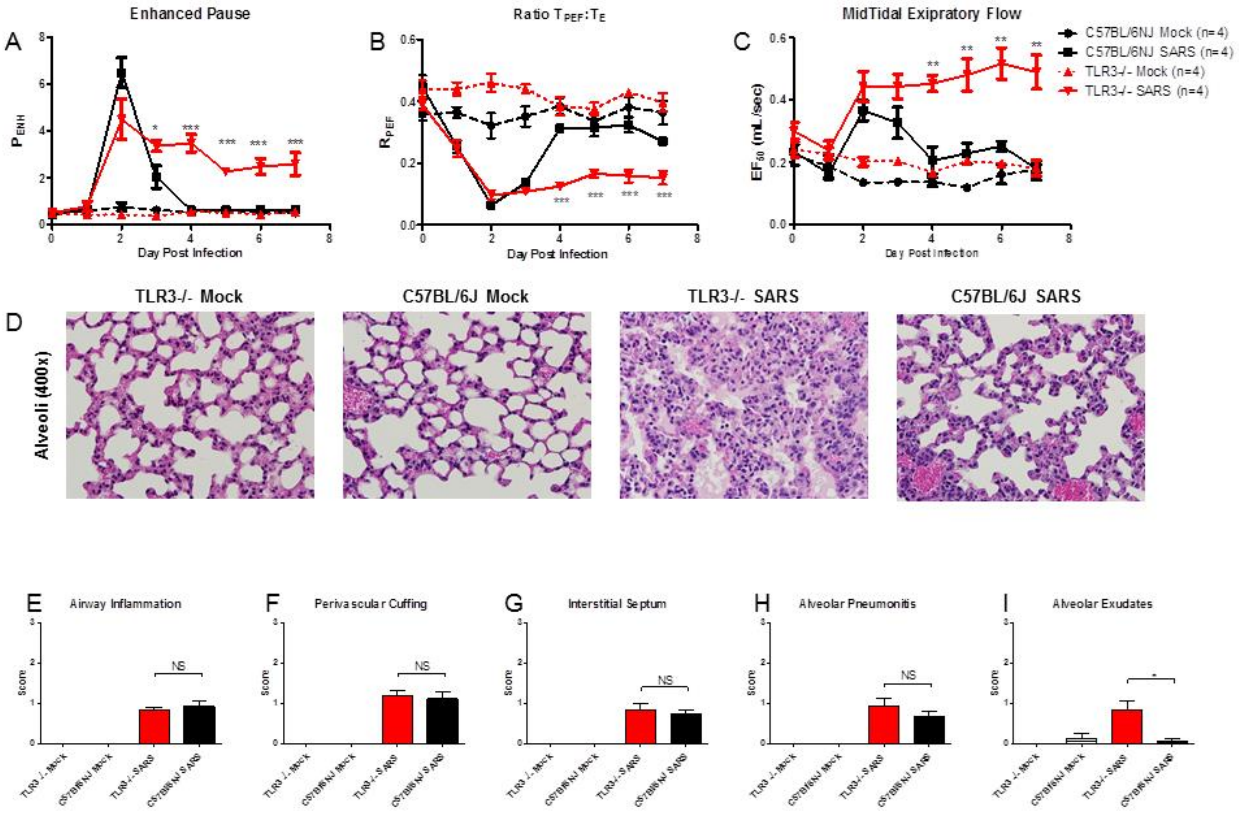

Figure 2.2 TLR3$^{-/-}$ Mice have Aberrant Lung Function and Pathology Resulting from SARS-CoV Infection.

Whole body plethysmography analysis shows that SARS-CoV infected TLR3$^{-/-}$ mice (solid red line) have alterations in lung functions compared to C57BL/6NJ mice (solid black line) including Enhanced Pause (P_{ENH}, a), Ratio TPEF:TE (R_{PEF}, b), and Midtidal Expiratory Flow (EF_{50}, c) over the course of seven days (dashed red line indicates TLR3$^{-/-}$ mock, dashed black line indicates C57BL/6NJ mock, *p<0.05, **p<0.01, ***p<0.001 by unpaired student's t-test). Histopathology analysis of formalin fixed H&E stained lung tissues indicates that while TLR3$^{-/-}$ (d, first panel) and C57BL/6J (d, second panel) mock inoculated mice have normal alveolar architecture; TLR3$^{-/-}$ mice infected with SARS-CoV (d, third panel) show signs of alveolar exudates not present in C57BL/6J mice infected with SARS-CoV (d, last panel) on day 7 postinfection. Histopathology

lung sections from day 7 postinfection were scored for SARS disease signs including airway inflammation (e), perivascular cuffing (f), thickening of the interstitial septa of alveoli (g), alveolar pneumonitis (h), and alveolar exudates (i). Histology sections were scored in a blinded manner, scores were evaluated for significance by unpaired student's *t*-test, $*p<0.05$, NS not significant.

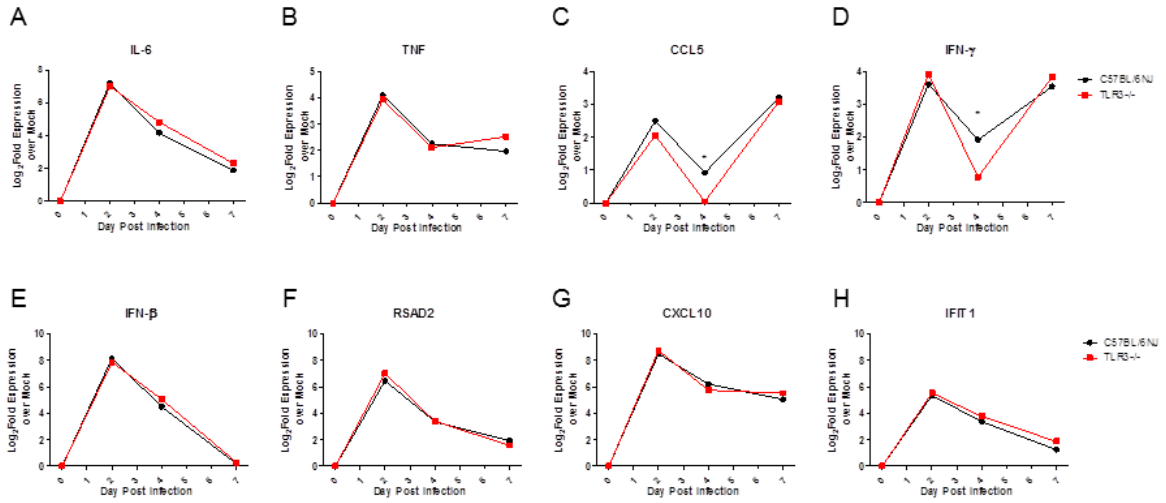

Figure 2.3. TLR3$^{-/-}$ Mice Show Few Alterations in Cytokine and IFN Signaling Responses to SARS-CoV Infection Compared to Wild Type Mice.

RNA expression profiles of cytokines and interferon stimulated genes (ISGs) downstream of TLR3 signaling measured by microarray analysis of IL-6 (a), TNF (b), CCL5 (c), IFNγ (d), IFNβ (e), RSAD2 (f), CXCL10 (g), and IFIT1 (h) from mock PBS inoculated TLR3$^{-/-}$ or C57BL/6NJ mice and TLR3$^{-/-}$ or C57BL/6NJ infected with 10^5 PFU of SARS-CoV (n=4-5 mice per group) . Differentially expressed genes indicated by * have >1.5 fold change and p>0.05.

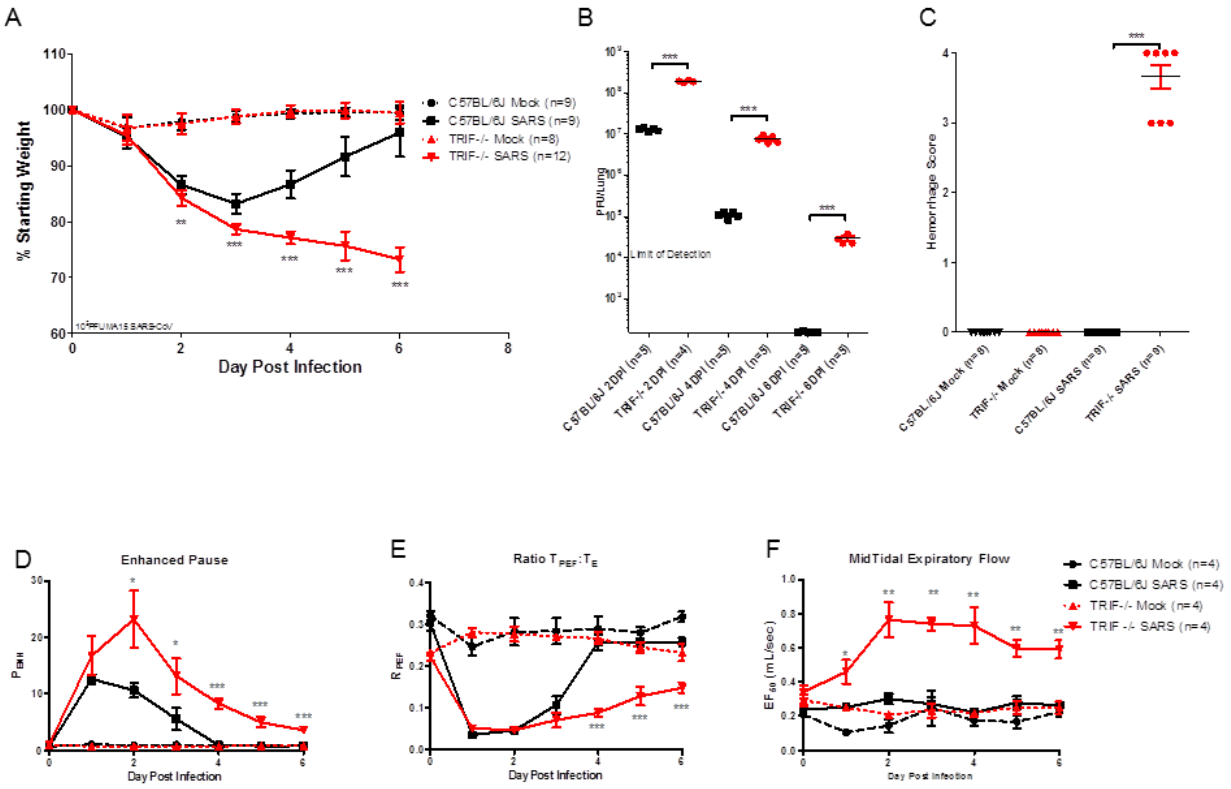

Figure 2.4 TRIF$^{-/-}$ Mice are Highly Susceptible to SARS-CoV Infection.

TRIF$^{-/-}$mice infected with SARS-CoV have significantly greater weight loss (a, $^{**}p<0.01$, $^{***}p<0.001$ by nonparametric Mann-Whitney Test where values indicate the mean percent starting weight, error bars indicate standard deviation), viral titers (b, $^{***}p<0.001$ by unpaired student's *t*-test), and lung hemorrhage scores (c, scored from 0-4, $^{***}p<0.001$ by unpaired student's *t*-test) than C57BL/6J mice infected with SARS-CoV over a 6 day course of infection. Whole body plethysmography analysis shows that SARS-CoV infected TRIF$^{-/-}$ mice (solid red line) have alterations in lung functions compared to SARS-CoV infected C57BL/6J mice (solid black line) including Enhanced Pause (P_{ENH}, d), Ratio TPEF:TE (R_{PEF}, e), and Midtidal Expiratory Flow (EF_{50}, f) over the course of six days (dashed red line indicates TRIF$^{-/-}$ mock, dashed black line indicates C57BL/6J mock; $^{*}p<0.05$, $^{**}p<0.01$, $^{***}p<0.001$ by unpaired student's *t*-test).

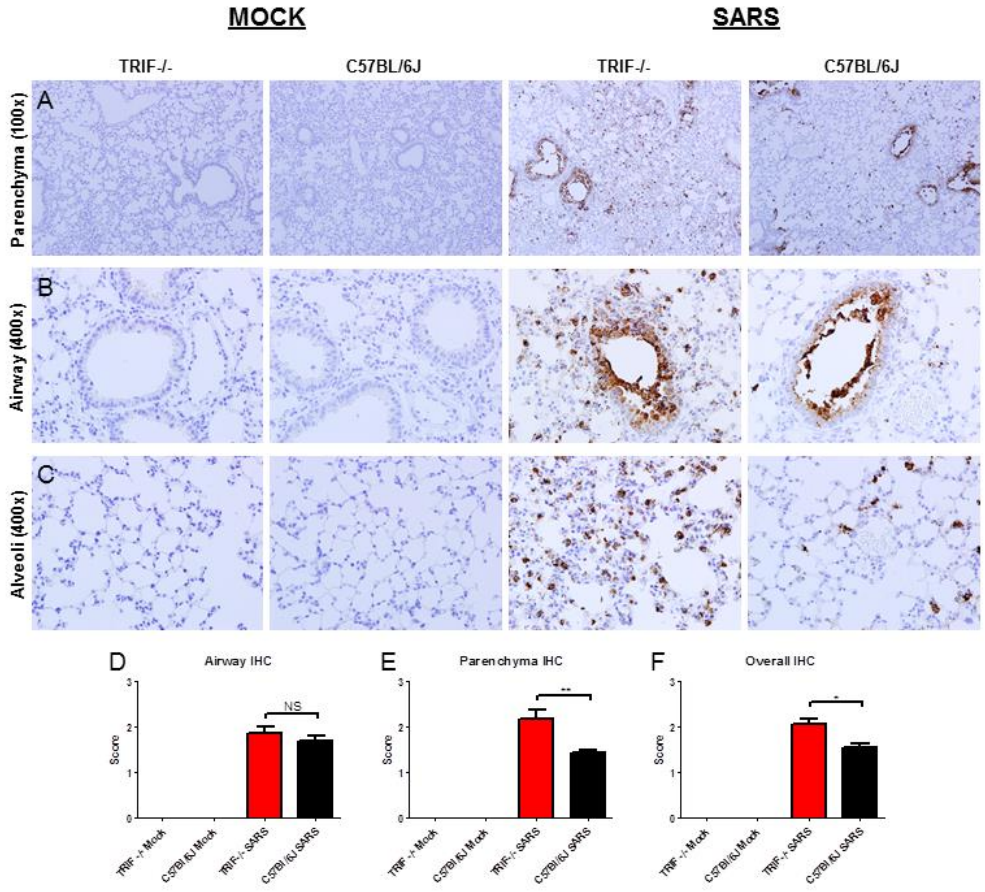

Figure 2.5 Increased Presence of Viral Antigen in the Lungs of TRIF$^{-/-}$ Mice.

Immunohistochemistry was used to stain for SARS-CoV nucleocapsid antigen in the lungs of TRIF$^{-/-}$ mock inoculated mice (first column a-c), C57BL/6J inoculated mice (second column a-c), TRIF$^{-/-}$ SARS-CoV infected mice (third column a-c), and C57BL/6J SARS-CoV infected mice (last column a-c) on day 2 postinfection with SARS-CoV. Immunohistochemistry lung sections from day 2 postinfection were scored for the presence of SARS nucleocapsid antigen Sections were scored in a blinded manner, scores were evaluated for significance by unpaired student's *t*-test; *p<0.05, **p<0.01, NS not significant.

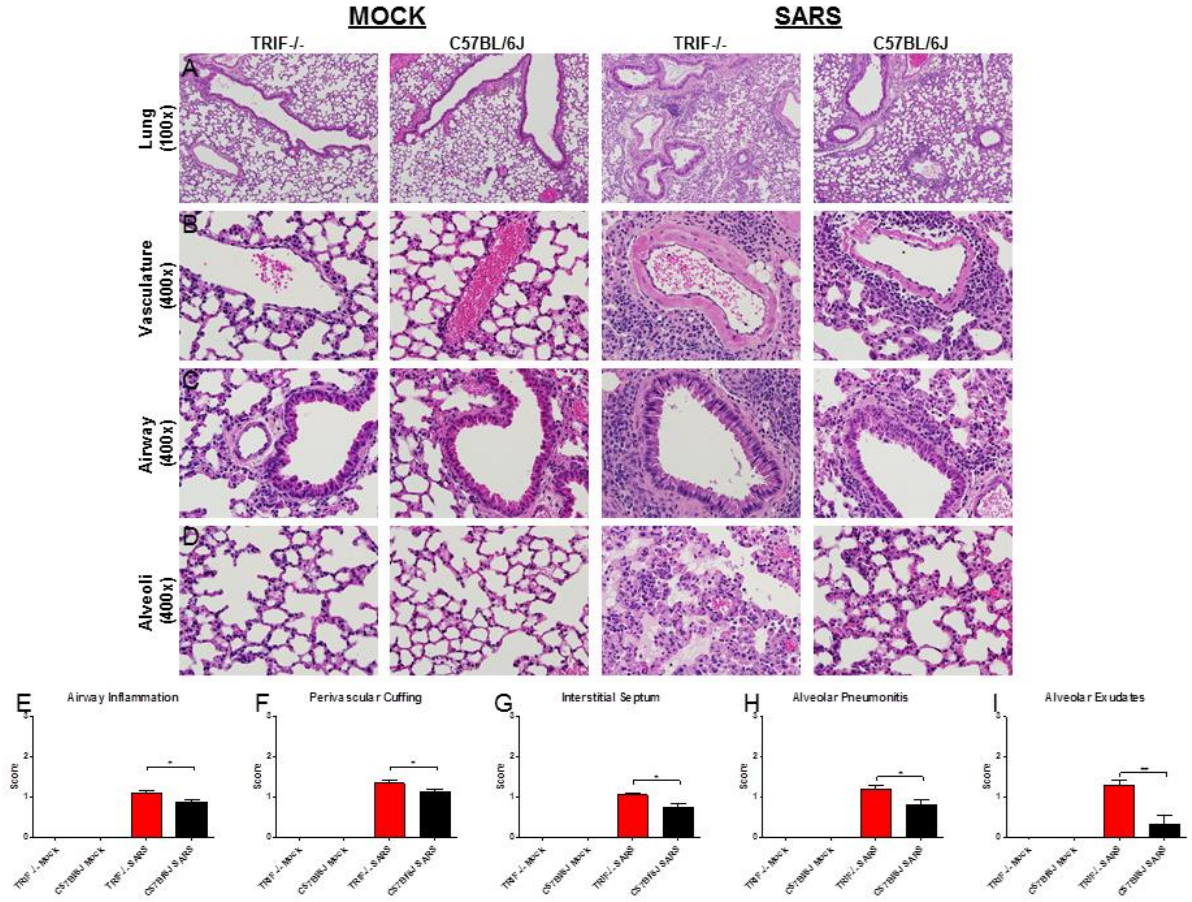

Figure 2.6. Increased Pathology of SARS-CoV in the Lungs of TRIF$^{-/-}$ Mice.

Histopathology analysis of formalin fixed H&E stained lung tissues indicates that while uninfected TRIF$^{-/-}$ mice (first column) and wild type mice (second column) have normal lung architecture, TRIF$^{-/-}$ mice infected with SARS-CoV (3rd column) show increased signs of SARS related pathology compared to wild type mice infected with SARS-CoV (last column) in the overall lung (a), vasculature (b), airways (c), and alveoli (d). Histopathology lung sections from day 6 postinfection were scored for SARS disease signs including airway inflammation (e), perivascular cuffing (f), thickening of the interstitial septa of alveoli (g), alveolar pneumonitis (h), and alveolar exudates (i). Histology sections were scored in a blinded manner, scores were evaluated for significance by unpaired student's *t*-test, *p<0.05, **p<0.01.

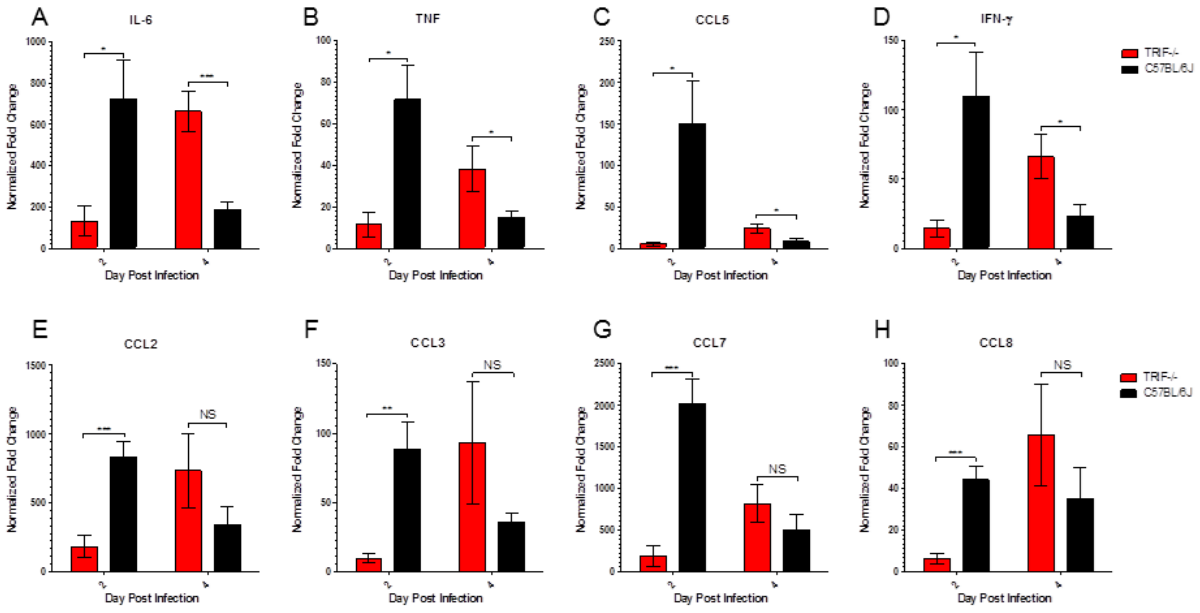

Figure 2.7 Aberrant Proinflammatory Cytokine and Chemokine Signaling in TRIF$^{-/-}$ Mice Infected with SARS-CoV.

RNA expression profiles of cytokines and chemokines downstream of TRIF and TLR signaling programs measured by qPCR analysis of IL-6 (a), TNF (b), CCL5 (c), IFNγ (d), CCL2(e), CCL3 (f), CCL7 (g), and CCL8 (h) from TRIF$^{-/-}$ (red bars) or wild type C57BL/6J (black bars) infected with 10^5 PFU of SARS-CoV normalized to mock TRIF$^{-/-}$ or wild type mice (n=4 mice per group) at day 2 and day 4 postinfection. Significant differences between groups were evaluated by an unpaired student's *t*-test, bar graphs show the mean normalized fold change on the day post infection, the error bars indicate one standard deviation from the mean; *p<0.05, ***p<0.001, NS not significant.

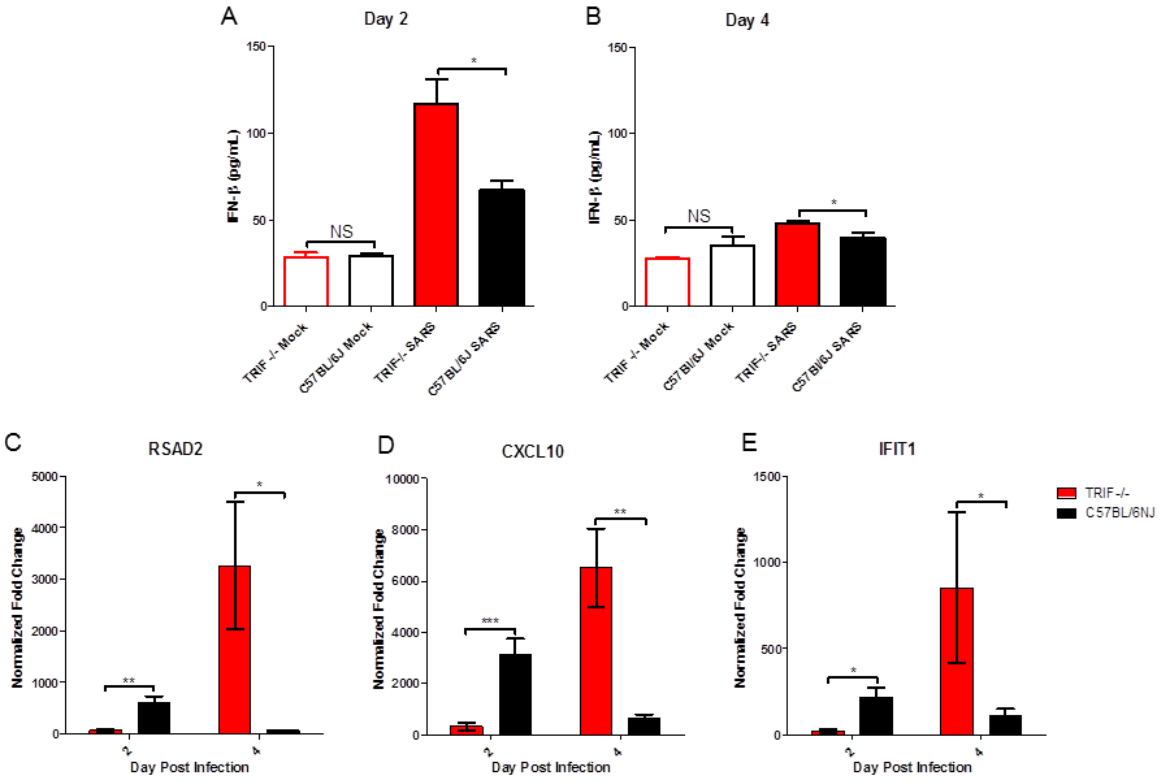

Figure 2.8 Aberrant Interferon and Interferon Stimulated Gene Responses in TRIF$^{-/-}$ Mice Infected with SARS-CoV.

TRIF$^{-/-}$ mice infected with SARS-CoV have significantly higher protein levels of IFNβ measured by ELSIA on day 2 (a) and day 4 (b) postinfection in lung homogenates. A RNA expression profiles of ISGs measured by qPCR analysis of RSAD2 (c), CXCL10 (d), and IFIT1 (e), TRIF$^{-/-}$ (red bars) or wild type C57BL/6J (black bars) infected with 10^5 PFU of SARS-CoV normalized to mock TRIF$^{-/-}$ or wild type mice at day 2 and day 4 postinfection. Significant differences between groups were evaluated by an unpaired student's *t*-test, bar graphs show the mean normalized fold change on the day post infection, the error bars indicate one standard deviation from the mean; *p<0.05, **p<0.01, ***p<0.001, NS not significant.

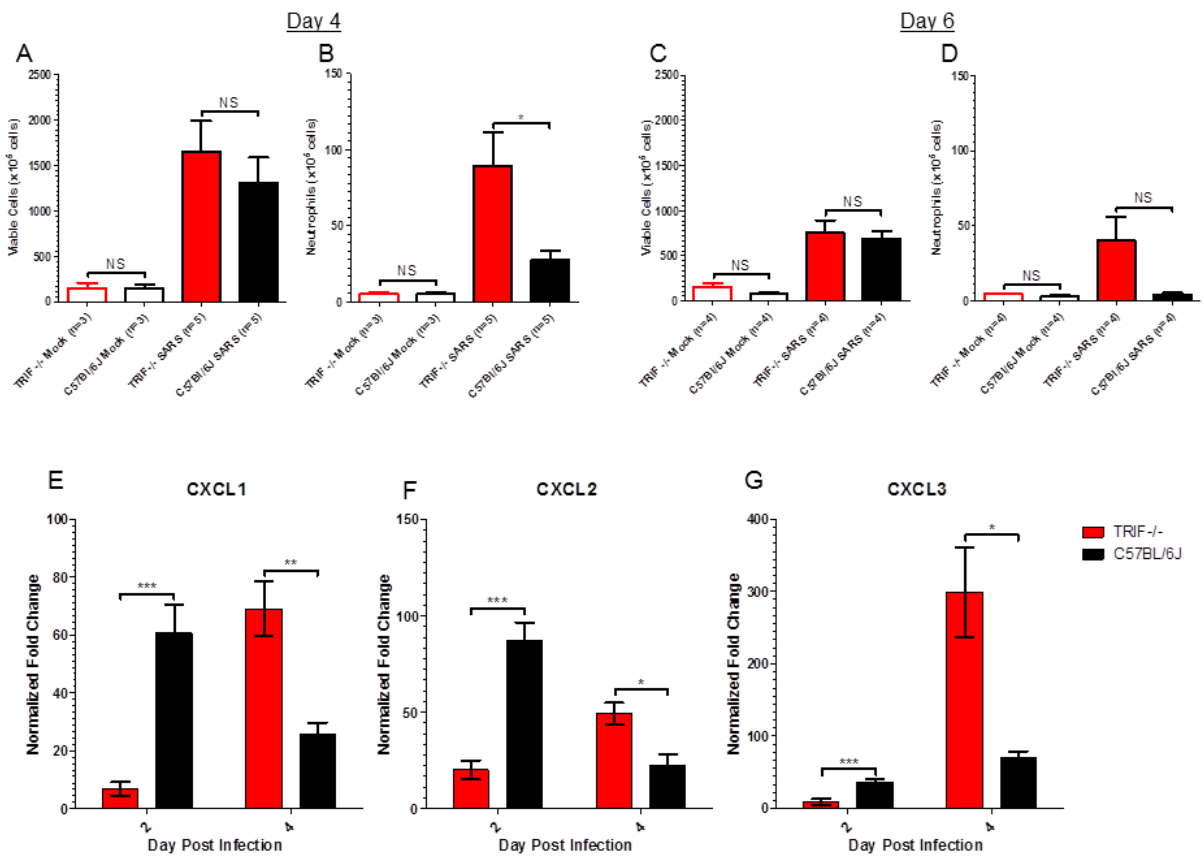

Figure 2.9 Greater Infiltration of Neutrophils into the Lungs of TRIF$^{-/-}$ Mice Infected with SARS-CoV and Aberrant Expression of Neutrophil Attractant Chemokines.

TRIF$^{-/-}$ mice have similar numbers of total infiltrating cells in the lungs on day 4 (a) and day 6 (c) postinfection compared to wild type mice infected with SARS-CoV, but significantly greater number of neutrophils at day 4 postinfection (b) but not significantly different at day 6 postinfection (d). Chemokines that influence neutrophil chemotaxis including CXCL1 (e), CXCL2 (f), and CXCL3 (g) were evaluated on days 2 and 4 postinfection, *p<0.05, **p<0.01, ***p<0.001, NS=not significant as evaluated by unpaired student's t-test.

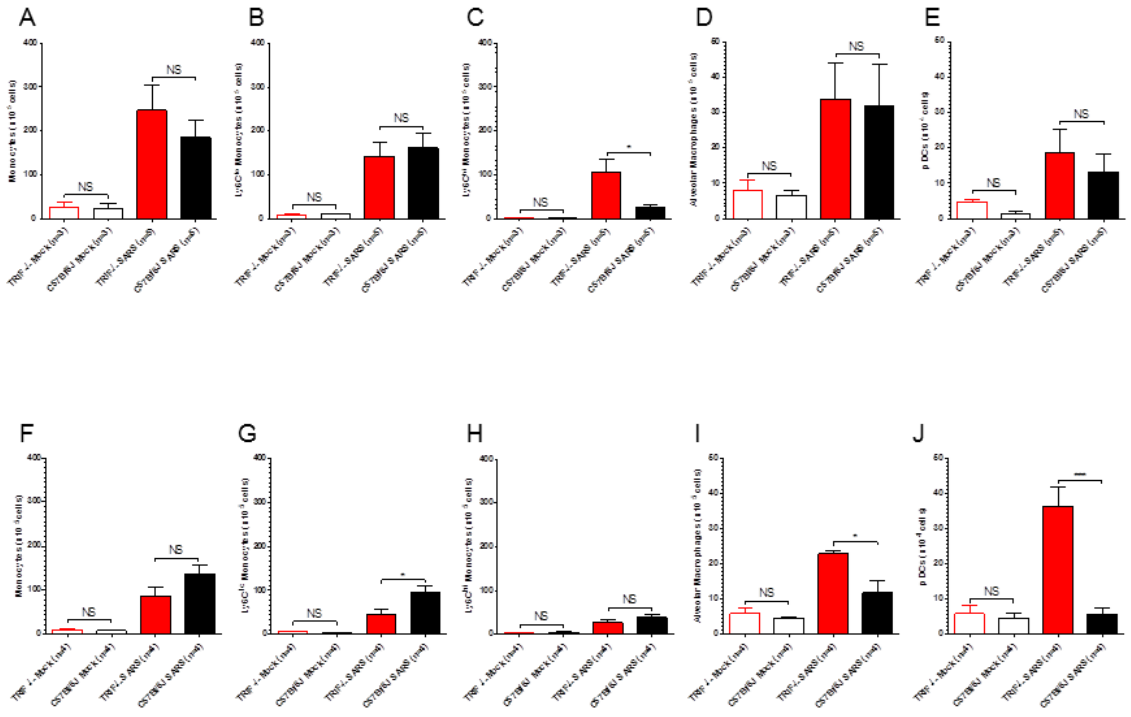

Figure 2.10 Significant Differences in Monocyte Derived Cell Populations in the Lungs of TRIF$^{-/-}$ Mice Infected with SARS-CoV.

At day 4 postinfection (a-e) the numbers of monocyte derived cells populations of total monocytes (a), Ly6C^{low} monocytes (b), Ly6C^{high} monocytes (c), alveolar macrophages (d), and plasmacytoid dendritic cells (e) were measured by flow cytometry in wild type and TRIF$^{-/-}$ mice, where the only statistically significant difference in cell populations measure was more LyC6^{high} monocytes in TRIF$^{-/-}$ mice infected with SARS-CoV compared to wild type mice infected with SARS-CoV. At day 6 postinfection (f-j) the numbers of monocyte derived cells populations of total monocytes (f), Ly6C^{low} monocytes (g), Ly6C^{high} monocytes (h), alveolar macrophages (i), and plasmacytoid dendritic cells (j) were measured by flow cytometry in wild type and TRIF$^{-/-}$ mice. Statistically significant differences in cell populations of LyC6^{low} monocytes, alveolar macrophages, and pDCs were measured in TRIF$^{-/-}$ mice infected with SARS-CoV compared to wild type mice infected with SARS-CoV n day 6 postinfection, but there was no significant

difference in total monocytes or Ly6C^{high} monocytes. Bar graphs are the average number of cells measured in each group with error bars indicating one standard deviation from the mean, statistically significant differences between groups were determine by an unpaired student's *t*-test, *p<0.05, ***p<0.001, and NS not significant.

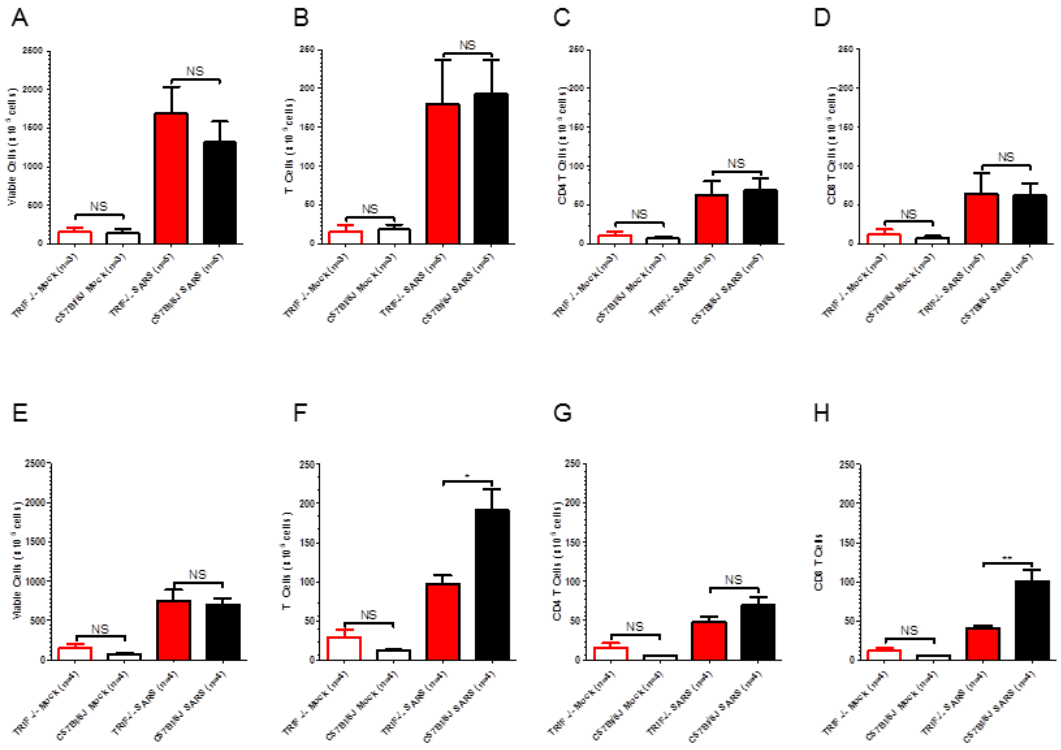

Figure 2.11 Decreased Infiltration of T Lymphocytes in TRIF$^{-/-}$ Mice Infected with SARS-CoV.

At day 4 postinfection (a-d) the numbers of lymphocyte derived cells populations of total lymphocytes (a), T cells (b), CD4^{+} T cells (c), and CD8^{+} T cells (d) were measured by flow cytometry in wild type and TRIF$^{-/-}$ mice, where no statistically significant differences in cell populations measure were observed. At day 6 postinfection (e-h) the numbers of lymphocyte derived cells populations of total lymphocytes (e), T cells (f), CD4^{+} T cells (g), and CD8^{+} T cells (h) were measured by flow cytometry in wild type and TRIF$^{-/-}$ mice. Statistically significant differences in cell populations of T cells and CD8+ T cells were measured in TRIF$^{-/-}$ mice infected with SARS-CoV compared to wild type mice infected with SARS-CoV on day 6 postinfection, but there was no significant difference in total lymphocytes or CD4+ T cells. Bar graphs are the average number of cells measured in each group with error bars indicating one

standard deviation from the mean, statistically significant differences between groups were determine by an unpaired student's *t*-test, *$p<0.05$, **$p<0.01$, and NS=not significant.

CHAPTER 3: TLR4 SIGNALING VIA TRAM/TRIF MEDIATES SARS-COV PATHOGENESIS

INTRODUCTION

Severe Acute Respiratory Syndrome coronavirus (SARS-CoV) and Middle East Respiratory Syndrome coronavirus (MERS-CoV) are highly pathogenic coronaviruses that likely emerged from bat reservoir host species into humans (34, 35, 40). The SARS pandemic of 2002-2004 took an economic toll in excess of $50 billion USD worldwide, indicating that coronavirus epidemics can have significant impact on tourism and the global economy, yet currently no approved coronavirus specific vaccines or antivirals exist to protect against emerging and re-emerging coronavirus threats (6, 190). The current MERS epidemic in the Arabian Peninsula (2012-present) has been accompanied by sporadic cases in Europe and North America in patients following travel to the Middle East, indicating that viral spread outside of the current geographic confines may occur (20, 21, 191). SARS-CoV and MERS-CoV both cause respiratory syndromes that each have high mortality rates, particularly in patients that progress to Acute Respiratory Distress Syndrome (ARDS), the most severe form of acute lung injury (12, 150).

In the most severe cases of MERS-CoV or SARS-CoV infection, patients develop ARDS, a syndrome characterized by severe lung damage that can result from viral infection as well as bacterial and chemical insults to the pulmonary compartment (7, 153, 192). SARS-CoV infections result in an atypical pneumonia with diffuse alveolar damage, with an overall mortality rate of 10%, but more severe disease in aged populations (>65 years) with mortality rates in excess of 50% (11, 193). MERS-CoV infection results in similar symptoms with a

similar predisposition to severe disease in aged populations, but with a higher overall mortality rate of 40% (22, 194). In addition to known coronavirus strains that infect humans, a large reservoir of antigenically distinct coronaviruses with unknown pathogenic potential exists in bat species (33); the emergence of coronaviruses may continue to serve as a factor that destabilizes "at risk" geographic regions where bat and human or livestock habitats overlap, with the threat of global spread. For this reason, development of coronavirus-specific antiviral therapeutics and vaccines that target conserved mechanisms of viral recognition by host species are highly desirable.

Pattern recognition receptors (PRRs) include families of cellular sensors that detect invading pathogens and initiate cellular defense signaling programs. Toll-like receptors (TLRs) are a family of PRRs that recognize bacterial, viral, and fungal pathogen associated molecular patterns (PAMPs) at cellular membrane structures including the plasma membrane and endosomes (75). Many TLRs that are implicated in the sensing of viruses including TLR3, TLR7, TLR8, and TLR9 recognize viral nucleic acid species in endosomes (158, 179). However, TLR2, TLR4, and TLR6 are located at the plasma membrane, and have been implicated in the sensing of viral glycoproteins (87, 91, 195). While the majority of TLRs utilize MyD88 as an adaptor protein to propagate host antiviral signaling cascades, TLR3 and TLR4 can both initiate MyD88-independent signaling programs through the adaptor TRIF (161, 162).

TLR4 is present in bronchial epithelial cells and alveolar cells at basal levels, but TLR4 expression increases upon infiltration of inflammatory cells in response to insults such as viral infections (196, 197). TLR4 is capable of signaling through either MyD88 or TRIF using two sorting adaptors: MAL (for MyD88-dependent signaling) and TRAM (for TRIF-dependent signaling) (198). The TLR4/TRAM/TRIF signaling cascade has been previously implicated in the exacerbation of ARDS caused by influenza virus infections and acid damage models (199).

Controversially, TLR4 has been identified as potentially mediating immunopathogenesis of influenza virus, and TLR4 antagonist Eritoran has been proposed as an immunomodulatory therapeutic for influenza virus infections (165). The role of TLR4 in highly pathogenic coronavirus infections is unclear, but previous studies identified that C3H/HeJ mice (that are naturally deficient in TLR4) are more susceptible to MHV infection than C3H/HeN (with wild type TLR4 signaling capability) (89). Data from a previous study indicated that TLR signaling through the adaptor molecule TRIF is a critical component to the host protective innate immune response to SARS-CoV infection (Chapter 2). Although $TLR3^{-/-}$ mice were more susceptible to SARS-CoV than wild type mice, $TLR3^{-/-}$ mice did not fully recapitulate $TRIF^{-/-}$ mice susceptibility phenotype to SARS-CoV infection measured by weight loss, survival, lung dysfunction, viral titer, or host mRNA signaling responses. Our previous work identified TLR signaling through both TRIF and MyD88 as key components of innate immune protection from lethal SARS-CoV disease in our mouse model, here we present evidence that TLR4 contributes to protective signaling in response to SARS-CoV infection in our mouse model via the sorting adaptor molecule TRAM.

MATERIALS & METHODS

Viruses, cells, and plaque assay.

All studies used a recombinant mouse adapted SARS-CoV-rMA15 virus that was developed by serial passage in the lungs of mice as has been previously described (60, 95). Virus stocks of an infectious clone of rMA15-SARS-CoV were propagated on Vero E6 cells(60). Quantification of virus in viral stocks and the lower left lobe of lungs from rMA-15-SARS-CoV infected mice were performed in Vero E6 cells (169). All experiments in this study using SARS-CoV-rMA15 were performed in a certified biosafety level 3 laboratory, using class II biological safety cabinet. Personal Protective Equipment for work with SARS-CoV-rMA15 included high-

efficiency particulate air (HEPA)-filtered powered air-purifying respirators (PAPRs), Tyvek suits, hoods, aprons, and booties.

Animals.

All animal housing and care were conducted according to University of North Carolina - Chapel Hill (Animal Welfare Assurance #A3410-01) Institutional Animal Care and Use Committee (IACUC) approved protocols. Animals were maintained in HEPA-filtered Sealsafe cages (Techniplast) during experiments with SARS-CoV-rMA15. Age matched female mice were obtained from Jackson labs: C57BL/6J (stock no. 000664) and $TLR4^{-/-}$ (stock no.007227). At ten weeks of age, mice were anesthetized with a mixture of ketamine/xylazine and inoculated intranasally with 50uL of either phosphate buffered saline (PBS) or 10^5 PFU of MA15-SARS-CoV in PBS. Lung tissues from days 2, 4, and 7 postinfection (C57BL/6J and $TLR4^{-/-}$ mice) or days 2, 4, 7, and 10 days postinfection (C57BL/6J and $TRAM^{-/-}$ mice) were collected for downstream analyses by plaque assay, histology and RNA analysis.

Whole body plethysmography.

Lung function was measured by unrestrained whole body plethysmography using IACUC approved protocols as has been previously described (170). Briefly, animals were introduced into randomized individual plethysmography chambers following calibration according to manufacturer protocols (Buxco). After a 30 min acclimation period, data on lung parameters was collected for 5 min measurement period. Data were analyzed by Finepoint software (Buxco) for established metrics of airway hyperresponsiveness and virus infection associated airway obstruction, including Enchanced Pause(P_{ENH}), Midtidal Expiratory Flow (EF_{50}), and Ratio of T_{PEF}:T_E (R_{PEF}). These measures have been defined previously (Chapter 2, Materials & Methods).

Differentially expressed gene identification.

Mouse lung homogenates in TRIzol were analyzed by microarray and full data set are available at Omics-lhv-discovery.wisc.edu in the pathway folder for Systems Virology Data/SARS/SM034. Differentially expressed gene targets were selected from data collected in a study previously described with transcriptomics data banked at NCBI Gene Expression Omnibus #GSE33266 (169). Briefly, this study performed microarray analysis on RNA from lungs of 10 week old female TLR4$^{-/-}$ or C57BL/6J mice infected with 10^5 PFU dose of mouse adapted SARS-CoV to identify differentially expressed genes compared to mock (PBS) inoculated mice. A linear fit model was used to determine differential expression (DE) for each transcript, requiring an absolute $\log_2$(fold change) >1.5 as well as a false discovery rate (FDR) adjusted *p* value of <0.05

RESULTS

Due to the differences in weight loss and survival between TRIF$^{-/-}$ and TLR3$^{-/-}$ mice infected with SARS-CoV in a previous study, we hypothesized that TLR4 may contribute to signaling through TRIF in response to SARS-CoV infection (Figure 3.1). To determine the role of TLR4 in the pathogenesis of SARS-CoV, we infected TLR4$^{-/-}$ mice and wild type C57BL6/J mice intranasally with 10^5 PFU of MA15-SARS-CoV. TLR4$^{-/-}$ mice lost a greater percentage of their starting weight, with statistically significant differences in weight loss compared to wild type mice on day 3-7 post infection, but are recovering from weight loss by 7 days post infection (Figure 3.2a, *p<0.05, ***p<0.001). TLR4$^{-/-}$ mice had significantly higher titers of virus in the lungs than wild type mice infected with SARS-CoV at days 2 (3 fold difference, ***p<0.001) and 4 (4 fold difference, *p<0.05) postinfection, but had cleared the virus by day 7 postinfection, similarly to wild type mice (Figure 3.2b). Notably, although signs of lung hemorrhage are absent in the wild type mice at day 7 postinfection, TLR4$^{-/-}$ mice showed varying degrees of

hemorrhage, but hemorrhage was present in all TLR4$^{-/-}$ mice infected with SARS-CoV (***p<0.001, Figure 3.2c).

TLR4- can signal in either a MyD88-dependent or TRIF-dependent manner via the usage of the sorting adaptor MAL or TRAM respectively. In order to discriminate between the effects of TLR4-MyD88-dependent signaling and TLR4-TRIF-dependent signaling, we infected 10-week female TRAM$^{-/-}$ mice and wild type C57BL6/J mice intranasally with 10^5 PFU of SARS-CoV. TRAM$^{-/-}$ mice retain the ability to signal through TLR4 in a MAL/MyD88-dependent manner, but cannot signal through TLR4 in TRAM/TRIF-dependent manner. TRAM$^{-/-}$ mice infected with SARS-CoV lose more weight than wild type mice (Figure 3.3a, ***p<0.001). TRAM$^{-/-}$ mice infected with SARS-CoV begin to recover from weight loss on day 4 postinfection, but fail to recover from weight loss by 10 days post infection, while wild type mice begin to recover from weight loss on day 4 postinfection and recover from weight loss by day 6 postinfection (Figure 3.3a). TRAM$^{-/-}$ mice have 3 fold higher titers than wild type mice infected with SARS-CoV on day 2 postinfection (**p<0.01) but not day 4 postinfection, and have cleared the virus by day 7 postinfection similarly to wild type mice, despite lack of recovery from weight loss (Figure 3.3b). TRAM$^{-/-}$ mice showed significantly more hemorrhage in their lungs at day 10 postinfection than wild type mice infected with SARS-CoV, which did not show any signs of hemorrhage (Figure 3.3c, ***p<0.001).

Because TLR4$^{-/-}$ mice and TRAM$^{-/-}$ mice infected with SARS-CoV displayed increased signs of disease severity compared to wild type mice, we used whole body plethysmography to determine if TLR4$^{-/-}$ and TRAM$^{-/-}$ mice showed signs of aberrant lung function compared to wild type mice following infection with SARS-CoV. TLR4$^{-/-}$ mice had increased P_{ENH} on day 2 postinfection (**p<0.01) compared to wild type mice (Figure 3.4a). TRAM$^{-/-}$ mice had higher P_{ENH} values on day 1 (**p<0.01) and day 4 (*p<0.05) postinfection, but the peak P_{ENH} value in

TRAM$^{-/-}$ mice infected with SARS-CoV did not differ significantly from wild type mice infected with SARS-CoV (Figure 3.4d). TLR4$^{-/-}$ mice had decreased R_{PEF} compared to wild type mice on days 5 and 6 postinfection (*p<0.05, Figure 3.3b). TRAM$^{-/-}$ mice had a lower R_{PEF} on day 1 postinfection, and on days 4 through 7 postinfection (Figure 3.4e, **p<0.01), while wild type mice infected with SARS-CoV have R_{PEF} values returned to baseline at day 4 postinfection. TLR4$^{-/-}$ mice had increased EF_{50} on day 2 postinfection, with a similar trend towards higher midtidal expiratory flow for the entirety of the infection period, while wild type mice experience a lower peak EF_{50} on day 3 postinfection that returned to baseline values by day 5 postinfection (Figure 3.4c). TRAM$^{-/-}$ mice had significantly higher EF_{50} at days 2 and 3 postinfection **(p<0.01) than wild type mice infected with SARS-CoV, but both wild type and TRAM$^{-/-}$ returned to baseline EF50 values by day 7 postinfection (Figure 3.4f). Similarities between TLR4$^{-/-}$ and TRAM$^{-/-}$ mice infected with SARS-CoV were expected, because disease signs indicated that TLR4, TRAM, and TRIF are involved in the protective signaling to SARS-CoV. However, slight difference exist between lung dysfunction measurements of TLR4$^{-/-}$ and TRAM$^{-/-}$ mice infected with SARS-CoV which may be explained by intact TLR4/MyD88-dependent signaling in TRAM$^{-/-}$ mice that does not exist in TLR4$^{-/-}$ mice infected with SARS-CoV.

Because differences were observed in TLR4$^{-/-}$ mice by weight loss, viral titer, and lung function compared to wild type mice infected with SARS-CoV, host mRNA responses to infection were evaluated by microarray. Cytokine and chemokine responses downstream of the TLR4 adaptors MyD88 and TRIF were evaluated for changes in RNA levels, and differences greater than two fold were considered significantly different between wild type and TLR4$^{-/-}$ mice infected with SARS-CoV on the same day postinfection. No significant differences in IL-6, TNF, CCL5, IFNγ, CCL2, CCL3, CCL7, or CCL8 between TLR4$^{-/-}$ mice and wild type mice infected with SARS-CoV were observed on days 2 or 4 postinfection (Figure 3.5a-h). On day 7

postinfection mRNA responses of CCL5, IFNγ, CCL2, and CCL7 in the TLR4$^{-/-}$ mice were expressed at levels two fold or greater than wild type mice infected with SARS-CoV (Figure 3.5c, 3.5d, 3.5e, 3.5g). Differences in interferons and interferon stimulated genes (ISGs) were also evaluated, as aberrant interferon responses to coronavirus infection has been observed in MERS and SARS patients. No differences were observed in IFNβ RNA levels at days 2 through 7 postinfection between TLR4$^{-/-}$ mice and wild type mice infected with SARS-CoV (Figure 3.6a). However, ISG responses of RSAD2, CXCL10, and IFIT1 in TLR4$^{-/-}$ mice were two fold less than wild type mice infected with SARS-CoV (Figure 3.6b, 3.6c, 3.6d). In addition, on days 4 and day 7 postinfection CXCL10 levels were a greater of two fold different in TLR4$^{-/-}$ mice infected with SARS-CoV compared to wild type mice (Figure 3.6c). Differences in these antiviral signaling programs between TLR4$^{-/-}$ and wild type mice indicates that TLR4 is likely to be involved in recognition of SARS-CoV, with signaling likely mediated by TRAM/TRIF leading to alterations in ISG signaling programs that establish an antiviral state in infected cells.

DISCUSSION

Toll-like Receptors (TLRs) represent an important early detection system for hosts that initiate innate immune signaling programs against invading pathogens. Our study indicates that TLR4 is involved in mediating the pathogenesis of SARS-CoV infection, likely by activating key ISG signaling programs. In the absence of TLR4, significantly less ISG signaling occurs, and significant differences in lung function parameters and higher viral titers were observed compared to wild type mice infected with SARS-CoV. It is likely that TLR4 signaling occurs in a TRIF-dependent manner through the sorting adaptor TRAM, as TRAM$^{-/-}$ mice recapitulate features of increased SARS-CoV pathogenesis similarly to TLR4$^{-/-}$ mice, including increased weight loss, similar alterations in lung parameters, higher viral titers, and exacerbation of some histological features of SARS-CoV disease. The involvement of TRAM signaling indicates that

the adaptor protein TRIF mediates a large part if not all of TLR4 signaling in response to SARS-CoV. However, while we have defined a role for TRIF in protection from lethal SARS-CoV infection in our mouse model (Chapter 2) and previous studies indicate that TLR signaling through MyD88 also mediates protection from lethal SARS-CoV disease additional studies are required to determine the relative contributions of MyD88-dependent and TRIF-dependent signaling downstream of TLR4 sensing of SARS-CoV (95). Host mRNA transcription profiles from $TRAM^{-/-}$ and $MAL^{-/-}$ mice infected with SARS-CoV would provide insight into if the differences in ISG signaling in the absence of TLR4 are dependent on cellular signaling programs via TRIF or MyD88.

The studies presented here and in Chapter 2 indicate that both TLR3 and TLR4 mediate a portion of TRIF-dependent TLR signaling necessary for survival of SARS-CoV in our mouse model. These are among the first observations of the role of individual TLRs in contributing to protection from SARS-CoV disease. Interestingly, the absence of either TLR3 or TLR4 does not lead to lethal SARS-CoV disease similarly to $TRIF^{-/-}$ mice infected with SARS-CoV, likely because absence of signaling via a single TLR may be compensated for by sensing of viral PAMPs by other PRRs. While there are several similarities in the phenotypes of $TLR3^{-/-}$ mice and $TLR4^{-/-}$ mice infected with SARS-CoV compared to wild type mice (increased weight loss followed by recovery, higher viral titers), $TLR3^{-/-}$ mice had few alterations in cytokine, chemokine, or ISG signaling, while $TLR4^{-/-}$ had a diminsihed ISG response compared to wild type mice. These differences in cellular signaling programs suggest that although weight loss and viral titer phenotypes may be similar between $TLR3^{-/-}$ and $TLR4^{-/-}$ mice, that other PRRs may be able to more easily compensate for the loss of TLR3 signaling than TLR4 signaling in the establishment of cellular antiviral signaling programs.

In other models of acute lung injury, TLR4$^{-/-}$ mice and TRIF$^{-/-}$ mice are less susceptible to lung injury mediated by the introduction of acid and IAV into the lung (199). Imai *et al.* observed that oxidized phospholipids, putative PAMPs potentially contributing to acute lung injury by activating TLR4 and signaling through TRIF, were present in ARDS patient samples resulting from infectious diseases like H5N1 IAV and SARS-CoV (199). The findings that TLR4$^{-/-}$ mice are resistant to acute lung injury via IAV and acid models are contrary to our findings here that TLR4$^{-/-}$ mice have significantly more disease resulting from SARS-CoV infection compared to wild type mice. One explanation for these conflicting data is that activation of TLR4 by oxidized phospholipid PAMPs may be detrimental in acid injury and IAV infection mouse models, but in the case of SARS-CoV infection the benefits of TLR4 sensing of PAMPs and subsequent ISG expression by innate immune signaling programs may outweigh the damaging effects of cellular signaling programs resulting from sensing of oxidized phospholipids by TLR4. Additional studies are needed to test the hypothesis that oxidized phospholipids act as PAMPs in SARS-CoV infection models of acute lung injury, or if cellular signaling programs downstream of TLR4 contribute to or prevent coronavirus induced lung injury.

Our data indicate that signaling via TLR4/TRAM/TRIF may be an important regulatory mechanism in protecting the host from SARS-CoV disease. However, this regulatory mechanism does not appear to be common among other respiratory viruses. TLR4 may serve not only as a PRR, but also as an entry co-factor that facilitates infection for a number of different respiratory viruses, including influenza viruses, adenoviruses, paramyxoviruses, and picornaviruses, playing a detrimental role in the host (88). While this viral entry co-factor phenotype has yet to be investigated with coronaviruses, it seems unlikely to be the case due to lower SARS-CoV titers in wild type mice than TLR4$^{-/-}$ mice, indicating that the presence of TLR4 plays a role in control of viral replication of SARS-CoV. Recently, it was shown that TLR4$^{-/-}$ mice are less susceptible

to influenza virus infection and an immunomodulatory approach using a TLR4 antagonist was proposed to have ameliorative properties for the treatment of influenza virus (165). These findings indicate that protective signaling via TLR4/TRAM/TRIF may be a unique feature in the pathogenesis of coronaviruses compared to other respiratory pathogens like influenza viruses, and that different cellular sensors recognize pathogens with similar clinical features and infecting similar cell types.

The emergence of highly pathogenic coronaviruses SARS-CoV and MERS-CoV has led to the discovery of a pool of highly diverse coronaviruses in bats, some of which may be poised to enter human or livestock populations during spillover events (200). Identification of conserved methods of host recognition of coronaviruses may be highly valuable resource for vaccine formulation and antiviral compound development against potentially emergent coronaviruses. Along with our evidence on the recognition of SARS-CoV by TLR4, TLR4 may also be capable of recognizing MHV, an indication of conserved method of identification of multiple coronaviruses by hosts *in vivo* (89). MHV infected C3H/HeJ mice (without functional TLR4) had decreased survival compared to C3H/HeN mice (with wild type TLR4) (89). However, inconsistencies in this model were that while fewer C3H/HeJ mice survived MHV infection compared to C3H/HeN mice, less lung function disruption was observed in C3H/HeJ compared to C3H/HeN mice measured by P_{ENH} and no differences in viral titer were observed in MHV infected C3H/HeJ mice compared to C3HHeN mice (89). In order to determine if TLR4 recognition of coronaviruses is a conserved mechanism of host protection against coronavirus disease, additional studies are needed to determine role of TLR4/TRAM/TRIF signaling in other coronavirus infections, including MERS-CoV and potentially emergent coronaviruses of bats.

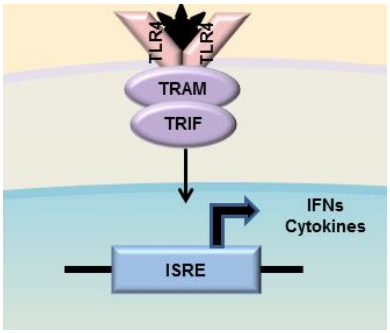

Figure 3.1 TLR4 Signals via TRAM to Utilize the Adaptor Protein TRIF

TLR4 detects pathogen associated molecular patterns (PAMPs) at the plasma membrane; in the sensing of viruses, this is likely to be the viral glycoprotein. Following detection of PAMPs, TLR4 is endocytosed (not shown) and signals from the endosome through the sorting adaptor TRAM to initiate TRIF-dependent signaling. The result of TRIF-dependent signaling via TLR4 is the induction of cytokines, chemokines, and ISGs in cellular signaling programs.

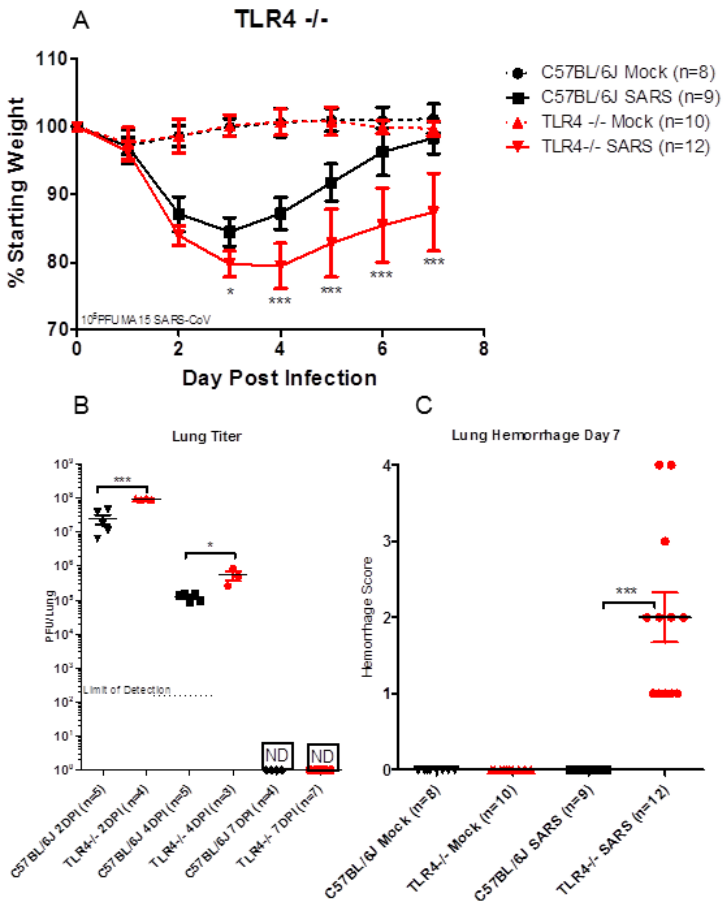

Figure 3.2 TLR4$^{-/-}$ Mice are More Susceptible to SARS-CoV Infection than Wild Type Mice.

TLR4$^{-/-}$ mice and wild type mice were infected intranasally with 10^5 PFU of SARS-CoV. Weight loss was measured each day post infection, and TLR4$^{-/-}$ mice lost significantly more weight compared to wild type mice on days 3-7 postinfection (a, *p<0.05, ***p<0.001 by nonparametric Mann-Whitney Test, values indicate the mean percent starting weight, error bars indicate standard deviation). Virus titer in the lung was measured by plaque assay, TLR4$^{-/-}$ mice had significantly higher virus titers in the lungs at days 2 and 4 postinfection, but had cleared the virus by day 7 postinfection, similarly to wild type mice (b, *p<0.05, ***p<0.001 by unpaired student's t-test, ND not detected by plaque assay). On day 7 postinfection, gross hemorrhage of

the lung was scored at the time of euthanasia, and TLR4$^{-/-}$ mice had varying degrees of hemorrhage in the lungs from mild to moderate, while wild type mice had none (c, ***$p<0.001$ by unpaired student's *t*-test).

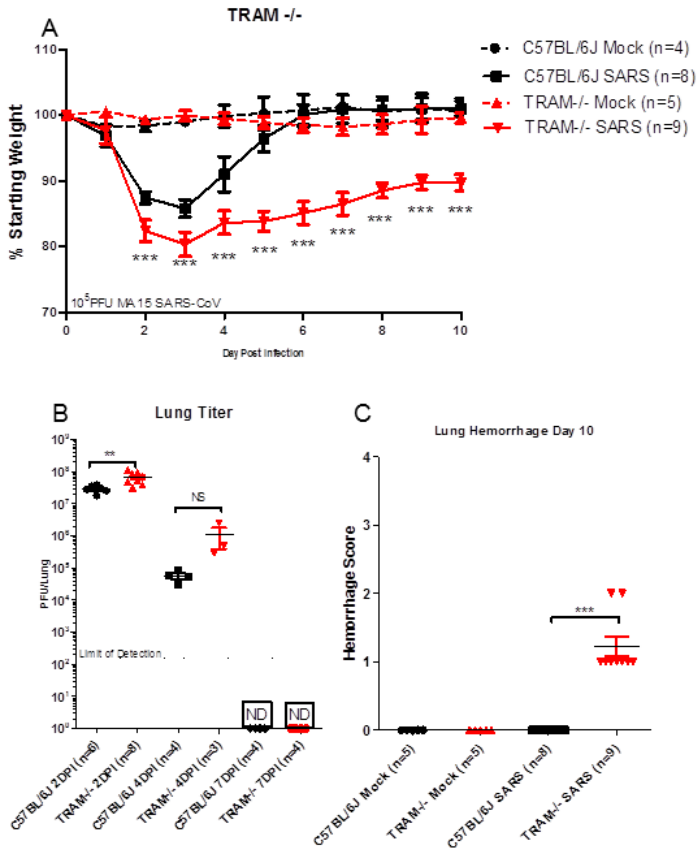

Figure 3.3 TRAM$^{-/-}$ Mice are More Susceptible to SARS-CoV Infection than Wild Type Mice.

Following infection with SARS-CoV, TRAM$^{-/-}$ mice and wild type mice were weighed daily to assess weight loss. TRAM$^{-/-}$ mice lost significantly more weight compared to wild type mice on days 2-10 postinfection (a, ***p<0.001 by nonparametric Mann-Whitney Test, values indicate the mean percent starting weight, error bars indicate standard deviation). TRAM$^{-/-}$ mice had significantly higher virus titers in the lungs at days 2 postinfection as measured by plaque assay, but differences were not significant at day 4 postinfection, and TRAM$^{-/-}$ mice and wild type mice both had no detectable virus in the lungs by day 7 postinfection (b, *p<0.05, NS not significant by unpaired student's t-test, ND not detected by plaque assay). Gross hemorrhage of

the lung was scored on day 10 postinfection at the time of euthanasia, and TRAM$^{-/-}$ mice had mild, but detectable, hemorrhage in the lungs, while wild type mice had none (c, ***$p<0.001$ by unpaired student's *t*-test).

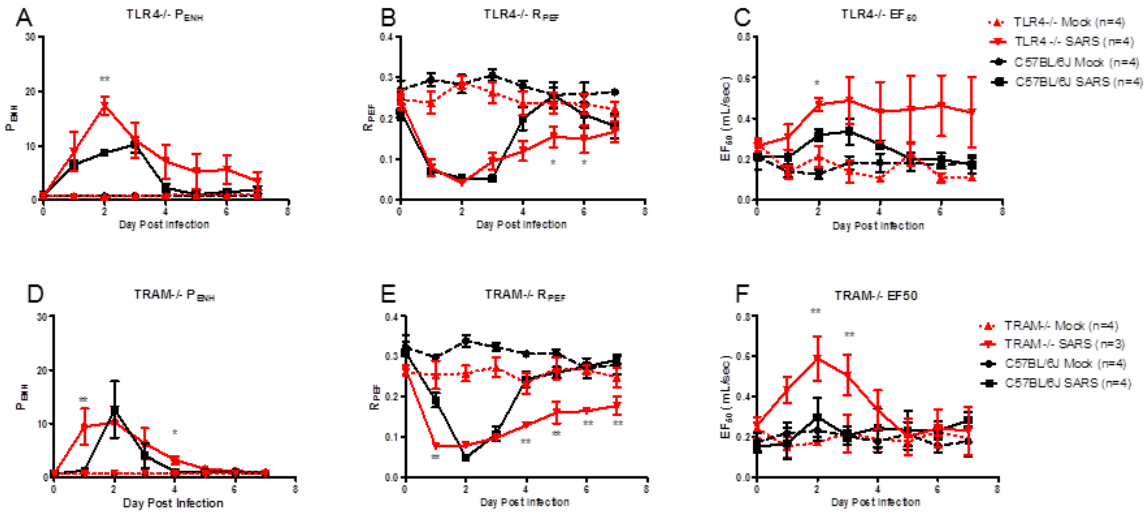

Figure 3.4 TLR4$^{-/-}$ mice and TRAM$^{-/-}$ mice have Similar Lung Dysfunction in Response to SARS-CoV Infection.

Following SARS-CoV infection, the lung function parameters of TLR4$^{-/-}$ mice (a-c) and TRAM$^{-/-}$ mice (d-f) were measured daily along with wild type mice and mock inoculated controls. Differences from wild type mice infected with SARS-CoV by the lung parameters of P_{ENH} (a, d,), R_{PEF} (b, e), and EF_{50} (c, f) were observed in TLR4$^{-/-}$ mice and TRAM$^{-/-}$ mice infected with SARS-CoV, but not mock inoculated controls. (*$p<0.05$, **$p<0.01$ by unpaired student's *t*-test)

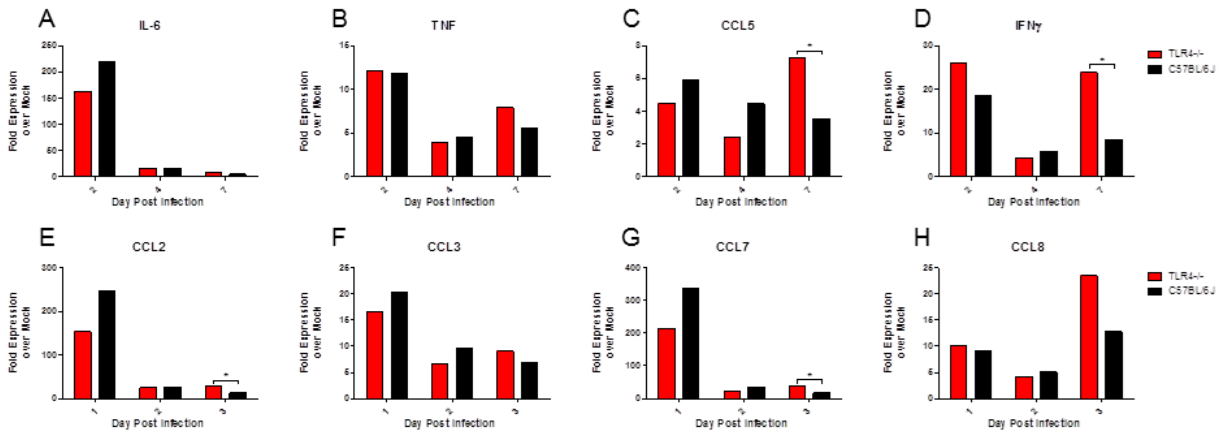

Figure 3.5. TLR4$^{-/-}$ mice have similar Cytokine and Chemokine host RNA responses to SARS-CoV Infection as Wild Type Mice.

Host mRNA responses of TLR4$^{-/-}$ mice and wild type mice were measured by microarray and normalized to mock inoculated controls. Few differences were observed in cytokine and chemokine responses downstream of TLR signaling that were evaluated, including IL-6 (a), TNF (b), CCL5 (c), IFNγ (d), CCL2 (e), CCL3 (f), CCL7 (g), and CCL8 (h). *Indicates genes with >1.5log$_2$(FoldChange) in expression between TLR4$^{-/-}$ and wild type controls.

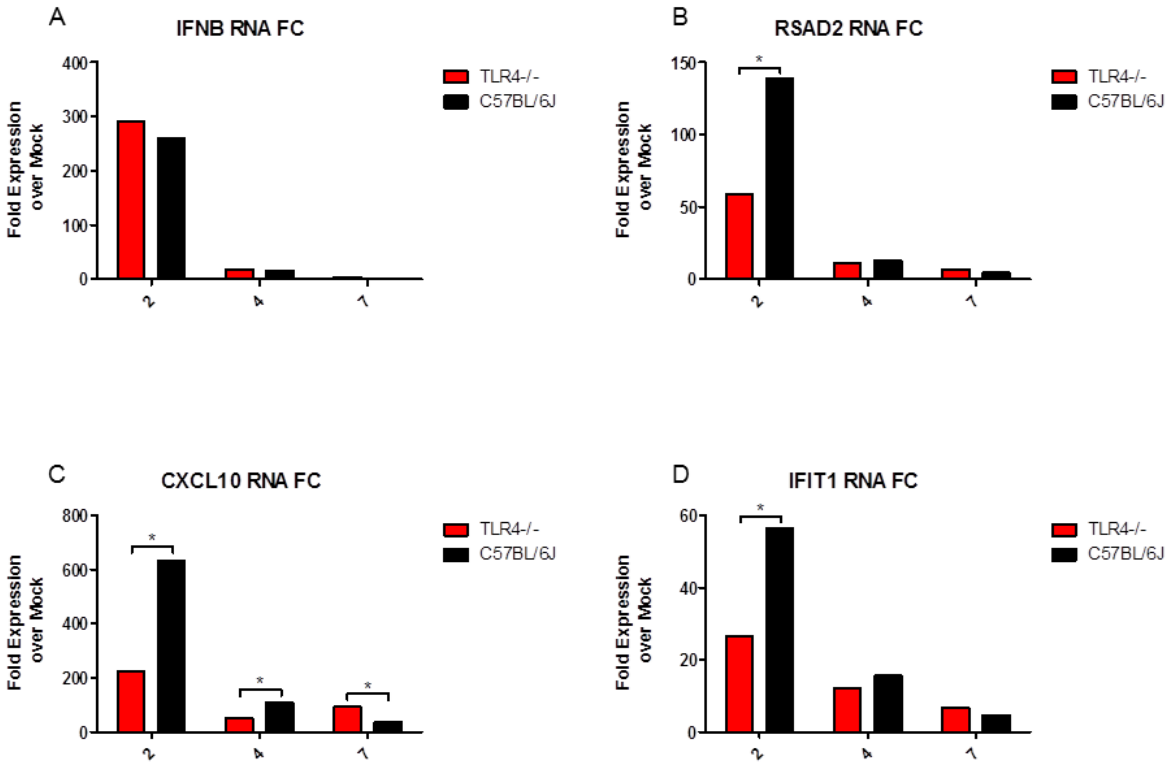

Figure 3.6 TLR4$^{-/-}$ Mice have a Deficient ISG Response to SARS-CoV Infection.

Host mRNA responses of TLR4$^{-/-}$ mice and wild type mice were measured by microarray and normalized to mock inoculated controls. No difference was observed in IFNβ (a) expression between TLR4$^{-/-}$ and wild type mice infected with SARS-CoV. However, differences in ISG expression including RSAD2 (b), CXCL10 (c), and IFIT1 (d) were observed on day 2 postinfection, with diminished ISG responses in TLR4$^{-/-}$ mice compared to wild type mice infected with SARS-CoV.*Indicates genes with >1.5log$_2$(FoldChange) in expression between TLR4$^{-/-}$ and wild type controls.

CHAPTER 4: SARS CORONAVIRUS NONSTRUCTURAL PROTEIN 7 ANTAGONIZES RIG-I INDUCED TYPE I INTERFERON SIGNALING[3]

INTRODUCTION

In late 2002 a respiratory syndrome characterized by atypical pneumonia emerged from the Guangdong Province in China, spreading from Southeast Asia to countries throughout the world (201). Severe Acute Respiratory Syndrome (SARS) infection was confirmed in 8096 patients by the end of the global outbreak in 2003, with 774 deaths resulting from the disease yielding an overall mortality rate of 9.6%; yet mortality rates in patients over the age of 65 were in excess of 50%, indicating that advanced age was a major risk factor for increased susceptibility to SARS disease (5, 202). A novel virus of the family *Coronaviridae,* SARS coronavirus (SARS-CoV) was determined to be the causative agent of the SARS outbreak (1, 2, 203). During the pandemic SARS initially presented as atypical pneumonia, but in the most severe cases could progress to Acute Respiratory Distress Syndrome (ARDS) characterized by diffuse alveolar damage (8, 11, 204). Despite attempts to treat SARS patients with antivirals such as ribavirin and interferon, none of the courses of therapy were proven to be efficacious against SARS-CoV infection (6). While the virus was eventually controlled by public health measures to limit viral spread, efforts to generate a vaccine against SARS-CoV have been fettered by the challenges of vaccine induced immunopathology and lack of protection against heterologous SARS-CoV variants, particularly in the elderly (65, 152). The emergence of Middle East Respiratory Syndrome coronavirus (MERS-CoV) in 2012, a novel coronavirus that has

infected more than 900 people with a high case fatality rate of approximately 40%, exposed potential public health vulnerabilities due to a lack of therapeutic strategies against highly pathogenic coronavirus infections (24, 150).

The hypothesis that highly pathogenic coronaviruses likely emerged by zoonotic transmission from bats, either directly to humans or via intermediate animal host species, was prompted by the discovery of bat coronaviruses (BtCoVs) from group 2b (SARS-like) including the highly similar BtCoV-HKU3, BtCoV-WIV1, and BtCoV-RsSHC014 (34-36). Surveillance for coronavirus specific sequences within bat populations has led to the recent discovery of BtCoV sequences on the continents of North America, South America, Europe, Africa, and Asia in 11 of 18 bat families and includes BtCoV-Appalachian Ridge from group 1b as well as BtCoV-HKU4 and BtCoV-HKU5 from group 2c (MERS-like) (reviewed in (200)). Little is known about the pathogenesis of these viruses in reservoir or human hosts or BtCoV potential for cross-species transmission (38, 39). Recent evidence of MERS and MERS-like coronaviruses in bat and camel populations indicates that zoonotic transmission will likely continue to seed future coronavirus emergence events (32, 205). While most bat coronaviruses appear to have enteric tropisms, human coronaviruses (HCoV) like HCoV-NL63 are primarily associated with mild respiratory diseases (common cold symptoms) while SARS-CoV and MERS-CoV infection resulted in more severe disease outcomes like acute lung injury and ARDS in approximately 20-30% of patients (203, 206, 207).

Analysis of immune responses from SARS patients indicates that continued increased expression of proinflammatory innate immune effectors (including cytokines, chemokines, interferons (IFNs), and interferon stimulated genes (ISGs)) past the acute phase of the disease

---

[3] This chapter has been reviewed by a peer-reviewed journal and is in preparation for re-submission as Totura AL, Frieman MB, Heise MT, and RS Baric. *SARS coronavirus nonstructural protein 7 antagonizes RIG-I induced type I interferon signaling.*

was correlated with poor disease outcome (severe SARS or death), while resolution of these same responses was seen in patients recovering from milder cases of SARS (16). This correlation, along with observations that prophylactic administration of IFNs in cell culture, murine, and primate models of SARS-CoV infection protected against viral replication has led to the hypothesis that differences in innate immune signaling, in particular that of IFNs, can contribute to acute coronavirus disease severity (67, 99, 208). Although some coronaviruses are resistant to antiviral effects of IFN treatment in culture, SARS-CoV and MERS-CoV are relatively sensitive to pretreatment of cells with IFN (70, 209-212). Type I IFNs are typically among the earliest components of the antiviral response, and can stimulate transcriptional regimes of ISGs in an autocrine and paracrine manner to protect both infected and uninfected cells (213). Airway epithelial cells, the target cells of SARS-CoV infection, are capable of secreting IFNs and other cytokines and chemokines to recruit immune cells in response to host sensing of viral infection (154). In addition to activating the innate immune response to viral infections, IFNs also prime adaptive immune responses which promote viral clearance.

Initiation of IFN signaling begins by the sensing of viral pathogen associated molecular patterns (PAMPs) by cellular pattern recognition receptors (PRRs). PRRs are localized to points of viral entry and viral replication including the plasma membrane, endosomes, and cytosol to ensure maximal detection of viral motifs. Cytosolic PRRs such as RIG-I and MDA5 detect viral RNAs that differ from cellular mRNAs by motifs such as 5'-ppp RNA, dsRNA, and ssRNA with poly-Uridine motifs (214, 215). Sensing of viral PAMPs by RIG-I or MDA5 results in translocation of the sensor to the mitochondria, where two N-terminal caspase activation and recruitment domains (CARDs) interact with CARDs of the adaptor molecule MAVS. MAVS transduces the signal through complexes of kinases including TBK1/IKKε and IKKα/IKKβ/IKKγ that phosphorylate the transcription factors IRF3 and IRF7, leading to the

formation of homodimers and heterodimers that enter the nucleus to begin transcription of type I IFNs including IFNα and IFNβ (216). While it has not been reported that RIG-I or MDA5 detect SARS-CoV RNAs during infection, RIG-I and MDA5 are capable of detecting MHV infection of oligodendrocytes and macrophages, indicating that coronaviruses with similar replication strategies are sensed by these pathways, and that IFNs are induced in response to viral RNA detection (81, 217).

To counteract innate immune recognition and establish viral replication, many pathogenic respiratory viruses encode antagonists of type I IFN signaling including Influenza A virus, respiratory syncytial virus, and SARS-CoV. Within the family *Coronaviridae*, coronaviruses MHV, TGEV, HCoV-NL63, and SARS-CoV encode proteins that block IFN induction by these signaling pathways (130, 218-222). SARS-CoV encodes eight proteins that have been identified as IFN antagonists, including nsp1, PLP, nsp7, nsp15, membrane glycoprotein, nucleocapsid, ORF3b, and ORF6 (104, 116, 131). Included in the list of IFN antagonists of SARS-CoV are nonstructural, structural, and accessory proteins. While accessory proteins are generally unique to each virus (or limited to closely related viruses) within the *Coronaviridae*, and structural proteins produce the antigenic variability between viruses, the sequences and functions of these essential nonstructural proteins are more highly conserved. The nonstructural protein 7 (nsp7) has a conserved function among coronaviruses: acting in concert with nsp8 as a secondary RNA Dependent RNA Polymerase (RdRp) and perhaps to function as an RNA processivity factor (145, 223). While nsp7 has been previously shown to be a stabilizing platform for the nsp7/nsp8 polymerase and processivity functions, here we present evidence that SARS-CoV nsp7 as well as the nsp7 from other mammalian coronaviruses acts as an IFN antagonist on the antiviral sensor RIG-I.

MATERIALS & METHODS

Cell Culture and Plasmids.

HEK293T cells (ATCC #CRL11268) were used for Luciferase Assay and Coimmunoprecipitation studies. 293T cells were cultured in Dulbecco's minimal essential medium (CellGro) with the addition of 10% FBS (Sigma), 1% L-glutamine (CellGro), and 1% penicillin/streptomycin (Sigma). Plasmids containing the IFNβ promoter with firefly luciferase reporter gene, FLAG-tagged RIG-I, FLAG-tagged NRIG, FLAG-tagged MAVS, MDA5, IKKe, and IRF3 have been described previously (116).

Cloning of Coronavirus nsp7 Plasmids.

SARS-CoV nsp7 and nsp9 (GenBank Accession AY27841), MHV nsp7 (GenBank Accession AY910861), and NL63 nsp7 (GenBank Accession FJ211861) were synthesized by amplification from full length infectious clone cDNA. Primers for SARS- CoV nsp7 (F:*5'*GAATTCACCatgtctaaaatgtctgacgtaaag*3'*, R: *5'*CCCGGGctgaagagtagcacggttatcgagc*3'*); SARS-CoV $nsp7_{1-42}$ (F: *5'*GAATTCACCatgtctaaaatgtctgacgtaaag*3'*, R: *5'*CCCGGGtgcaagaagaatatcattgtggagttg*3'*); SARS-COV $nsp7_{43-67}$ (*5'*GAATTCACCatgaaagacacaactgaagctttcg*3'*, R: *5'*CCCGGGgtctacagcaccctgcatggatagcaaaac*3'*); SARS-CoV $nsp7_{68-83}$ (F: *5'*GAATTCACCatgattaataggttgtgcgagg*3'*, R: *5'*CCCGGGctgaagagtagcacggttatcgagc*3'*); SARS-CoV nsp9 (F: *5'*GAATTCACCatgaataatgaactgagtccagtagc*3'*, R: *5'*gatcCCCGGGctgaagacgtactgtagcagctaaactgc3'); MHV nsp7 (F: *5'*GAATTCACCatgtcaagattgacggatgttaaatg*3'*, R: *5'*CCCGGGctgtaaggcttgcaagacagtattgtcg*3'*); NL63 nsp7 (F: *5'*gatcGAATTCACCatgtccaaactgactgatttgaagtg*3'* R: *5'*CCCGGGctgaagggtgctactattatcaaaataag*3'*) were generated to include an ATG start codon

(underlined in primer sequences) and EcoRI/XmaI restriction sites (capital letters in primer sequences) for each coronavirus nsp construct. Expression plasmids were generated using 5' EcoRI and 3' XmaI restriction sites for insertion into pCAGGs/GFP vector. SARS nsp7 alanine scanning mutants (codon replacement GCC), BtCoV-AR nsp7 (GenBank Accession HQ585094), BtCoV-HKU4 nsp7 (GenBank Accession NC_009019), and BtCoV-HKU5 nsp7 (GenBank Accession NC_009020) were synthesized by BioBasic for 5'EcoRI and 3'XmaI insertion into pCAGGS/GFP plasmids similarly as above. All resulting plasmid constructs were sequence verified and expression of tagged coronavirus proteins was verified by western blot analysis.

IFNβ Reporter Luciferase Assays.

As previously described, a luciferase reporter assay was used in 293T cells to analyze IFN expression (116). Briefly, an expression construct containing the luciferase ORF and the IFNβ promoter (IFNβ/luc) and an upstream inducer of IFN such as RIG-I, MDA5, NRIG, MAVS, IKKε, or IRF3 were cotransfected with either a SARS-CoV nsp9 (control) plasmid or the designated CoV nsp7 plasmid. Transfection of 100ng of each plasmid into 48 well plates of 293T cells was performed with the X-tremeGENE DNA transfection reagent as directed by the manufacturer (Roche). GFP expression was observed for verification of transfection efficiency at 24 hours post-transfection, cells were then lysed and assayed for luciferase expression using the Dual-Glo luciferase reagent (Promega) per the manufacturer's instructions using a luminometer. The ratio of experimental induction of luciferase to mock treatment is graphed in each figure, as well as total relative light units (RLU) collected. Polyinosinic-polycytidylic acid (pI:C, Invivogen) stimulation of RIG-I (low molecular weight pI:C ,average size of 0.2-1 kb) or MDA5(high molecular weight pI:C, average size of 1.5-8 kb) was performed by addition of 100ng of pI:C/LyoVec complex to cells 12 hours post-transfection with reporter plasmid system, then allowing 24 hours for pI:C stimulation before cell lysis and luciferase detection.

Protein CoIPs and Western Blot Analysis.

Western blot analysis of all expression constructs generated for this study was performed to ensure expression of tagged proteins. GFP-tagged nsp constructs and FLAG-tagged NRIG constructs were transfected into 293T cells seeded in 12 well plates using X-tremeGENE DNA transfection reagent according to manufacturer protocols (Roche). Twenty-four hours post transfection, cells were lysed with 1%NP-40 lysis buffer (20 mM Tris-HCl (pH 7.5), 150 mM NaCl, 1% NP-40, and protease inhibitor cocktail (Roche)) and following centrifugation at 13,000 rpm for 15 min at 4C the supernatant was collected for further analysis. Western blot analysis was completed using NuPage SDS-PAGE protocols, apparatus, buffers, and gels (all Life Technologies) before transfer to PVDF membranes. Anti-FLAG (mouse and rabbit-Sigma), anti-GFP (rabbit-Clontech, mouse-Sigma), and anti-βactin (mouse-Sigma) antibodies were used for detection of tagged proteins.

For GFP and FLAG immunoprecipitations, protein G Dynabeads (Life Technologies) complexes were formed with either anti-GFP (Clontech) or anti-FLAG (Sigma) antibody for 1 h on a rotating wheel at 4C. After incubation, the bead-antibody complex was washed three times with lysis buffer, blocked with mock 293T lysate for 1 hour at 4C (no transfected proteins), washed three times with lysis buffer before use with immunoprecipitations. Twenty-five microliters of protein G/GFP or proteinG/FLAG beads were used for each immunoprecipitation reaction with five hundred microliters of lysed 293T transfected supernatant rotated overnight (8 hours) at 4°C for gentle mixing. Immunoprecipitations were washed three times with lysis buffer at 4°C. The protein extract-bead mixture was then resuspended in buffer before boiling and immediate western blot analysis or storage at -80C.

RESULTS

SARS-CoV nsp7 Antagonizes IFN Induced by the RIG-I Signaling Pathway

Using Venezuelan equine encephalitis virus replicon particles (VRPs), we have previously demonstrated the SARS-CoV nsp7 expression significantly suppressed IFN induction (116). While the SARS-CoV IFN antagonists nsp1, PLP, ORF6, and nsp15 were capable of completely blocking the induction of IFN detectable by IFN bioassay, SARS-CoV nsp7 exhibited only partially blocked IFN induction and expression under these conditions. Evidence within the literature is unclear as to whether RLR type receptors are capable of sensing SARS-CoV, but dsRNA replication intermediates of coronaviruses had been detected outside of double membrane vesicles where coronavirus replication is thought to occur (224). Because of the robust induction of IFN that normally occurs from the stimulation of RIG-I, we tested the effect of nsp7 on IFN production induced by components of the RIG-I signaling pathway. 293T cells were co-transfected with SARS-CoV nsp7 or SARS-CoV nsp9 along with upstream components of the RIG-I signaling pathway and an IFNβ Luciferase reporter plasmid. SARS-CoV nsp9 was chosen as a negative control because it is expressed equivalently, similarly sized and derived from the same polyprotein precursors, but has not identified as an IFN antagonist by the VRP screen (116). In addition, SARS-CoV nsp9 protein has been identified as having dsDNA and ssRNA binding properties with an essential but not well defined role in viral replication (reviewed in (225)).

Expression of the N-terminal CARD domains of RIG-I (labeled as NRIG) in the absence of the C-terminal regulatory domains results in robust induction of IFNβ as detected by luciferase assay ((226), Figure 4.1a, 4.1e). In support of earlier findings, expression of SARS-CoV nsp9 did not diminish the IFN levels induced by NRIG as detected by luciferase assay. In

the presence of SARS-CoV nsp7, the amount of IFN generated by co-transfection of NRIG is significantly reduced by about 7 fold ($p<0.001$, Figure 4.1a, 4.1e). A similar trend is seen with other components of the RIG-I signaling pathway, including MAVS, IKKε, and IRF3, where nsp7 expression results in significantly less IFN induction as compared to the nsp9 control ($p<0.05$, Figure 4.1b-d, 4.1f-h). Because the most significant effect of SARS-CoV nsp7 on IFN induction by RIG-I signaling occurs in the presence of NRIG (Figure 4.1a, 4.1e; compared to rest of Figure 4.1), we tested whether there was an interaction between NRIG and SARS-CoV nsp7 by coimmunoprecipitation. NRIG protein coimmunoprecipitates with SARS-CoV nsp7 but not SARS-CoV nsp9, indicating the potential for protein-protein interaction between RIG-I and SARS-CoV nsp7 (Figure 4.3a, 4.3b, 4.3c).

RIG-I shares similar non-self nucleic acid sensory functions with MDA5, but the two PRRs signal in response to different RNA ligands within the cell (214). When stimulated with appropriate pI:C ligands (Figure 4.2 legend), RIG-I and MDA5 produce robust amounts of IFN (Figure 4.2a, 4.2b). 293T cells were transfected with RIG-I or MDA5 and either SARS-CoV nsp7 or SARS-CoV nsp9, followed by stimulation with the appropriate pI:C ligand. After pI:C stimulation, SARS-CoV nsp7 showed a similar effect of antagonism of IFN induced by RIG-I, where significantly less IFN was produced in the presence of SARS-CoV nsp7 than in the presence of SARS-CoV nsp9 control ($p<0.01$, Figure 4.2a). Interestingly, there is no statistically significant effect of SARS-CoV nsp7 on MDA5 induction of IFN signaling, indicating a degree of specificity for the antagonist effect of SARS-CoV nsp7 on IFN production induced by RIG-I signaling (Figure 4.2b).

Fine Mapping of nsp7-NRIG Interaction Domains

Previous studies of the SARS-CoV nsp7/nsp8 complex identified separate domains of SARS-CoV nsp7 including 3 N-terminal helices HB1 (residues 1-21), HB2 (residues 30-42),

HB3 (residues 44-63) and a C-terminal helix HCT (residues 70-78) (145). To test the hypothesis that the structural domains of SARS-CoV nsp7 have different effects on IFN antagonism activity, we independently cloned and expressed the unique structural helices of SARS-CoV nsp7 into three domains: SARS-CoV nsp7$_{1-42}$, SARS-CoV nsp7$_{43-67}$, and SARS-CoV nsp7$_{68-83}$ (Figure 4.4a). Because helices HB1 and HB2 contain overlapping sites responsible for surrounding the central channel formed by the nsp7/8 complex, they were expressed as a single construct (145). In contrast to nsp7$_{1-42}$ and nsp7$_{68-83}$, when transfected into cells nsp7$_{43-67}$ did not express protein, indicating that this central part of nsp7 may need to be stabilized by SARS-CoV nsp7$_{43-67}$ and/or SARS-CoV nsp7$_{68-83}$ for expression (Figure 4.4d). By luciferase assay, expression of SARS-CoV nsp7$_{1-42}$ suppressed IFN when induced by NRIG similarly to expression of full length SARS-CoV nsp7 (p<0.005, Figure 4.4b, 4.4c). SARS-CoV nsp7$_{68-83}$ also suppressed IFN induction slightly but significantly (p<0.005), indicating that there may be some limited IFN antagonism activity in the C-terminal portion of the protein. However, by coimmunoprecipitation, SARS-CoV nsp7$_{1-42}$ retains the interaction with NRIG similarly to full length SARS-CoV nsp7, while SARS-CoV nsp7$_{68-83}$ did not coimmunoprecipitate with NRIG under identical conditions, suggesting the that the major antagonism activity is encoded in the N-terminal domains of nsp7 (Figure 4.4d).

Because the IFN antagonism activity in SARS-CoV nsp7 is located in the N-terminal structural domain of the protein, we hypothesized that there are critical amino acid residues within the N-terminal domain of SARS-CoV nsp7 that are responsible for the IFN antagonism activity as measured by luciferase assay and coimmunoprecipitation with NRIG. To test this hypothesis, we generated a panel of SARS-CoV nsp7 mutants, where sets of 5 amino acids across the N-terminal portion of the protein were replaced with alanine amino acid residues (SARS-CoV nsp7$_{Ala1-5}$, SARS-CoV nsp7$_{Ala6-10}$, SARS-CoV nsp7$_{Ala11-15,}$ SARS-CoV nsp7$_{Ala16-20,}$

SARS-CoV nsp7$_{Ala21-25,}$ SARS-CoV nsp7$_{Ala26-30,}$ SARS-CoV nsp7$_{Ala31-35,}$ SARS-CoV nsp7$_{Ala36-40,}$ and SARS-CoV nsp7$_{Ala41-45}$ (Figure 4.5a). SARS-CoV nsp7$_{Ala6-10}$ did not express when transfected into 293T cells, but the expression of all of the other mutants was robust, as confirmed by western blot (Figure 4.5c). SARS-CoV nsp7$_{Ala21-25}$, SARS-CoV nsp7$_{Ala26-30}$, SARS-CoV nsp7$_{Ala31-35}$ SARS-CoV nsp7$_{Ala36-40}$ retain a significant level of IFN antagonism activity as compared with the wild type SARS-CoV nsp7, while the IFN antagonism activity of SARS-CoV nsp7$_{Ala1-5}$, SARS-CoV nsp7$_{Ala11-15}$, SARS-CoV nsp7$_{Ala16-20}$, and SARS-CoV nsp7$_{Ala41-45}$ displayed little if any IFN antagonism activity (Figure 4.5b). In addition, SARS-CoV nsp7$_{Ala1-5}$, SARS-CoV nsp7$_{Ala11-15}$, SARS-CoV nsp7$_{Ala16-20}$ mutants lost the ability of nsp7 to Co-IP with NRIG, suggesting that ablation of the IFN antagonism activity in these mutants is most likely associated with weakened interaction between NRIG and nsp7 (Figure 4.5d). These data suggested that the amino acids in the N-terminal region of the protein play a defining role in the IFN antagonism capability of the protein.

Phylogenetically Distinct Coronavirus nsp7 Proteins Antagonize RIG-I Signaling

Because the N-terminal region of the SARS-CoV nsp7 protein is responsible for the IFN antagonism and is highly conserved between members of the family *Coronaviridae* (Figure 4.6a, 4.7a), we hypothesized that IFN antagonism activity of nsp7 is also conserved between representative phylogenetically distant coronaviruses HCoV-NL63 (coronavirus group 1b), and MHV (coronavirus group 2a) compared to SARS-CoV nsp7 (coronavirus group 2b). Analysis of the amino acid sequence of the homologous proteins of nsp7 from the human coronavirus HCoV-NL63 (coronavirus group 1b), the murine coronavirus MHV (coronavirus group 2a), and SARS-CoV (coronavirus group 2b) showed a high degree of identity in the primary sequence of the protein (Table 4.1), particularly in the N-terminus (Figure 4.6a). Based on these protein sequence analyses we hypothesized that the nsp7 of other coronaviruses may also share similar

IFN antagonist activities. To test this hypothesis by luciferase assay, nsp7 from both MHV and HCoV-NL63 were expressed ectopically and showed a similar level of antagonism of NRIG induced IFN as the nsp7 from SARS-CoV (p>0.005, Figure 4.6b, 4.6c). By coimmunoprecipitation studies, the nsp7 from MHV and NL63 interact directly with NRIG as has been described earlier for the nsp7 from SARS-CoV (Figure 4.6d). These data indicated that the IFN antagonist activity of nsp7 may be a conserved function across the family *Coronaviridae*, even among more distantly related members with differences in host tropism and pathogenic potential.

Bat coronaviruses represent a phylogenetically diverse pool of potentially emergent mammalian viruses with unknown pathogenic potential in human and animal populations. Few studies have investigated the activity of select epidemic precursor viral strains for their ability to antagonize human sensing and signaling programs. Group 2c BtCoVs HKU4 and HKU5 are closely related to the recently emerged MERS-CoV; BtCoV- HKU5 shares complete identity with MERS-CoV in the 20 N-terminal amino acids of nsp7, while BtCoV-HKU4 differs from MERS-CoV by only a single amino acid in this region (Figure 4.7a). High sequence identity exists between homologous BtCoV nsp7 coding sequences and other well-known and characterized coronaviruses like MHV, NL63 and SARS-CoV (Table 4.1, Figure 4.8). To test whether evolutionary adaptations during viral emergence are essential for BtCoV nsp7 mediated IFN antagonism, the nsp7 genes from several precursor strain bat coronaviruses were tested for the ability to antagonize IFN sensing and signaling programs. By luciferase assay, BtCoVs nsp7 antagonized IFN signaling by 2-3 fold, while SARS-CoV nsp7 antagonized IFN signaling by 7 fold, indicating a decreased capacity for BtCoV nsp7 antagonism of IFN signaling programs compared to the epidemic strain SARS-CoV nsp7 (Figure 4.7b-g). However, co-immunoprecipitation assays of the BtCoV nsp7 proteins pulled down the NRIG protein with the

BtCoV nsp7 proteins similarly as described for SARS-CoV nsp7, indicating that there is still an association between RIG-I and BtCoV nsp7 proteins (Figure 4.7h).

DISCUSSION

Coronaviruses are highly endemic in bat species, and it is estimated that each species of bat may harbor several unique coronaviruses, providing a rich pool of antigenically unique and highly divergent precursor strains for cross-species transmission and adaptation to human and other mammalian populations (33). The availability of closely related bat and human emerging coronaviruses, like BtCoV-HKU3, BtCoV-WIV-I, and SARS-CoV or BtCoV-HKU4, BtCoV-HKU5 and MERS-CoV, provides a novel opportunity to evaluate conserved viral antagonism features across distinct species barriers. Coronavirus nsp7 is a highly conserved essential viral replicase protein that associates tightly with nsp8 to mitigate both a primer independent RNA polymerase activity as well as potential functions in polymerase processivity (145, 223). In this study we have presented evidence that nonstructural protein 7 (nsp7) from SARS-CoV and several phylogenetically diverse coronaviruses antagonizes interferon induction via the RIG-I pathway.

Coronaviruses likely replicate in double membrane vesicles (DMVs), and the compartmentalization of replication has several potential functions that would be advantageous to viruses: sequestering viral RNAs for further packaging and shielding of degradation products or replication intermediates from cytoplasmic sensors like RLRs. While dsRNA replication intermediates are found within DMVs at early times postinfection (4 hours), they are also detected in the cytoplasm at later times postinfection (8 hours) where they may be susceptible to host sensing machinery (224). Cellular sensors like IFIT and MDA5 pathways are capable of recognition of unmethylated 2'-O RNA generated by replication of SARS-CoV mutant virus with impaired nsp16 function, indicating that RNA intermediates are localized for detection by

host recognition mechanisms (170). In addition, MHV replication is detected by RIG-I and MDA5 while having similar replication intermediates as other coronaviruses, but also conservation of the nsp7 IFN antagonism described in this study (Figure 4.6, (217)). These data support the idea that CoV replication intermediates are available for cellular sensing programs, and that coronavirus nsp7 IFN antagonism activity may not be capable of completely shielding the virus from host recognition or long term prevention of IFN responses. These observations agree with our data of partial but not complete ablation of IFN responses after overexpression of nsp7 from VRP and plasmid vectors (Figures 4.1, 4.6, 4.7, and (116)).

The RIG-I-like Receptor (RLR) family of sensors recognizes non-self RNAs to initiate cell intrinsic innate immune signaling programs that generate a strong interferon response, culminating in an antiviral state in both infected as well as neighboring cells (214). Viruses with genomes utilizing replication intermediates composed of non-self RNA patterns in the cytoplasm are vulnerable to recognition by RIG-I and MDA5. A common strategy employed by RNA viruses to evade IFN responses is by early expression of nonstructural proteins to directly disable upstream mediators of IFN signaling (reviewed in (227)). The nonstructural protein 7 (nsp7) of coronaviruses specifically antagonizes IFN signaling by RIG-I but not MDA5 (Figure 4.2). Although RIG-I and MDA5 are the most closely related within the RLR family, the N-terminal CARD domains responsible for downstream signaling interactions, shown in our study to be antagonized by SARS-CoV nsp7 (Figure 4.1a, 4.1e, 4.3b, 4.3c), share only 23% amino acid sequence identity in the N-terminal CARD domains, compared to 35% amino acid sequence identity in the C-terminal helicase domains (76). In a similar manner to coronavirus nsp7, nonstructural proteins of other viruses also antagonize the more diverse N-terminal domain of RIG-I: NS2 of RSV binds the N-terminal CARD domains of RIG-I and influenza virus NS1 inhibits ubiquitination of the N-terminal CARD domains of RIG-I (228, 229). Swine and avian

origin influenza NS1 proteins inhibit RIG-I in a similar manner to NS1 of human influenza strains, a similar finding to our observations that BtCoV nsp7 inhibits RIG-I through similar mechanisms to SARS-CoV (Figure 4.7).

The primary targets of SARS-CoV, influenza virus, and RSV are cells within the lung, suggesting the importance of IFN signaling to the protection of the respiratory compartment. It should be noted that mammalian coronaviruses with the nsp7 IFN antagonism function described here may have cellular tropism outside of the respiratory compartment, including the majority of BtCoVs identified by oral or rectal swabs, but that IFN antagonism of RIG-I by BtCoV nsp7 remains conserved. Analyses of the RIG-I protein of bats and humans found that the proteins are 82% identical in amino acid sequence, and that they exhibit similar patterns of tissue expression(230). Bat cells with native bat RIG-I expression are susceptible to IFN induction through RLR stimulation by pI:C indicating intact and functional cytoplasmic PAMP sensing machinery (230).

The family *Coronaviridae* contains the largest positive polarity RNA genomes in nature. Multiple interferon antagonists have been identified in the genomes of several different coronaviruses, including the nonstructural proteins, structural proteins and the highly variable virus specific accessory proteins. SARS-CoV encodes multiple proteins with recognized functions of innate immune antagonism particularly aimed at interferon including nsp1, PLP, nsp7, nsp15, ORF6, membrane glycoprotein, and nucleocapsid proteins. The redundancy of SARS-CoV IFN antagonists that target components of the same or similar antiviral pathways could be related to temporal and spatial differences in interferon stimulated gene expression noted during SARS-CoV and MERS-CoV infection (180). Although coronavirus replication initiates very soon after viral entry into the cell, data on host responses of infected cells suggests aberrations in early IFN and ISG production related to SARS-CoV control of host defense

mechanisms: Yoshikawa *et al.* describe NF-kB mediated host transcription happening earlier (12h post infection) than IRF3/7 mediated transcription (48h post infection) (47). This delay in the timing of early antiviral events may allow SARS-CoV to establish foothold within the lung before immune response is activated. Once activated, response is skewed toward NF-kB inflammatory response with potentially detrimental effects, including a potential for progression to ARDS (180). The conserved nature of the nsp7 control of IFN response and of IFN antagonism in general by members of the coronavirus family suggests that the control of this host response may be necessary and advantageous for coronaviruses during the replication cycle. Accordingly, observation of ISG responses in SARS-CoV and MERS-CoV infected cells shows a delay in the induction of interferon stimulated genes that is not present in cells infected with influenza viruses (180).

The nsp7 IFN antagonism activity described herein appears to be a highly conserved feature of a large number of *Coronaviridae* with a diverse host range, tissue tropism and pathogenecities. While the coronaviruses are very similar within the proteins of the replicase (ORF1ab), they are typically much more diverse within the accessory proteins, which are specific to a particular virus or very closely related viruses. MERS-CoV, BtCoV-HKU4 and BtCoV-HKU5 demonstrate IFN antagonism via induction by RIG-I, IRF3, or TNF via the ORF4b protein, a group specific accessory protein with conserved function between these viruses of group 2c, which are very similar (231). However, SARS-CoV ORF3b IFN antagonism function is not conserved in 2 out of 3 BtCoV strains tested, even though all 3 of the BtCoVs are phylogenetically characterized as group 2b (138). While these accessory proteins are generally not required for viral replication but may play an additional role in pathogenesis, the more conserved functions of nonstructural proteins within ORF1ab are typically necessary for viable virus infection of cells. The nsp1 of SARS-CoV encodes an IFN antagonism function

that is strongest in nsp1 protein from SARS-CoV and the BtCoV most closely related to SARS-CoV from group 2b, while nsp1 from BtCoV from group 2c and group 2d retained IFN antagonism activity, but was less effective than SARS-CoV nsp1 (122). Antagonism of host innate responses by the papain-like protease of several phylogenetically diverse coronaviruses including SARS-CoV, MERS-CoV and HCoV-NL63 is a well conserved function of a coronavirus replicase protein (116, 232, 233). These data suggest that the conservation of antagonism of innate immune responses by replicase proteins including nsp7 may be shared between highly diverse coronaviruses, while IFN antagonism activity in accessory proteins may be limited to very closely related viruses, particularly between BtCoV virus strains.

In coronaviruses, the portion of the viral genome encoding nsp7 through nsp10 is required for viral replication, including not only the nsp7 protein but also the specific order of the individual proteins within the ORF1a polyprotein (234). Deletions in nsp7 of MHV leads to a nonviable virus, which may be due to the role of nsp7 in an nsp7/nsp8 complex in addition to the IFN antagonists functions described in this study. The nsp7/nsp8 conformation has been described as a hexadecameric supercomplex containing a central channel situated for nucleic acid binding (145). The nsp7 basic residues R21 and K32 situated along RNA binding channel in the RdRp and processivity complex are not essential for RNA binding within the complex or IFN antagonism activity (Figure 4.5), and nsp7 has no RNA binding activity in the absence of nsp8 (223). The N terminal helical bundle region of the first 20 amino acids of nsp7 is critically important for IFN antagonism activity (Figures 4.4, 4.5) and also for the hydrophobic core in formation with the supercomplex with nsp8 and Gln19 forms a hydrogen bond with nsp8 (145). Due to the overlap of the residues of importance for both nsp7 interferon antagonism as well as the formation of the nsp7/nsp8 complex, the creation of viable viruses deficient in nsp7 IFN antagonism activity but intact in the essential RdRp function has not proven successful.

Descriptions of the nsp7/nsp8 supercomplex formation have used the analogy of nsp7 being the "mortar" which holds the "bricks" of nsp8 together, and it may be reasonable to speculate that nsp7 performs a similar binding function of sequestering RIG-I protein in prevention of IFN signaling, although additional studies are needed to confirm this characterization. Competition may exist between nsp8 and RIG-I for nsp7 binding.

Following the emergence highly pathogenic coronaviruses in humans of SARS-CoV in 2002 and MERS-CoV in 2012, a reservoir of coronaviruses has been described within bat populations that has only begun to be characterized in terms of pathogenesis and cross-species transmission potential (41). The emergence of SARS-CoV and MERS-CoV in geographically distant regions of Southeast China and the Arabian Peninsula respectively indicates that it may be difficult to predict highly pathogenic coronavirus emergence events based on geographic proximity to previous known outbreaks. Unlike accessory protein antagonism activities that do not appear to be conserved between distantly related viruses, the conserved nsp7 dual functions of nsp7/nsp8 complex formation and IFN antagonism may be essential for cross-species replication efficiencies of BtCoV and other mammalian coronaviruses not previously assessed in models of coronavirus pathogenesis and emergence. The lack of efficacy of generalized antivirals including interferon and ribavirin in ameliorating the SARS-CoV pandemic of 2002-2003, difficulties in generating efficacious coronavirus vaccines, and the increase in size of susceptible aged populations (>65 years) worldwide, particularly within developed and developing nations make discovery of a highly conserved drug target between multiple coronaviruses a priority in terms of protecting against emergent viruses with highly pathogenic potential. The dual functions encoded in the N-terminal 20 amino acids of coronavirus nsp7 proteins during RNA transcription and replication and IFN antagonist activity make it an attractive antiviral target for ameliorating both viral replication and disease outcomes.

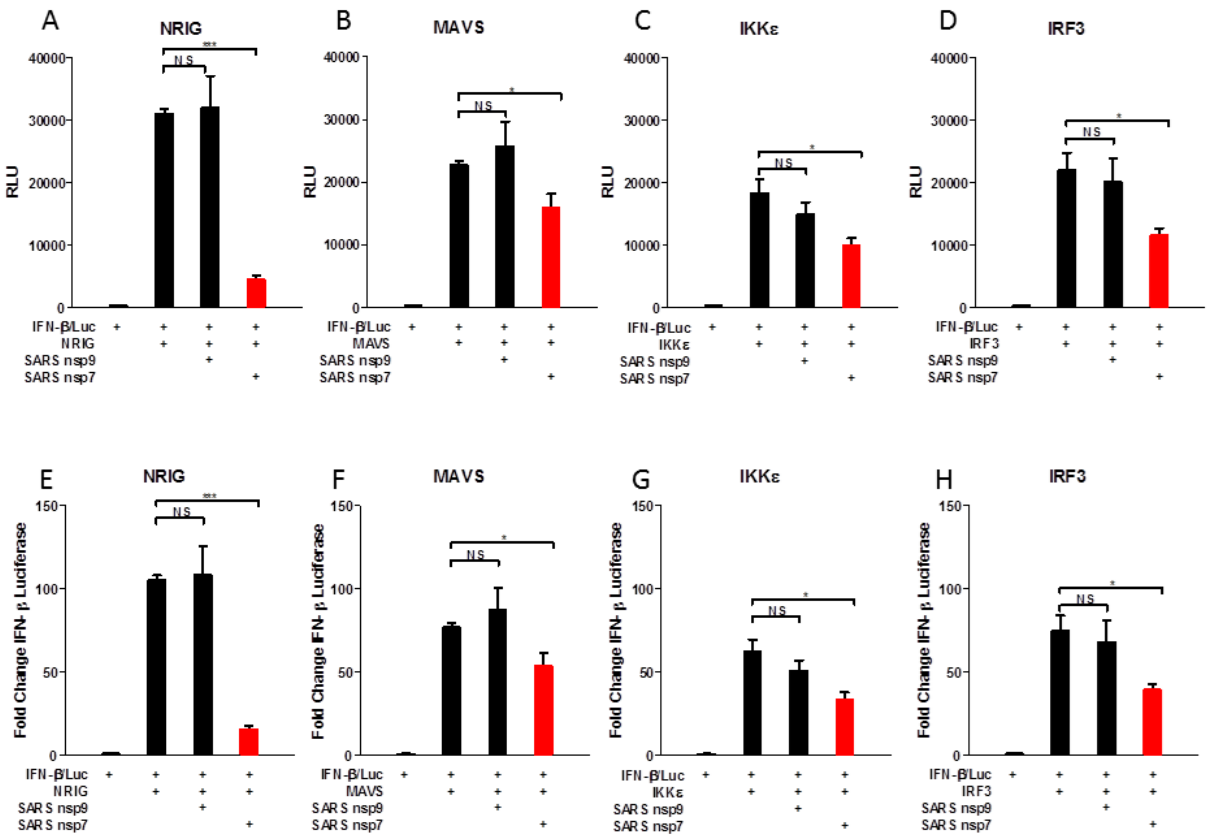

Figure 4.1 SARS-CoV nsp7 Antagonizes IFN Induced by the RIG-I Pathway.

HEK293T cells were transfected with 100ng of IFNβ/luc reporter gene; 100ng of NRIG (constitutively active RIG-I mutant a,e), MAVS (b,f), IKKe (c,e) or IRF3 (d,h); and 100ng of SARS-CoV nsp7 or nsp9. At 24 hours after transfection, cells were lysed and luciferase units were recorded and expressed as either relative light units (RLU, a-d) or fold change compared to IFNβ/luc transfection (e-h). Data shown are a representative experiment completed in triplicate wells. (Error bars indicate one standard deviation from the mean; NS not significant,*p>0.05; ***p>0.001)

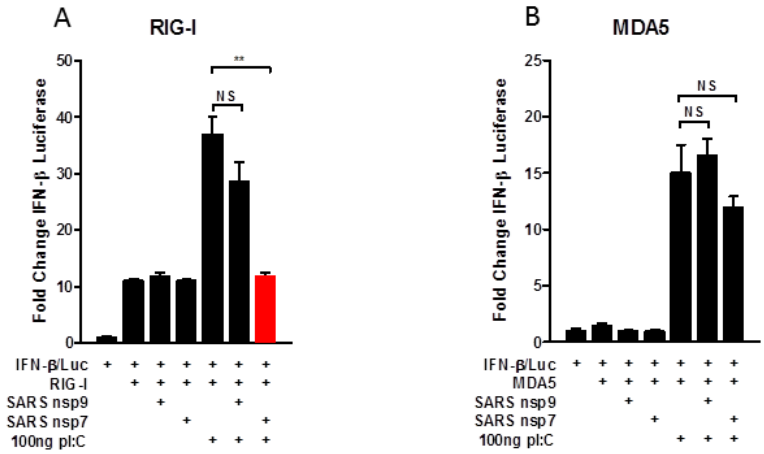

Figure 4.2 SARS-CoV nsp7 Antagonizes IFN Production Induced by pI:C Stimulation of RIG-I, but not pI:C Stimulation of MDA5.

HEK293T cells were transfected with 100ng of IFNβ/luc reporter gene; 100ng of RIG-I (a) or MDA5 (b); and 100ng of SARS-CoV nsp7 or nsp9. At 12 hours post transfection, 100 ng of the appropriate pI:C ligand was lipofected into cultures to stimulate RIG-I (a, low molecular weight pI:C average size of 0.2-1 kb) or MDA5(b, high molecular weight pI:C average size of 1.5-8 kb) induction of IFNβ/luc. At 36 hours after transfection, cells were lysed and luciferase units were recorded and expressed as fold change compared to IFNβ/luc transfection. Data shown are a representative experiment completed in triplicate wells. (Error bars indicate one standard deviation from the mean; NS not significant, **p>0.01)

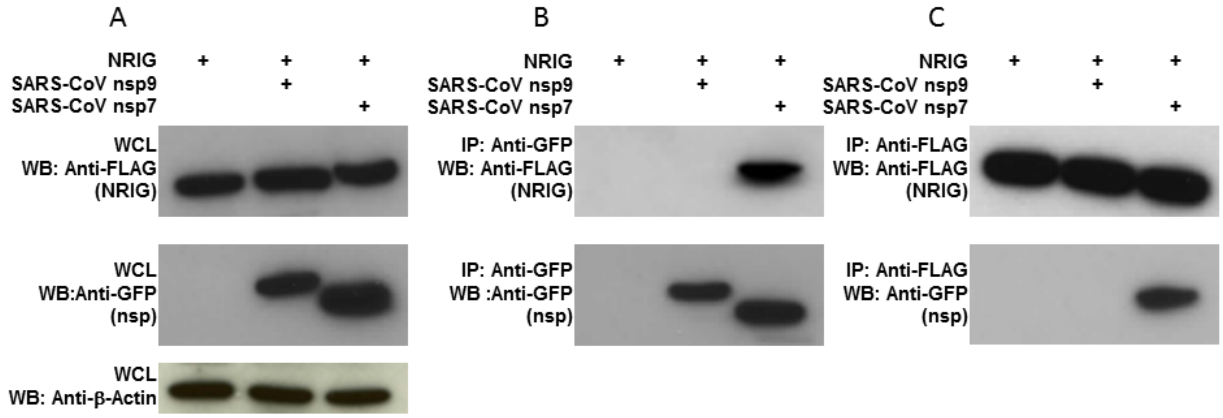

Figure 4.3 The SARS-CoV nsp7 Protein Interacts with NRIG Protein by co-Immunoprecipitation Assay.

HEK293T cells were transfected with 100ng of NRIG (constitutively active RIG-I mutant), and 100ng of SARS-CoV nsp7 or SARS-CoV nsp9. At 24 hours after transfection, cells were lysed and whole cell lysates (a) were assayed by Western Blot for SARS-CoV nsp 7 and nsp9 expression (anti-GFP), NRIG expression (anti-FLAG) and β-actin expression for loading control. Co-immunoprecipitation assays were performed overnight to pull down for either SARS-CoV nsps (IP anti-GFP, panel b) or NRIG (IP anti-FLAG, panel c) and NRIG and SARS-CoV nsp expression was assayed by Western Blot. Data shown are from a representative experiment.

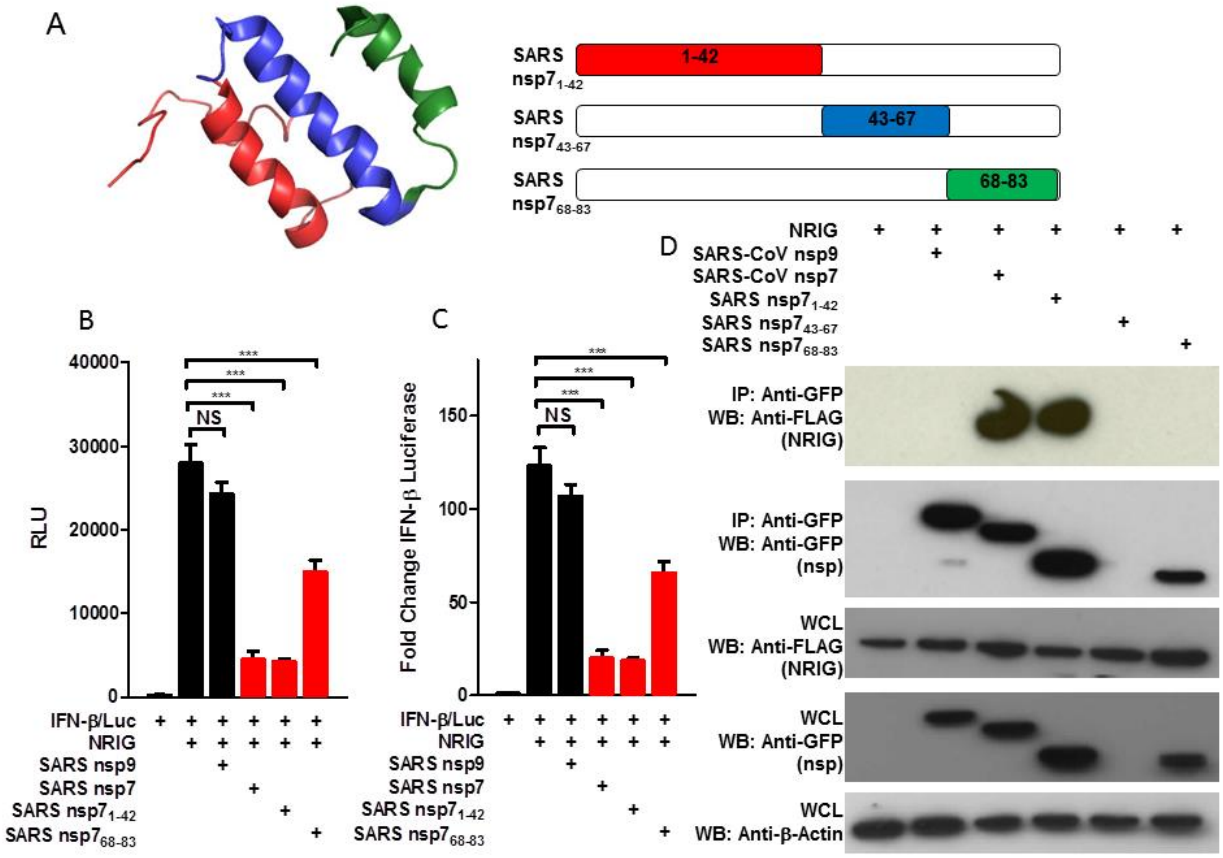

Figure 4.4 The N-terminal Domain of SARS-CoV nsp7 Antagonizes RIG-I Mediated IFN Induction.

Analysis of protein structure of SARS-CoV nsp7 (a) informed the division of the proteins into three domains: SARS-CoV nsp7$_{1-42}$, SARS-CoV nsp7$_{43-67}$, SARS-CoV nsp7$_{68-83}$. HEK293T cells were transfected with 100ng of IFNβ/luc reporter gene; 100ng of NRIG (constitutively active RIG-I mutant); and 100ng of SARS-CoV nsp7, SARS-CoV nsp7$_{1-42}$, SARS-CoV nsp7$_{43-67}$, SARS-CoV nsp7$_{68-83}$ or SARS-CoV nsp9. At 24 hours after transfection, cells were lysed and luciferase units were recorded and expressed as either relative light units (RLU, b) or fold change compared to IFNβ/luc transfection (c). Data shown are a representative experiment completed in triplicate wells. (Error bars indicate one standard deviation from the mean; NS not significant, **p>0.01; ***p>0.001) For co-immunoprecipitation experiments, HEK293T cells were

transfected with 100ng of NRIG and 100ng of SARS-CoV nsp7, SARS-CoV $nsp7_{1-42}$, SARS-CoV $nsp7_{43-67}$, SARS-CoV $nsp7_{68-83}$ or SARS-CoV nsp9. At 24 hours after transfection, cells were lysed and whole cell lysates (d, bottom three rows) were assayed by Western Blot for SARS-CoV nsp expression (anti-GFP), NRIG expression (anti-FLAG) and β-actin expression for loading control. Co-immunoprecipitation assays were performed overnight to pull down for SARS-CoV nsp7, SARS-CoV $nsp7_{1-42}$, SARS-CoV $nsp7_{43-67}$, SARS-CoV $nsp7_{68-83}$ or SARS-CoV nsp9 (IP anti-GFP); NRIG and SARS-CoV nsp expression was assayed by Western Blot (d, top two rows). Data shown are from a representative experiment.

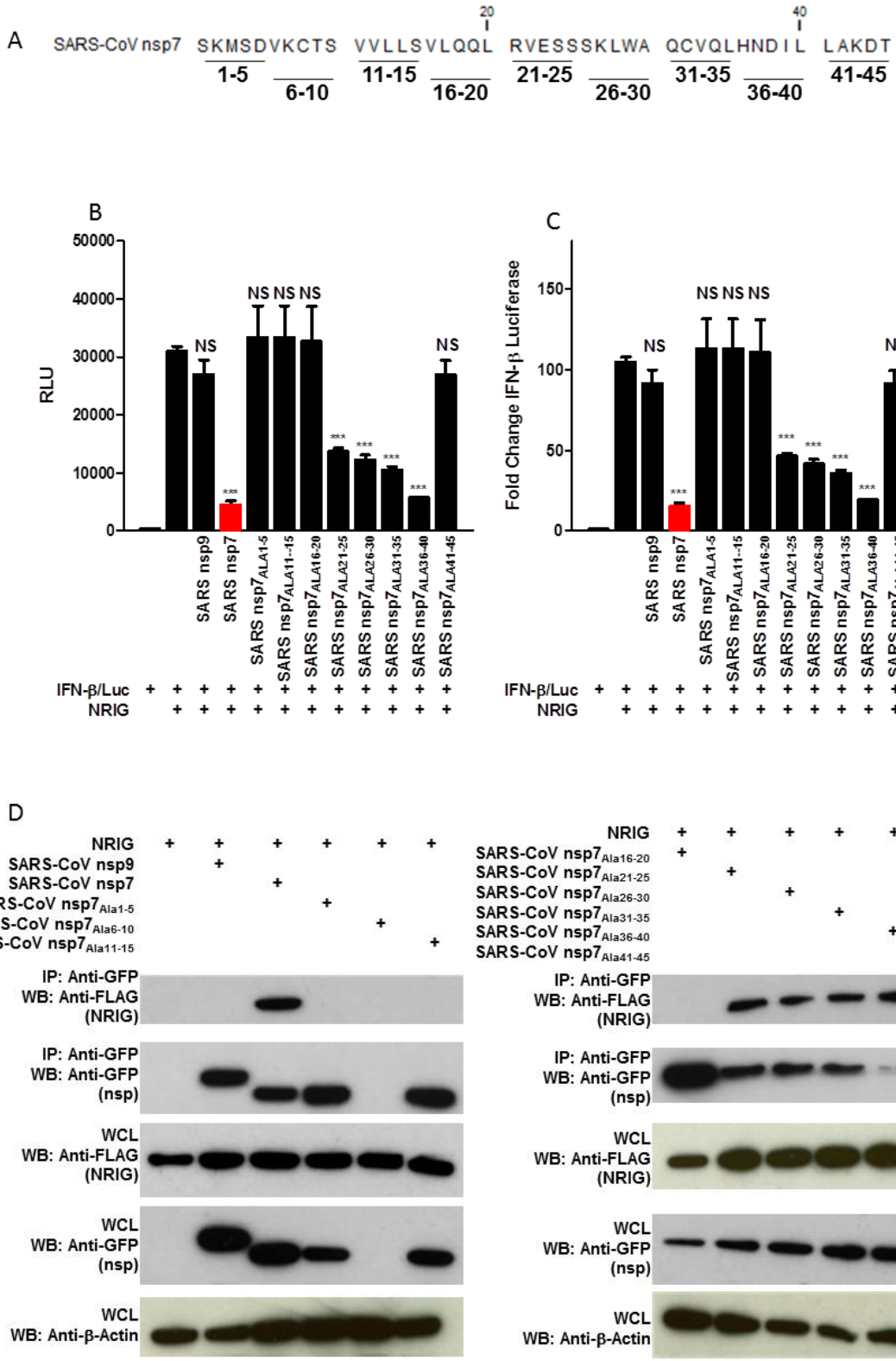
A
SARS-CoV nsp7 SKMSDVKCTS VVLLSVLQQL RVESSSKLWA QCVQLHNDIL LAKDT
20
40
1-5
6-10
11-15
16-20
21-25
26-30
31-35
36-40
41-45
B
RLU
50000
40000
30000
20000
10000
0
NS NS NS
NS
NS
***
SARS nsp9
SARS nsp7
SARS nsp7ALA1-5
SARS nsp7ALA11--15
SARS nsp7ALA16-20
SARS nsp7ALA21-25
SARS nsp7ALA26-30
SARS nsp7ALA31-35
SARS nsp7ALA36-40
SARS nsp7ALA41-45
IFN-β/Luc
NRIG
C
Fold Change IFN-β Luciferase
150
100
50
0
NS NS NS
NS
NS
***
SARS nsp9
SARS nsp7
SARS nsp7ALA1-5
SARS nsp7ALA11--15
SARS nsp7ALA16-20
SARS nsp7ALA21-25
SARS nsp7ALA26-30
SARS nsp7ALA31-35
SARS nsp7ALA36-40
SARS nsp7ALA41-45
IFN-β/Luc
NRIG
D
NRIG
SARS-CoV nsp9
SARS-CoV nsp7
SARS-CoV nsp7Ala1-5
SARS-CoV nsp7Ala6-10
SARS-CoV nsp7Ala11-15
IP: Anti-GFP
WB: Anti-FLAG
(NRIG)
IP: Anti-GFP
WB: Anti-GFP
(nsp)
WCL
WB: Anti-FLAG
(NRIG)
WCL
WB: Anti-GFP
(nsp)
WCL
WB: Anti-β-Actin
NRIG
SARS-CoV nsp7Ala16-20
SARS-CoV nsp7Ala21-25
SARS-CoV nsp7Ala26-30
SARS-CoV nsp7Ala31-35
SARS-CoV nsp7Ala36-40
SARS-CoV nsp7Ala41-45
IP: Anti-GFP
WB: Anti-FLAG
(NRIG)
IP: Anti-GFP
WB: Anti-GFP
(nsp)
WCL
WB: Anti-FLAG
(NRIG)
WCL
WB: Anti-GFP
(nsp)
WCL
WB: Anti-β-Actin

Figure 4.5 Alanine Scanning Across the N-Terminal Domain of SARS-CoV nsp7 Maps the IFN Antagonism Activity to 20 N-Terminal Amino Acid Residues.

Alanine residues were used to replace sets of 5 amino acid blocks across the N-terminus of SARS-CoV nsp7 in the domain previously defined for IFN antagonism activity (a). HEK293T cells were transfected with 100ng of IFNβ/luc reporter gene; 100ng of NRIG (constitutively active RIG-I mutant); and 100ng of SARS-CoV nsp7, SARS-CoV $nsp7_{Ala1-5}$, SARS-CoV $nsp7_{Ala6-10}$, SARS-CoV $nsp7_{Ala11-15,}$ SARS-CoV $nsp7_{Ala16-20,}$ SARS-CoV $nsp7_{Ala21-25,}$ SARS-CoV $nsp7_{Ala26-30,}$ SARS-CoV $nsp7_{Ala31-35,}$ SARS-CoV $nsp7_{Ala36-40,}$ and SARS-CoV $nsp7_{Ala41-45}$ or SARS-CoV nsp9. At 24 hours after transfection, cells were lysed and luciferase units were recorded and expressed as either relative light units (RLU, b) or fold change compared to IFNβ/luc transfection (c). Data shown are a representative experiment completed in triplicate wells. (Error bars indicate one standard deviation from the mean; NS not significant, ***p>0.001) For co-immunoprecipitation experiments, HEK293T cells were transfected with 100ng of NRIG and 100ng of SARS-CoV nsp7 (wild type), SARS-CoV nsp7 alanine scanning mutant, or SARS-CoV nsp9. At 24 hours after transfection, cells were lysed and whole cell lysates (d, bottom three rows) were assayed by Western Blot for SARS-CoV nsp expression (anti-GFP), NRIG expression (anti-FLAG) and β-actin expression for loading control. Co-immunoprecipitation assays were performed overnight to pull down for SARS-CoV nsp7 (wild type), SARS-CoV nsp7 alanine scanning mutant, or SARS-CoV nsp9 (IP anti-GFP); NRIG and SARS-CoV nsp expression was assayed by Western Blot (d, top two rows). Data shown are from a representative experiment.

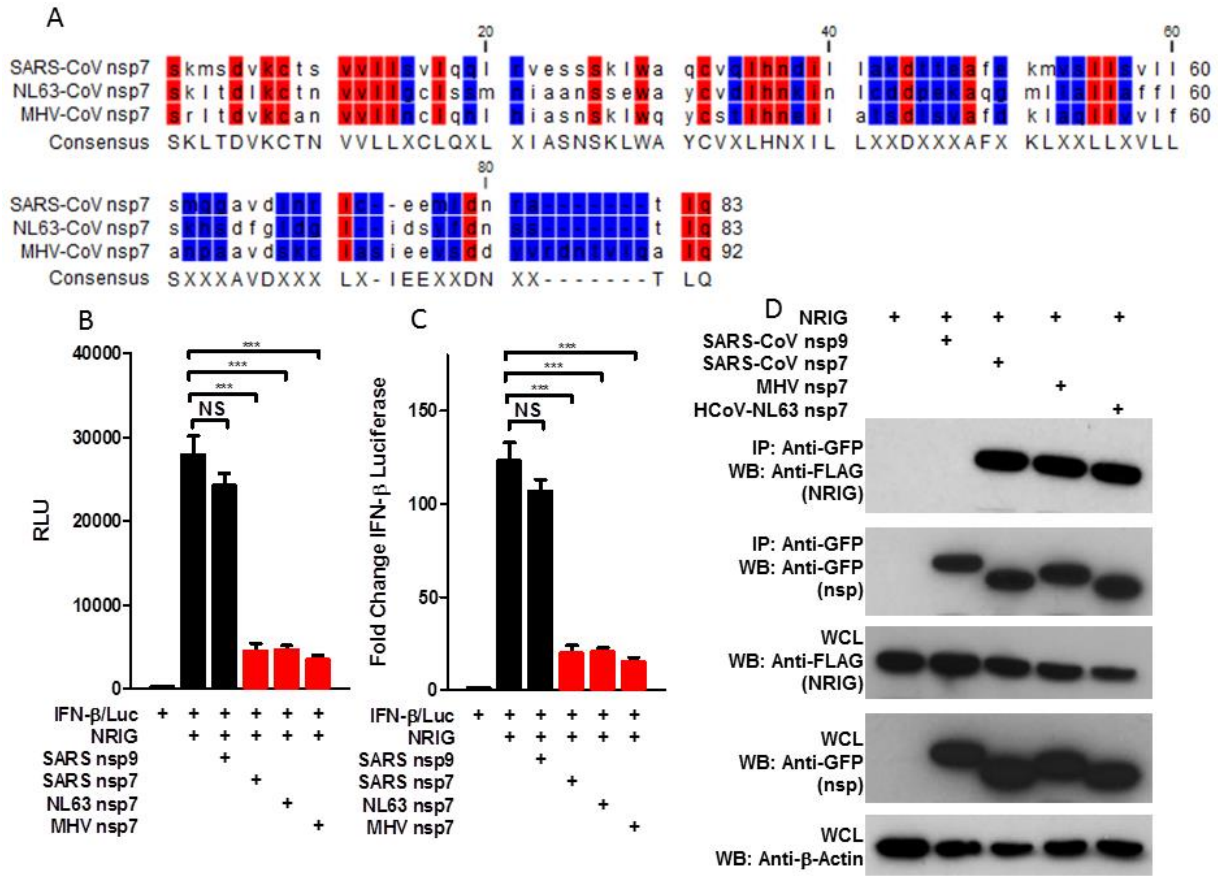

Figure 4.6 Coronaviruses MHV nsp7 and NL63 nsp7 Antagonize RIG-I Mediated Induction of IFN by a Similar Mechanism to SARS-CoV nsp7.

Alignment of nsp7 from coronaviruses SARS-CoV, HCoV-NL63 and MHV shows highly conserved amino acids in the N-terminal region with defined IFN antagonism activity for SARS-CoV nsp7 (a, red color indicates amino acids conserved in all three sequences compared, blue color indicates unique amino acid in each virus). HEK293T cells were transfected with 100ng of IFNβ/luc reporter gene; 100ng of NRIG (constitutively active RIG-I mutant); and 100ng of SARS-CoV nsp7, HCoV-NL63 nsp7, MHV nsp7 or SARS-CoV nsp9. At 24 hours after transfection, cells were lysed and luciferase units were recorded and expressed as either relative light units (RLU, b) or fold change compared to IFNβ/luc transfection (c). Data shown are a representative experiment completed in triplicate wells. (Error bars indicate one standard

deviation from the mean; NS not significant, ***p>0.001) For co-immunoprecipitation experiments, HEK293T cells were transfected with 100ng of NRIG and 100ng of SARS-CoV nsp7, HCoV-NL63 nsp7, MHV nsp7 or SARS-CoV nsp9. At 24 hours after transfection, cells were lysed and whole cell lysates (e, bottom three rows) were assayed by Western Blot for SARS-CoV nsp expression (anti-GFP), NRIG expression (anti-FLAG) and β-actin expression for loading control. Co-immunoprecipitation assays were performed overnight to pull down for SARS-CoV nsp7, HCoV-NL63 nsp7, MHV nsp7 or SARS-CoV nsp9 (IP anti-GFP); NRIG and SARS-CoV nsp expression was assayed by Western Blot (e, top two rows). Data shown are from a representative experiment.

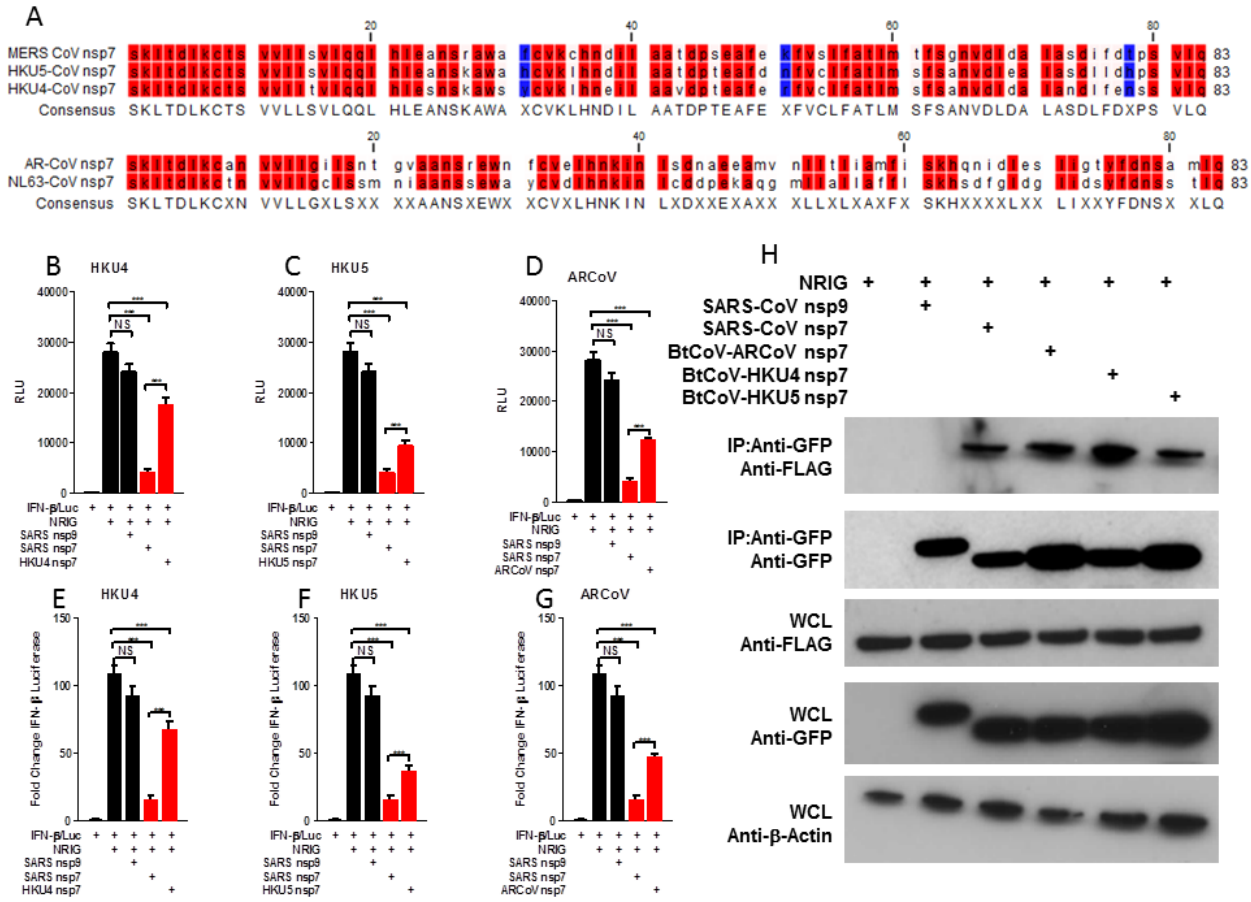

Figure 4.7 BtCoV nsp7 from Epidemic Precursor Viral Strains Antagonize RIG-I Mediated Induction of IFN.

Alignment of nsp7 from coronaviruses MERS-CoV, BtCoV-HKU4, and BtCoV-HKU5, or HCoV-NL63 and BtCoV-AR shows highly conserved amino acids in the N-terminal region with defined IFN antagonism activity for SARS-CoV nsp7 (a, red indicates amino acid conservation in all sequences compared, white indicates differences in 1 sequence, blue indicates unique amino acid residues in all sequences). HEK293T cells were transfected with 100ng of IFNβ/luc reporter gene; 100ng of NRIG (constitutively active RIG-I mutant); and 100ng of SARS-CoV nsp7, BtCoV-HKU4, BtCoV-HKU5, and BtCoV-AR nsp7, or SARS-CoV nsp9. At 24 hours after transfection, cells were lysed and luciferase units were recorded and expressed as either relative light units (RLU, b-d) or fold change compared to IFNβ/luc transfection (e-g).

Data shown are a representative experiment completed in triplicate wells. (Error bars indicate one standard deviation from the mean; NS not significant, ***p>0.001) For co-immunoprecipitation experiments, HEK293T cells were transfected with 100ng of NRIG and 100ng of SARS-CoV nsp7, BtCoV-HKU4, BtCoV-HKU5, and BtCoV-AR nsp7 or SARS-CoV nsp9. At 24 hours after transfection, cells were lysed and whole cell lysates (h, bottom three rows) were assayed by Western Blot for SARS-CoV nsp expression (anti-GFP), NRIG expression (anti-FLAG) and β-actin expression for loading control. Co-immunoprecipitation assays were performed overnight to pull down for SARS-CoV nsp7, BtCoV-HKU4, BtCoV-HKU5, and BtCoV-AR nsp7, or SARS-CoV nsp9 (IP anti-GFP); NRIG and SARS-CoV nsp expression was assayed by Western Blot (e, top two rows). Data shown are from a representative experiment.

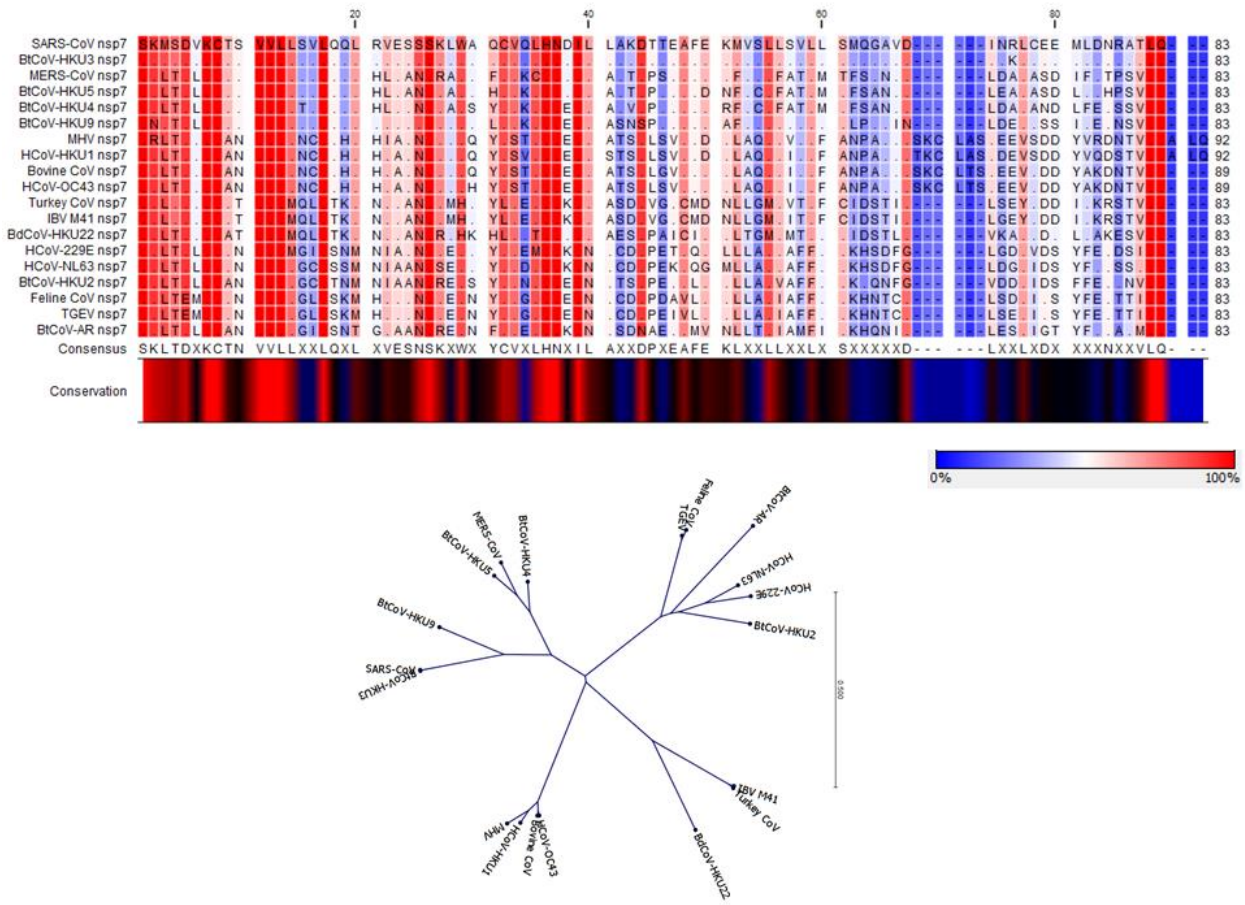

Figure 4.8 Primary Sequence Alignment of Homologous nsp7 Proteins of Coronaviruses

Alignment of coronaviruses from group 2b (SARS-CoV, BtCoV-HKU3), group 2c (MERS-CoV, BtCoV-HKU4, BtCoV-HKU5), group 2d (BtCoV-HKU9), group 2a (MHV, HCoV-HKU1, BCoV, HCoV-OC43), group 3 (TCoV, IBV M41, BtCoV-HKU22), group 1b (HCoV-NL63, HCoV-229E, BtCoV-HKU2, BtCoV-AR), and group 1a (TGEV, FCoV) demonstrates that the conservation of the N-terminus of nsp7 is highly conserved across all genogroups within the *Coronaviridae* (a). A radial dendrogram of amino acid sequence of nsp7 from these viruses sorts them into the standard genogroups (b).

	SARS-CoV	BtCoV-HKU3	MERS-CoV	BtCoV-HKU4	BtCoV-HKU5	HCoV-NL63	BtCoV-AR	CoV-MHV
SARS-CoV	x							
BtCoV-HKU3	99%	x						
MERS-CoV	55%	55%	x					
BtCoV-HKU4	54%	54%	78%	x				
BtCoV-HKU5	57%	57%	84%	83%	x			
HCoV-NL63	40%	40%	45%	47%	45%	x		
BtCoV-AR	37%	37%	43%	43%	45%	63%	x	
CoV-MHV	38%	38%	38%	41%	41%	33%	29%	x

Table 4.1 Primary Sequence Analysis of Homologous nsp7 Proteins of Coronaviruses.

The Clustal Omega tool was used to align the amino acid sequence of nsp7 from coronaviruses SARS-CoV, BtCoV-HKU3, MERS-CoV, BtCoV-HKU4, BtCoV-HKU5, HCoV-NL63, BtCoV-AR, and CoV-MHV. Values are recorded as percent identity between homologous nsp7 proteins of two coronaviruses in the table.

CHAPTER 5: DISCUSSION, SUMMARY, AND FUTURE DIRECTIONS

IMPORTANCE OF THE INNATE IMMUNE RESPONSE TO SARS-COV INFECTION

The innate immune response of the host is the earliest recognition system that discriminates "self" from "non-self" to initiate cell intrinsic signaling programs protective against invading pathogens. Our lab has previously demonstrated that both the timing as well as the content of innate immune responses to highly pathogenic coronavirus infections are important components of host protection or susceptibility to severe disease in models of SARS-CoV and MERS-CoV infection (Chapter 2, Chapter 3,(95, 180)). These findings are in accordance with studies of SARS and MERS patients, where aberrant innate immune responses correlate with severe disease and death from coronavirus infection (16, 23). The recognition of viral pathogen associated molecular patterns (PAMPs) by host pattern recognition receptors (PRRs) is the first step in the regulation of innate immune response to coronavirus infections. In the studies presented here, we identify the importance of PRRs in the antiviral immune response to SARS-CoV, both in the context of host recognition of SARS-CoV infection by Toll-Like Receptors (TLRs, Chapter 2 and Chapter 3) as well as viral antagonism of RIG-I-like Receptor (RLR, Chapter 4) signaling.

SIGNALING THROUGH TLR3 DRIVES A PROTECTIVE HOST RESPONSE TO SARS-COV

Network integration analysis of a systems biology study identified TLR3 and MyD88 as potential key regulators of pathogenesis in the host response to SARS-CoV infection of a mouse model (175). Previous studies demonstrated the susceptibility of MyD88$^{-/-}$ mice to SARS-CoV

infection, indicating that TLR signaling is an important aspect of the protective innate immune response in our animal model (95). Recognition of SARS-CoV by a specific TLR had not been described, nor had the MyD88-independent TLR response to SARS-CoV infection. In Chapter 2, we presented evidence that TLR3$^{-/-}$ mice experienced increased weight loss, viral titer, lung dysfunction, and histological disease signs over the course of infection with SARS-CoV compared to wild type mice. TLR3$^{-/-}$ mice recovered from SARS-CoV infection, albeit more slowly than wild type mice, and the majority of TLR3$^{-/-}$ mice survived SARS-CoV infection. Surprisingly, few effects were observed on the transcription of host proinflammatory response genes downstream of TLR3, including interferons and ISGs, in TLR3$^{-/-}$ mice compared to wild type mice following SARS-CoV infection. These data indicate that although TLR3 may be important for initial recognition of SARS-CoV and control of high viral titers, other pathogen recognition pathways (particularly those that recognize viral dsRNA species such as RIG-I and MDA5) may be able to compensate for innate immune signaling features that provide protection to lethal SARS-CoV infection.

THE TLR ADAPTOR TRIF PROTECTS MICE FROM LETHAL SARS-COV DISEASE

Because TLR3 signals in a MyD88-independent manner through the TLR adaptor TRIF, the effect of SARS-CoV infection on TRIF$^{-/-}$ mice was tested. TRIF$^{-/-}$ mice were much more susceptible to SARS-CoV infection than wild type mice or TLR3$^{-/-}$ mice. TRIF$^{-/-}$ mice showed marked differences in SARS-CoV disease measured by decreased survival, increased weight loss, increased viral titers in the lungs, increased lung pathology, increased lung dysfunction, alterations in infiltrating cell populations, and aberrant cytokine, chemokine, and ISG host responses compared to wild type mice. In a previous study, MyD88$^{-/-}$ mice infected with SARS-CoV had similar phenotypes to TRIF$^{-/-}$ mice in our study with respect to weight loss, survival, viral titers, and lung pathology, but showed few differences in infiltrating cell populations

compared to wild type mice despite diminished cytokine and chemokine signaling programs (95). The contrast between the cellular signaling programs and infiltration of inflammatory cells in mice deficient in either of the two central adaptor proteins for TLR signaling (MyD88 and TRIF) indicates that although each pathway contributes to innate immune protection for survival of SARS-CoV infection, the TLRs recognizing viral PAMPs may be active in different cell types that contribute to the host response to SARS-CoV.

TLR4 SIGNALING VIA TRAM/TRIF IS PROTECTIVE AGAINST SARS-COV INFECTION

TRIF$^{-/-}$ mice are highly susceptible to SARS-CoV infection, indicating the TLRs that signal using TRIF are part of a protective component to the host innate immune response to SARS-CoV infection. TLR3$^{-/-}$ mice only partially replicated the phenotype of TRIF$^{-/-}$ mice, indicating that additional TLRs may be involved in generating TRIF related responses to SARS-CoV infections. Because TLR4 can also signal in a TRIF-dependent manner, TLR4$^{-/-}$ mice were infected with SARS-CoV and evaluated for SARS disease signs, as described in Chapter 3. TLR4$^{-/-}$ mice infected with SARS-CoV had increased weight loss, viral titer, lung dysfunction and lung pathology disease signs compared to wild type mice. TLR4 uses the sorting adaptor TRAM to signal through TRIF in a MyD88-independent manner, so TRAM$^{-/-}$ mice were infected with SARS-CoV to determine TLR4/TRIF-dependent responses to infection. Mice deficient in the sorting adaptor TRAM that were infected with SARS-CoV replicated many aspects of the TLR4$^{-/-}$ phenotype, including increased weight loss, higher viral titers, and alterations in lung function parameters as well as lung pathology compared to wild type mice infected with SARS-CoV. Similarities between the phenotypes of TLR4$^{-/-}$ mice and TRAM$^{-/-}$ mice infected with SARS-CoV suggest that TRIF signaling is partially generated by a TLR4 response to SARS-CoV infection. TLR4$^{-/-}$ mice had few changes in cytokine and chemokine signaling programs in response to SARS-CoV infection compared to wild type mice, but TLR4$^{-/-}$ mice had significantly

lower ISG responses at early times postinfection compared to wild type mice infected with SARS-CoV. Based on these studies we conclude that it is likely that TLR3 and TLR4 each signal through the TLR adaptor protein TRIF in response to SARS-CoV infection and contribute to a protective innate immune response in the host.

FUTURE DIRECTIONS: TOLL-LIKE RECEPTOR STUDIES

Although TRIF$^{-/-}$ and MyD88$^{-/-}$ mice are both highly susceptible to SARS-CoV infection compared to wild type mice, differences were observed in infiltrating cell populations as well as the ISG, cytokine, and chemokine responses of TRIF$^{-/-}$ and MyD88$^{-/-}$ mice infected with SARS-CoV. In TRIF$^{-/-}$ mice, greater numbers of infiltrating cell types including alveolar macrophages, inflammatory Ly6C^{high} monocytes, plasmacytoid dendritic cells, and neutrophils were observed at later times postinfection, while few differences were observed in MyD88$^{-/-}$ mice compared to wild type mice infected with SARS-CoV. In addition, although the number of infiltrating cell populations were not significantly different in MyD88$^{-/-}$ mice compared to wild type mice, MyD88$^{-/-}$ mice did not produce similarly robust amounts of cytokines or chemokines in response to SARS-CoV infection as wild type mice. TRIF$^{-/-}$ mice produced very little ISG, cytokine, or chemokine responses at early times postinfection, but generated more robust amounts of these antiviral effector molecules at later times postinfection. Future studies to evaluate the contributions of these two adaptors of TLR signaling in either hematopoietic or resident lung cells would aid in determining if these signaling program differences arise by the usage of different TLR signaling pathways in cell types of different origin. Previous studies using bacterial pneumonia models had determined that the presence of MyD88 in both hematopoietic and resident lung cells contributed to survival from *Klebsiella pneumonia* infection, while the presence of TRIF in hematopoietic cells but not resident cells contributed to protection against lethal bacterial pneumonia (235). Using a similar approach for SARS-CoV infection of bone

marrow chimeras of TRIF$^{-/-}$ and MyD88$^{-/-}$ mice could determine the importance of TLR signaling by resident lung cells and hematopoietic cells in SARS-CoV survival as well as the relative contributions of these cell types to aberrant cellular signaling programs similar to those in MERS and SARS patients with severe disease.

In Chapter 3, TLR4$^{-/-}$ mice were identified as more susceptible to SARS-CoV infection, and TRAM$^{-/-}$ mice that have no TLR4 signaling through the adaptor molecule TRIF replicated many aspects of the TLR4$^{-/-}$ mouse phenotype compared to wild type mice infected with SARS-CoV. However, TLR4 may also signal through the sorting adaptor protein MAL to initiate MyD88-dependent signaling programs, and studies in MAL$^{-/-}$ mice may identify what role, if any, TLR4/MAL/MyD88-dependent signaling has in SARS-CoV infection. Microarray studies on host RNA responses of MAL$^{-/-}$ and TRAM$^{-/-}$ mice compared to wild type mice infected with SARS-CoV would provide additional insight into how TLR4 specific differences in ISG signaling in particular are generated. In addition, TLR4 is well-described as sensor of bacterial ligands such as lipopolysaccharide (LPS), and additional studies on antibiotic depletion of microbiota and the impact this has on SARS-CoV infection of TLR4$^{-/-}$, TRAM$^{-/-}$, TRIF$^{-/-}$ and wild type mice could provide valuable insight into the role of commensal bacteria in coronavirus pathogenesis.

Although we identified the role of TLR3, TLR4, TRAM, and TRIF in the protective host innate immune response to SARS-CoV infection, we did not directly test the molecular components of SARS-CoV virions to determine what pathogen associated molecular patterns (PAMPs) cause TLR stimulation in the context of SARS-CoV infection. The involvement of TLR3 in SARS-CoV pathogenesis and control of viral titers suggests that TLR3 may detect dsRNA species in the endosome during part of the viral life cycle including viral entry, virion uncoating, genome replication, virion packaging, or viral egress, but has not been confirmed

experimentally. TLR4 has previously been shown to detect viral glycoproteins, and approaches to determine if TLR4 can detect SARS-CoV glycoproteins in cell lines are currently being optimized (87). Because TLR4 has been implicated in the pathogenesis of SARS-CoV (Chapter 3) as well as MHV, it would seem reasonable that conserved elements of the coronavirus virion may be detected by TLR4 (89). Additional studies investigating potentially diverse PAMPs of BtCoVs could determine if TLR4 recognition of coronaviruses is a conserved mechanism of host detection of infection. Information about SARS-CoV virion components that act as PAMPs to stimulate TLRs as well as their effects on downstream cellular signaling programs could help inform optimal vaccine formulations for emerging and reemerging coronavirus pathogens.

Previous studies have shown that pI:C, a TLR3 agonist, can provide protection against SARS-CoV disease in a mouse model, in agreement with our findings that TLR3 stimulation is a key component in the innate immune response to SARS-CoV (166). Evidence that UV inactivated vaccine formulations of SARS-CoV administered in combination with TLR3 and TLR4 agonists as adjuvants averts vaccine induced immunopathology upon re-challenge with SARS-CoV, indicates that further characterization of TLR stimulating compounds in SARS-CoV virions and vaccine formulations would provide additional information for refinements in coronavirus vaccine platform development (167). In addition, it has been demonstrated that stimulation of TLRs in combination can have synergistic effects on proinflammatory cytokine signaling, which may be important in the design of adjuvants for optimal vaccine performance (236).

Highly pathogenic respiratory viruses, including SARS-CoV, MERS-CoV, H5N1 IAV, and H7N9 IAV are serious threats to public health that are currently circulating in zoonotic reservoirs with the potential for spillover events into livestock or human populations. Although highly pathogenic coronaviruses and influenza viruses infect similar tissues in humans, the

respiratory compartment is a complicated organ of resident pneumocyte cells and infiltrating immune cells that may have differing cellular programs to mitigate different types of invading pathogens. TLR agonists and antagonists have proposed utility as antiviral or immunomodulatory compounds with properties to ameliorate symptoms caused by highly pathogenic viruses. Studies on influenza virus pathogenesis have controversially identified potential for TLR4 antagonists as therapeutic compounds to ameliorate severe cytokine responses following influenza virus infection (165). Our research would argue against the usage of antagonists of TLRs in the treatment of coronavirus infections like SARS and MERS, due to the protective role of TLR3, TLR4, TRIF and MyD88 in our model of SARS-CoV infection. Comparisons of cellular signaling programs following infection with SARS, MERS, and influenza highlights the differences between highly pathogenic respiratory viruses that share many similar clinical features making it likely that the development of coronavirus and influenza virus specific antivirals might not target the same pathways (180).

Currently, all of our studies on the contributions of TLR pathways against highly pathogenic coronavirus disease have used knockout mice in a C57BL/6J genetic background, which completely ablates signaling by a gene in an inbred mouse that does not replicate the variable response to viral infections seen in human populations. Future studies that include the collaborative cross resource of genetically diverse mice could be used in immunogenetics studies to investigate allelic variation in TLR related genes and their potential impact on SARS-CoV pathogenesis (237). TRIF polymorphisms that result in altered TRIF-dependent signaling exist in humans and can confer susceptibility to herpesvirus infections (238). However, the limited number of patients in SARS and MERS outbreaks combined with the rarity of TLR related allelic variants in the human population makes it difficult to study the contributions of TLR genes in the context of humans infected with highly pathogenic coronaviruses. The collaborative

cross, a recombinant inbred panel of mice would be a model that encompasses the variation in human background to evaluate the contributions of the TLR genes in diverse genetic backgrounds that more closely approximate what might be expected in human populations if a significant outbreak of highly pathogenic coronaviruses occurred.

CORONAVIRUS NSP7 IS AN INTERFERON ANTAGONIST

In Chapter 4, we described studies that identified that SARS-CoV nonstructural protein 7 (nsp7) is an interferon (IFN) antagonist. SARS-CoV nsp7 blocks RIG-I mediated induction of IFN, but not IFN induction by MDA5. In addition, SARS-CoV nsp7 coimmunprecipitated with NRIG, a constitutively active truncation mutant of RIG-I. Division of SARS-CoV nsp7 into individually expressed structural domains localized the IFN antagonism and NRIG protein-protein interaction of SARS-CoV nsp7 in the N-terminal domain. Alanine scanning across the N-terminal domain of SARS-CoV nsp7 mapped the IFN antagonism and NRIG interaction to a critical block of 20 amino acids at the N-terminus of the protein. Phylogenetic analysis of nsp7 protein sequences identified conservation of these residues in the N-terminus of nsp7 from coronaviruses from multiple branches of the family *Coronaviridae*, including well studied coronaviruses such as MHV (group 2a) and NL63 (group 1b) as well as less characterized BtCoVs from diverse viral lineages (group 2c and group 1b). Studies on IFN activity and NRIG protein-protein interactions confirmed a conservation of IFN antagonism activity in nsp7 from all coronaviruses tested in this study.

Aberrant IFN responses have been identified in SARS and MERS patients, and have been linked to poor disease outcomes in patients with highly pathogenic coronavirus infections (16, 23). Current antiviral therapeutic interventions focus on the administration of approved general antiviral drugs such as interferon and ribavirin, but preliminary studies indicate that these drugs have not been effective in ameliorating SARS or MERS disease (6, 24). IFN antagonists are

often considered a prime target for the design of new antiviral intervention platforms, due to their ability to subdue the initial phases of the innate response to viral infection. However, for coronaviruses the heterogeneity of accessory proteins (conserved only among closely related coronaviruses) or highly-variable structural proteins make these less attractive options even if immunomodulatory activity is identified. In contrast, nucleotide and protein sequences of nonstructural proteins are more highly conserved across the *Coronaviridae* than either accessory proteins or structural proteins, and many nsps are required for replication competent virus, including nsp7, the interferon antagonist characterized in Chapter 4.

Surveillance of coronavirus sequences within bat populations has provided a glimpse of a diverse pool of antigenically distinct viruses within groups 1 and 2 of the coronaviruses (38, 39). As these viruses are likely to be the source of coronavirus emergence events into livestock or other intermediate hosts into human populations, it is important to try to determine the pathogenic potential of viruses that may not be easily cultured in cell lines or assessed with animal models: for many of the BtCoVs, partial genomic sequence and phylogeny are the only analyses that have been completed (200). Analysis of activity of other BtCoV IFN antagonists has yielded mixed results, with the IFN antagonists accessory protein ORF4b of MERS-CoV, BtCoV-HKU4, and BtCoV-HKU5 all having similar levels of IFN antagonism activity, while accessory protein ORF3b of SARS-CoV and SARS-like-CoVs of bats have different levels of IFN antagonism activity (138, 231). In our study, we found that while BtCoV-HKU4, BtCoV-HKU5, and BtCoV-AR nsp7 maintained protein-protein interactions with NRIG, nsp7 from these BtCoVs antagonized IFN induction to a lesser degree than nsp7 from SARS-CoV. With the list of newly discovered BtCoV sequences constantly growing, screening for IFN antagonism activity may be a potential way to isolate BtCoV proteins with the potential for interacting with

human host cell machinery, a useful approach in the absence of building an infectious clone or for BtCoVs that cannot be grown in culture.

FUTURE DIRECTIONS OF NSP7 STUDIES

Currently, studies are ongoing to determine if MERS-CoV nsp7 retains IFN antagonism activity, which seems likely because other group 2c viruses BtCoV-HKU4 and BtCoV-HKU5 have IFN antagonism activity described in Chapter 4. Additional studies are needed to directly compare the nsp7 activity between epidemic and BtCoV precursor pairs, including SARS-CoV/BtCoV-HKU3; HCoV-NL63/BtCoV-HKU2/BtCoV-AR; and MERS-CoV/BtCoV-HKU4/BtCoV-HKU5. These analyses may provide essential data on whether IFN antagonism activity in precursor viral strains identified in bats predicts pathogenic potential in epidemic strains or provides insight into the emergent potential of BtCoV viruses.

Currently, platforms to generate coronavirus vaccines using inactivated virus have been troubled by reduced efficacy in aged animal models of infection and vaccine induced immunopathology in young animal models (65, 152). Live attenuated vaccines are being vigorously pursued, but would require robust mechanisms of attenuation that could be applicable across multiple viral strains, as well as vaccines that generate heterologous immunity to multiple potentially emergent coronaviruses in bats (239). Incorporation of multiple attenuating mutations would be highly desirable in live–attenuated vaccine approaches, as would mechanisms to prevent vaccine recombination events with other coronaviruses circulating in human populations. Identification of critical amino acid residues in the N-terminal region of SARS-CoV nsp7 may provide a map to cripple the IFN antagonism activity of nsp7 by amino acid substitutions as part of a live attenuated vaccine backbone. However, the difficulties with this approach are that the residues identified here as important for nsp7 IFN antagonism activity are also residues that are important for nsp7/nsp8 complex formation, an essential part of the

coronavirus replication machinery (145). It may not be possible to generate nsp7 mutants that retain the ability to form the nsp7/nsp8 complex but no longer antagonize IFN, but further studies are needed to confirm this characterization. However, because these N-terminal amino acids are highly conserved in coronaviruses, if residues could be identified to generate nsp7 mutant viruses without the nsp7 IFN antagonism activity that are still replication competent, this approach could be a useful component in a platform to rationally design live attenuated vaccine strains across multiple strains of mammalian infecting viruses within the *Coronaviridae*.

CONCLUSION OF DISSERTATION

Less than two decades into the 21st century we have already seen the emergence of two highly pathogenic coronaviruses in humans with the potential for high mortality rates and significant economic impacts: SARS-CoV and MERS-CoV. In addition, epizootic coronaviruses in livestock are threats to agriculturally important animals (such as PEDV in pigs) as well as potential hotbeds for CoV cross-species spillover into human populations (such as MERS-CoV from camels). The studies described herein enhance our understanding of host innate immune genes that render protection or susceptibility to SARS-CoV infection in animal model systems.

Surveys in bats around the world indicate a phylogenetically diverse coronavirus reservoir with unknown emergent potential exists in many different bat species covering a wide geographic range, making study of these BtCoVs a priority in coronavirus research. While factors for prediction of cross-species transmission and pandemic emergence potential remain elusive, our studies provide evidence that an important conserved aspect of coronavirus pathogenesis is the manipulation and control of innate immune responses in the host. Understanding how coronaviruses antagonize the earliest recognition of "non-self" responses in the host and conservation of this manipulation within the coronavirus family, especially among populations of potentially emergent viruses in reservoirs, may be important factors in i.) the

identification of pandemic threats, ii.) the design of coronavirus vaccine platforms, and iii.) the development of antiviral drugs against coronavirus infections. Advancements in these three key areas of viral research are critical as the emergence of highly pathogenic coronaviruses may continue to be a threat to human health and economic stability in the decades to come.

REFERENCES

1. **Drosten C, Gunther S, Preiser W, van der Werf S, Brodt H-R, Becker S, Rabenau H, Panning M, Kolesnikova L, Fouchier RAM, Berger A, BurguiÃ¨re A-M, Cinatl J, Eickmann M, Escriou N, Grywna K, Kramme S, Manuguerra J-C, MÃ¼ller S, Rickerts V, StÃ¼rmer M, Vieth S, Klenk H-D, Osterhaus ADME, Schmitz H, Doerr HW.** 2003. Identification of a Novel Coronavirus in Patients with Severe Acute Respiratory Syndrome. New England Journal of Medicine **348:**1967-1976.

2. **Ksiazek TG, Erdman D, Goldsmith CS, Zaki SR, Peret T, Emery S, Tong S, Urbani C, Comer JA, Lim W, Rollin PE, Dowell SF, Ling A-E, Humphrey CD, Shieh W-J, Guarner J, Paddock CD, Rota P, Fields B, DeRisi J, Yang J-Y, Cox N, Hughes JM, LeDuc JW, Bellini WJ, Anderson LJ.** 2003. A Novel Coronavirus Associated with Severe Acute Respiratory Syndrome. New England Journal of Medicine **348:**1953-1966.

3. **Li W, Moore MJ, Vasilieva N, Sui J, Wong SK, Berne MA, Somasundaran M, Sullivan JL, Luzuriaga K, Greenough TC, Choe H, Farzan M.** 2003. Angiotensin-converting enzyme 2 is a functional receptor for the SARS coronavirus. Nature **426:**450-454.

4. **Hui DSC, Chan MCH, Wu AK, Ng PC.** 2004. Severe acute respiratory syndrome (SARS): epidemiology and clinical features. Postgraduate Medical Journal **80:**373-381.

5. 2003, posting date. World Health Organization: Summary of probable SARS cases with onset of illness from 1 November 2002 to 31 July 2003. [Online.]

6. **Stockman LJ, Bellamy R, Garner P.** 2006. SARS: Systematic Review of Treatment Effects. PLoS Med **3:**e343.

7. **Tsushima K, King LS, Aggarwal NR, Gorordo AD, D'Alessio FR, Kubo K.** 2009. Acute Lung Injury Review Intern. Med **48:**621-630.

8. **Hwang DM, Chamberlain DW, Poutanen SM, Low DE, Asa SL, Butany J.** 2004. Pulmonary pathology of severe acute respiratory syndrome in Toronto. Mod Pathol **18:**1-10.

9. **Chow K-C, Hsiao C-H, Lin T-Y, Chen C-L, Chiou S-H.** 2004. Detection of Severe Acute Respiratory Syndrome Associated Coronavirus in Pneumocytes of the Lung. American Journal of Clinical Pathology **121:**574-580.

10. **Sims AC, Baric RS, Yount B, Burkett SE, Collins PL, Pickles RJ.** 2005. Severe Acute Respiratory Syndrome Coronavirus Infection of Human Ciliated Airway Epithelia: Role of Ciliated Cells in Viral Spread in the Conducting Airways of the Lungs. Journal of Virology **79:**15511-15524.

11. **Lew TWK, Kwek T-K, Tai D, Earnest A, Loo S, Singh K, Kwan KM, Chan Y, Yim CF, Bek SL, Kor AC, Yap WS, Chelliah YR, Lai YC, Goh S-K.** 2003. Acute Respiratory Distress Syndrome in Critically Ill Patients With Severe Acute Respiratory Syndrome. JAMA **290:**374-380.

12. 2003, posting date. World Health Organization: SARS case fatality ratio, incubation period. [Online.]

13. **Kong SL, Chui P, Lim B, Salto-Tellez M.** 2009. Elucidating the molecular physiopathology of acute respiratory distress syndrome in severe acute respiratory syndrome patients. Virus Research **145:**260-269.

14. **Baas T, Taubenberger JK, Chong PY, Chui P, Katze. MG.** 2006. SARS-CoV Virus-Host Interactions and Comparative Etiologies of Acute Respiratory Distress Syndrome as Determined by Transcriptional and Cytokine Profiling of Formalin-Fixed Paraffin-Embedded Tissues Journal of Interferon & Cytokine Research **26:**309-317.

15. **Wong CK, Lam CWK, Wu AKL, Ip WK, Lee NLS, Chan IHS, Lit LCW, Hui DSC, Chan MHM, Chung SSC, Sung JJY.** 2004. Plasma inflammatory cytokines and chemokines in severe acute respiratory syndrome. Clinical & Experimental Immunology **136:**95-103.

16. **Cameron MJ, Ran L, Xu L, Danesh A, Bermejo-Martin JF, Cameron CM, Muller MP, Gold WL, Richardson SE, Poutanen SM, Willey BM, DeVries ME, Fang Y, Seneviratne C, Bosinger SE, Persad D, Wilkinson P, Greller LD, Somogyi R, Humar A, Keshavjee S, Louie M, Loeb MB, Brunton J, McGeer AJ, Network tCSR, Kelvin DJ.** 2007. Interferon-Mediated Immunopathological Events Are Associated with Atypical Innate and Adaptive Immune Responses in Patients with Severe Acute Respiratory Syndrome. Journal of Virology **81:**8692-8706.

17. **Zaki AM, van Boheemen S, Bestebroer TM, Osterhaus ADME, Fouchier RAM.** 2012. Isolation of a Novel Coronavirus from a Man with Pneumonia in Saudi Arabia. New England Journal of Medicine **367:**1814-1820.

18. **de Groot RJ, Baker SC, Baric RS, Brown CS, Drosten C, Enjuanes L, Fouchier RAM, Galiano M, Gorbalenya AE, Memish ZA, Perlman S, Poon LLM, Snijder EJ, Stephens GM, Woo PCY, Zaki AM, Zambon M, Ziebuhr J.** 2013. Middle East

Respiratory Syndrome Coronavirus (MERS-CoV): Announcement of the Coronavirus Study Group. Journal of Virology **87:**7790-7792.

19. 2014. European Centre for Disease Prevention and Control: Epidemiological update: Middle East respiratory syndrome coronavirus (MERS-CoV) 05 Nov 2014.

20. **Kapoor M, Pringle K, Kumar A, Dearth S, Liu L, Lovchik J, Perez O, Pontones P, Richards S, Yeadon-Fagbohun J, Breakwell L, Chea N, Cohen NJ, Schneider E, Erdman D, Haynes L, Pallansch M, Tao Y, Tong S, Gerber S, Swerdlow D, Feikin DR.** 2014. Clinical and Laboratory Findings of the First Imported Case of Middle East Respiratory Syndrome Coronavirus to the United States. Clinical Infectious Diseases.

21. **Al-Tawfiq JA, Zumla A, Memish ZA.** Travel implications of emerging coronaviruses: SARS and MERS-CoV. Travel Medicine and Infectious Disease.

22. **Alghamdi IG.** 2014. The pattern of Middle East respiratory syndrome coronavirus in Saudi Arabia: a descriptive epidemiological analysis of data from the Saudi Ministry of Health. International journal of general medicine **7:**417-423.

23. **Faure E, Poissy J, Goffard A, Fournier C, Kipnis E, Titecat M, Bortolotti P, Martinez L, Dubucquoi S, Dessein R, Gosset P, Mathieu D, Guery B.** 2014. Distinct Immune Response in Two MERS-CoV-Infected Patients: Can We Go from Bench to Bedside? PLoS ONE **9:**e88716.

24. **Al-Tawfiq JA, Momattin H, Dib J, Memish ZA.** 2014. Ribavirin and interferon therapy in patients infected with the Middle East respiratory syndrome coronavirus: an observational study. International Journal of Infectious Diseases **20:**42-46.

25. **Raj VS, Mou H, Smits SL, Dekkers DHW, Muller MA, Dijkman R, Muth D, Demmers JAA, Zaki A, Fouchier RAM, Thiel V, Drosten C, Rottier PJM, Osterhaus ADME, Bosch BJ, Haagmans BL.** 2013. Dipeptidyl peptidase 4 is a functional receptor for the emerging human coronavirus-EMC. Nature **495:**251-254.

26. **Wevers BA, van der Hoek L.** 2009. Recently Discovered Human Coronaviruses. Clinics in Laboratory Medicine **29:**715-724.

27. **Vijgen L, Keyaerts E, Moës E, Thoelen I, Wollants E, Lemey P, Vandamme A-M, Van Ranst M.** 2005. Complete Genomic Sequence of Human Coronavirus OC43: Molecular Clock Analysis Suggests a Relatively Recent Zoonotic Coronavirus Transmission Event. Journal of Virology **79:**1595-1604.

28. **Stevenson GW, Hoang H, Schwartz KJ, Burrough ER, Sun D, Madson D, Cooper VL, Pillatzki A, Gauger P, Schmitt BJ, Koster LG, Killian ML, Yoon KJ.** 2013. Emergence of Porcine epidemic diarrhea virus in the United States: clinical signs, lesions, and viral genomic sequences. Journal of Veterinary Diagnostic Investigation **25:**649-654.

29. **Yount B, Curtis KM, Fritz EA, Hensley LE, Jahrling PB, Prentice E, Denison MR, Geisbert TW, Baric RS.** 2003. Reverse genetics with a full-length infectious cDNA of severe acute respiratory syndrome coronavirus. Proceedings of the National Academy of Sciences **100:**12995-13000.

30. **Frieman M, Yount B, Sims A, Deming D, Morrison T, Sparks J, Denison M, Heise M, Baric R, Perlman S, Holmes K.** 2006. SARS Coronavirus Accessory ORFs Encode Luxury Functions
p. 149-152, The Nidoviruses, vol. 581. Springer US.

31. **Song H-D, Tu C-C, Zhang G-W, Wang S-Y, Zheng K, Lei L-C, Chen Q-X, Gao Y-W, Zhou H-Q, Xiang H, Zheng H-J, Chern S-WW, Cheng F, Pan C-M, Xuan H, Chen S-J, Luo H-M, Zhou D-H, Liu Y-F, He J-F, Qin P-Z, Li L-H, Ren Y-Q, Liang W-J, Yu Y-D, Anderson L, Wang M, Xu R-H, Wu X-W, Zheng H-Y, Chen J-D, Liang G, Gao Y, Liao M, Fang L, Jiang L-Y, Li H, Chen F, Di B, He L-J, Lin J-Y, Tong S, Kong X, Du L, Hao P, Tang H, Bernini A, Yu X-J, Spiga O, Guo Z-M, Pan H-Y, He W-Z, Manuguerra J-C, Fontanet A, Danchin A, Niccolai N, Li Y-X, Wu C-I, Zhao G-P.** 2005. Cross-host evolution of severe acute respiratory syndrome coronavirus in palm civet and human. Proceedings of the National Academy of Sciences of the United States of America **102:**2430-2435.

32. **Alagaili AN, Briese T, Mishra N, Kapoor V, Sameroff SC, de Wit E, Munster VJ, Hensley LE, Zalmout IS, Kapoor A, Epstein JH, Karesh WB, Daszak P, Mohammed OB, Lipkin WI.** 2014. Middle East Respiratory Syndrome Coronavirus Infection in Dromedary Camels in Saudi Arabia. mBio **5**.

33. **Anthony SJ, Epstein JH, Murray KA, Navarrete-Macias I, Zambrana-Torrelio CM, Solovyov A, Ojeda-Flores R, Arrigo NC, Islam A, Ali Khan S, Hosseini P, Bogich TL, Olival KJ, Sanchez-Leon MD, Karesh WB, Goldstein T, Luby SP, Morse SS, Mazet JAK, Daszak P, Lipkin WI.** 2013. A Strategy To Estimate Unknown Viral Diversity in Mammals. mBio **4**.

34. **Lau SKP, Woo PCY, Li KSM, Huang Y, Tsoi H-W, Wong BHL, Wong SSY, Leung S-Y, Chan K-H, Yuen K-Y.** 2005. Severe acute respiratory syndrome coronavirus-like virus in Chinese horseshoe bats. Proceedings of the National Academy of Sciences of the United States of America **102:**14040-14045.

35. **Li W, Shi Z, Yu M, Ren W, Smith C, Epstein JH, Wang H, Crameri G, Hu Z, Zhang H, Zhang J, McEachern J, Field H, Daszak P, Eaton BT, Zhang S, Wang L-F.** 2005. Bats Are Natural Reservoirs of SARS-Like Coronaviruses. Science **310:**676-679.

36. **Ge X-Y, Li J-L, Yang X-L, Chmura AA, Zhu G, Epstein JH, Mazet JK, Hu B, Zhang W, Peng C, Zhang Y-J, Luo C-M, Tan B, Wang N, Zhu Y, Crameri G, Zhang S-Y, Wang L-F, Daszak P, Shi Z-L.** 2013. Isolation and characterization of a bat SARS-like coronavirus that uses the ACE2 receptor. Nature **503:**535-538.

37. **Yang Y, Du L, Liu C, Wang L, Ma C, Tang J, Baric RS, Jiang S, Li F.** 2014. Receptor usage and cell entry of bat coronavirus HKU4 provide insight into bat-to-human transmission of MERS coronavirus. Proceedings of the National Academy of Sciences **111:**12516-12521.

38. **Woo PCY, Wang M, Lau SKP, Xu H, Poon RWS, Guo R, Wong BHL, Gao K, Tsoi H-w, Huang Y, Li KSM, Lam CSF, Chan K-h, Zheng B-j, Yuen K-y.** 2007. Comparative Analysis of Twelve Genomes of Three Novel Group 2c and Group 2d Coronaviruses Reveals Unique Group and Subgroup Features. Journal of Virology **81:**1574-1585.

39. **Donaldson EF, Haskew AN, Gates JE, Huynh J, Moore CJ, Frieman MB.** 2010. Metagenomic Analysis of the Viromes of Three North American Bat Species: Viral Diversity among Different Bat Species That Share a Common Habitat. Journal of Virology **84:**13004-13018.

40. **van Boheemen S, de Graaf M, Lauber C, Bestebroer TM, Raj VS, Zaki AM, Osterhaus ADME, Haagmans BL, Gorbalenya AE, Snijder EJ, Fouchier RAM.** 2012. Genomic Characterization of a Newly Discovered Coronavirus Associated with Acute Respiratory Distress Syndrome in Humans. mBio **3**.

41. **Agnihothram S, Yount BL, Donaldson EF, Huynh J, Menachery VD, Gralinski LE, Graham RL, Becker MM, Tomar S, Scobey TD, Osswald HL, Whitmore A, Gopal R, Ghosh AK, Mesecar A, Zambon M, Heise M, Denison MR, Baric RS.** 2014. A Mouse Model for Betacoronavirus Subgroup 2c Using a Bat Coronavirus Strain HKU5 Variant. mBio **5**.

42. **Leong WF, Tan HC, Ooi EE, Koh DR, Chow VTK.** 2005. Microarray and real-time RT-PCR analyses of differential human gene expression patterns induced by severe acute respiratory syndrome (SARS) coronavirus infection of Vero cells. Microbes and Infection **7:**248-259.

43. **Dosch SF, Mahajan SD, Collins AR.** 2009. SARS coronavirus spike protein-induced innate immune response occurs via activation of the NF-κB pathway in human monocyte macrophages in vitro. Virus Research **142:**19-27.

44. **Li L, Wo J, Shao J, Zhu H, Wu N, Li M, Yao H, Hu M, Dennin RH.** 2003. SARS-coronavirus replicates in mononuclear cells of peripheral blood (PBMCs) from SARS patients. Journal of clinical virology : the official publication of the Pan American Society for Clinical Virology **28:**239-244.

45. **Sims AC, Burkett SE, Yount B, Pickles RJ.** 2008. SARS-CoV replication and pathogenesis in an in vitro model of the human conducting airway epithelium. Virus Research **133:**33-44.

46. **Tseng C-TK, Tseng J, Perrone L, Worthy M, Popov V, Peters CJ.** 2005. Apical Entry and Release of Severe Acute Respiratory Syndrome-Associated Coronavirus in Polarized Calu-3 Lung Epithelial Cells. Journal of Virology **79:**9470-9479.

47. **Yoshikawa T, Hill TE, Yoshikawa N, Popov VL, Galindo CL, Garner HR, Peters CJ, Tseng C-T.** 2010. Dynamic Innate Immune Responses of Human Bronchial Epithelial Cells to Severe Acute Respiratory Syndrome-Associated Coronavirus Infection. PLoS ONE **5:**e8729.

48. **Martina BEE, Haagmans BL, Kuiken T, Fouchier RAM, Rimmelzwaan GF, van Amerongen G, Peiris JSM, Lim W, Osterhaus ADME.** 2003. Virology: SARS virus infection of cats and ferrets. Nature **425:**915-915.

49. **van den Brand JMA, Haagmans BL, Leijten L, van Riel D, Martina BEE, Osterhaus ADME, Kuiken T.** 2008. Pathology of Experimental SARS Coronavirus Infection in Cats and Ferrets. Veterinary Pathology Online **45:**551-562.

50. **Roberts A, Vogel L, Guarner J, Hayes N, Murphy B, Zaki S, Subbarao K.** 2005. Severe Acute Respiratory Syndrome Coronavirus Infection of Golden Syrian Hamsters. Journal of Virology **79:**503-511.

51. **Subbarao K, McAuliffe J, Vogel L, Fahle G, Fischer S, Tatti K, Packard M, Shieh W-J, Zaki S, Murphy B.** 2004. Prior Infection and Passive Transfer of Neutralizing Antibody Prevent Replication of Severe Acute Respiratory Syndrome Coronavirus in the Respiratory Tract of Mice. Journal of Virology **78:**3572-3577.

52. **Glass WG, Subbarao K, Murphy B, Murphy PM.** 2004. Mechanisms of Host Defense following Severe Acute Respiratory Syndrome-Coronavirus (SARS-CoV) Pulmonary Infection of Mice. The Journal of Immunology **173:**4030-4039.

53. **Baas T, Roberts A, Teal TH, Vogel L, Chen J, Tumpey TM, Katze MG, Subbarao K.** 2008. Genomic Analysis Reveals Age-Dependent Innate Immune Responses to Severe Acute Respiratory Syndrome Coronavirus. Journal of Virology **82:**9465-9476.

54. **Yang X-h, Deng W, Tong Z, Liu Y-x, Zhang L-f, Zhu H, Gao H, Huang L, Liu Y-l, Ma C-m, Xu Y-f, Ding M-x, Deng H-k, Qin C.** 2007. Mice Transgenic for Human Angiotensin-converting Enzyme 2 Provide a Model for SARS Coronavirus Infection. Comparative Medicine **57:**450-459.

55. **Netland J, Meyerholz DK, Moore S, Cassell M, Perlman S.** 2008. Severe Acute Respiratory Syndrome Coronavirus Infection Causes Neuronal Death in the Absence of Encephalitis in Mice Transgenic for Human ACE2. Journal of Virology **82:**7264-7275.

56. **Rockx B, Baas T, Zornetzer GA, Haagmans B, Sheahan T, Frieman M, Dyer MD, Teal TH, Proll S, van den Brand J, Baric R, Katze MG.** 2009. Early Upregulation of Acute Respiratory Distress Syndrome-Associated Cytokines Promotes Lethal Disease in an Aged-Mouse Model of Severe Acute Respiratory Syndrome Coronavirus Infection. Journal of Virology **83:**7062-7074.

57. **Roberts A, Paddock C, Vogel L, Butler E, Zaki S, Subbarao K.** 2005. Aged BALB/c Mice as a Model for Increased Severity of Severe Acute Respiratory Syndrome in Elderly Humans. Journal of Virology **79:**5833-5838.

58. **De Albuquerque N, Baig E, Ma X, Zhang J, He W, Rowe A, Habal M, Liu M, Shalev I, Downey GP, Gorczynski R, Butany J, Leibowitz J, Weiss SR, McGilvray ID, Phillips MJ, Fish EN, Levy GA.** 2006. Murine Hepatitis Virus Strain 1 Produces a Clinically Relevant Model of Severe Acute Respiratory Syndrome in A/J Mice. Journal of Virology **80:**10382-10394.

59. **Day CW, Baric R, Cai SX, Frieman M, Kumaki Y, Morrey JD, Smee DF, Barnard DL.** 2009. A new mouse-adapted strain of SARS-CoV as a lethal model for evaluating antiviral agents in vitro and in vivo. Virology **395:**210-222.

60. **Roberts A, Deming D, Paddock CD, Cheng A, Yount B, Vogel L, Herman BD, Sheahan T, Heise M, Genrich GL, Zaki SR, Baric R, Subbarao K.** 2007. A Mouse-Adapted SARS-Coronavirus Causes Disease and Mortality in BALB/c Mice. PLoS Pathog **3:**e5.

61. **Sheahan T, Whitmore A, Long K, Ferris M, Rockx B, Funkhouser W, Donaldson E, Gralinski L, Collier M, Heise M, Davis N, Johnston R, Baric RS.** 2011. Successful Vaccination Strategies That Protect Aged Mice from Lethal Challenge from Influenza Virus and Heterologous Severe Acute Respiratory Syndrome Coronavirus. Journal of Virology **85:**217-230.

62. **Frieman M, Yount B, Agnihothram S, Page C, Donaldson E, Roberts A, Vogel L, Woodruff B, Scorpio D, Subbarao K, Baric RS.** 2012. Molecular Determinants of Severe Acute Respiratory Syndrome Coronavirus Pathogenesis and Virulence in Young and Aged Mouse Models of Human Disease. Journal of Virology **86:**884-897.

63. **Rockx B, Sheahan T, Donaldson E, Harkema J, Sims A, Heise M, Pickles R, Cameron M, Kelvin D, Baric R.** 2007. Synthetic Reconstruction of Zoonotic and Early Human Severe Acute Respiratory Syndrome Coronavirus Isolates That Produce Fatal Disease in Aged Mice. Journal of Virology **81:**7410-7423.

64. **Aylor DL, Valdar W, Foulds-Mathes W, Buus RJ, Verdugo RA, Baric RS, Ferris MT, Frelinger JA, Heise M, Frieman MB, Gralinski LE, Bell TA, Didion JD, Hua K, Nehrenberg DL, Powell CL, Steigerwalt J, Xie Y, Kelada SNP, Collins FS, Yang IV, Schwartz DA, Branstetter LA, Chesler EJ, Miller DR, Spence J, Liu EY, McMillan L, Sarkar A, Wang J, Wang W, Zhang Q, Broman KW, Korstanje R, Durrant C, Mott R, Iraqi FA, Pomp D, Threadgill D, Pardo-Manuel de Villena F, Churchill GA.** 2011. Genetic analysis of complex traits in the emerging Collaborative Cross. Genome Research **21:**1213-1222.

65. **Bolles M, Deming D, Long K, Agnihothram S, Whitmore A, Ferris M, Funkhouser W, Gralinski L, Totura A, Heise M, Baric RS.** 2011. A Double-Inactivated Severe Acute Respiratory Syndrome Coronavirus Vaccine Provides Incomplete Protection in Mice and Induces Increased Eosinophilic Proinflammatory Pulmonary Response upon Challenge. Journal of Virology **85:**12201-12215.

66. **McAuliffe J, Vogel L, Roberts A, Fahle G, Fischer S, Shieh W-J, Butler E, Zaki S, St. Claire M, Murphy B, Subbarao K.** 2004. Replication of SARS coronavirus administered into the respiratory tract of African Green, rhesus and cynomolgus monkeys. Virology **330:**8-15.

67. **Haagmans BL, Kuiken T, Martina BE, Fouchier RAM, Rimmelzwaan GF, van Amerongen G, van Riel D, de Jong T, Itamura S, Chan K-H, Tashiro M, Osterhaus ADME.** 2004. Pegylated interferon-α protects type 1 pneumocytes against SARS coronavirus infection in macaques. Nature Medicine **10:**290-293.

68. **Smits SL, de Lang A, van den Brand JMA, Leijten LM, van Ijcken WF, Eijkemans MJC, van Amerongen G, Kuiken T, Andeweg AC, Osterhaus ADME, Haagmans**

BL. 2010. Exacerbated Innate Host Response to SARS-CoV in Aged Non-Human Primates. PLoS Pathog **6:**e1000756.

69. **Smits SL, van den Brand JMA, de Lang A, Leijten LME, van IJcken WF, van Amerongen G, Osterhaus ADME, Andeweg AC, Haagmans BL.** 2011. Distinct Severe Acute Respiratory Syndrome Coronavirus-Induced Acute Lung Injury Pathways in Two Different Nonhuman Primate Species. Journal of Virology **85:**4234-4245.

70. **Kindler E, Jónsdóttir HR, Muth D, Hamming OJ, Hartmann R, Rodriguez R, Geffers R, Fouchier RAM, Drosten C, Müller MA, Dijkman R, Thiel V.** 2013. Efficient Replication of the Novel Human Betacoronavirus EMC on Primary Human Epithelium Highlights Its Zoonotic Potential. mBio **4**.

71. **Cockrell AS, Peck KM, Yount BL, Agnihothram SS, Scobey T, Curnes NR, Baric RS, Heise MT.** 2014. Mouse Dipeptidyl Peptidase 4 Is Not a Functional Receptor for Middle East Respiratory Syndrome Coronavirus Infection. Journal of Virology **88:**5195-5199.

72. **Zhao J, Li K, Wohlford-Lenane C, Agnihothram SS, Fett C, Zhao J, Gale MJ, Baric RS, Enjuanes L, Gallagher T, McCray PB, Perlman S.** 2014. Rapid generation of a mouse model for Middle East respiratory syndrome. Proceedings of the National Academy of Sciences **111:**4970-4975.

73. **de Wit E, Rasmussen AL, Falzarano D, Bushmaker T, Feldmann F, Brining DL, Fischer ER, Martellaro C, Okumura A, Chang J, Scott D, Benecke AG, Katze MG, Feldmann H, Munster VJ.** 2013. Middle East respiratory syndrome coronavirus (MERS-CoV) causes transient lower respiratory tract infection in rhesus macaques. Proceedings of the National Academy of Sciences **110:**16598-16603.

74. **Rathinam VAK, Fitzgerald KA.** 2011. Cytosolic surveillance and antiviral immunity. Current Opinion in Virology **1:**455-462.

75. **Arpaia N, Barton GM.** 2011. Toll-like receptors: key players in antiviral immunity. Current Opinion in Virology **1:**447-454.

76. **Yoneyama M, Kikuchi M, Matsumoto K, Imaizumi T, Miyagishi M, Taira K, Foy E, Loo Y-M, Gale M, Akira S, Yonehara S, Kato A, Fujita T.** 2005. Shared and Unique Functions of the DExD/H-Box Helicases RIG-I, MDA5, and LGP2 in Antiviral Innate Immunity. The Journal of Immunology **175:**2851-2858.

77. **Satoh T, Kato H, Kumagai Y, Yoneyama M, Sato S, Matsushita K, Tsujimura T, Fujita T, Akira S, Takeuchi O.** 2010. LGP2 is a positive regulator of RIG-I and MDA5-mediated antiviral responses. Proceedings of the National Academy of Sciences **107:**1512-1517.

78. **Pichlmair A, Schulz O, Tan CP, Naslund TI, Liljestrom P, Weber F, Reis e Sousa C.** 2006. RIG-I-Mediated Antiviral Responses to Single-Stranded RNA Bearing 5'-Phosphates. Science **314:**997-1001.

79. **Baum A, Sachidanandam R, Garcia-Sastre A.** 2011. Preference of RIG-I for short viral RNA molecules in infected cells revealed by next-generation sequencing. Proceedings of the National Academy of Sciences **107:**16303-16308.

80. **Kato H, Takeuchi O, Mikamo-Satoh E, Hirai R, Kawai T, Matsushita K, Hiiragi A, Dermody TS, Fujita T, Akira S.** 2008. Length-dependent recognition of double-stranded ribonucleic acids by retinoic acid-inducible gene-I and melanoma differentiation associated gene 5. The Journal of Experimental Medicine **205:**1601-1610.

81. **Roth-Cross JK, Bender SJ, Weiss SR.** 2008. Murine Coronavirus Mouse Hepatitis Virus Is Recognized by MDA5 and Induces Type I Interferon in Brain Macrophages/Microglia. Journal of Virology **82:**9829-9838.

82. **Kawai T, Takahashi K, Sato S, Coban C, Kumar H, Kato H, Ishii KJ, Takeuchi O, Akira S.** 2005. IPS-1, an adaptor triggering RIG-I- and Mda5-mediated type I interferon induction. Nature Immunology **6:**981-988.

83. **Lin R, Lacoste J, Nakhaei P, Sun Q, Yang L, Paz S, Wilkinson P, Julkunen I, Vitour D, Meurs E, Hiscott J.** 2006. Dissociation of a MAVS/IPS-1/VISA/Cardif-IKKε Molecular Complex from the Mitochondrial Outer Membrane by Hepatitis C Virus NS3-4A Proteolytic Cleavage. Journal of Virology **80:**6072-6083.

84. **Chariot A, Leonardi A, MÃ¼ller Jr, Bonif M, Brown K, Siebenlist U.** 2002. Association of the Adaptor TANK with the IκB Kinase (IKK) Regulator NEMO Connects IKK Complexes with IKKε and TBK1 Kinases. Journal of Biological Chemistry **277:**37029-37036.

85. **Zandi E, Rothwarf DM, Delhase M, Hayakawa M, Karin M.** 1997. The IκB Kinase Complex (IKK) Contains Two Kinase Subunits, IKKα and IKKβ, Necessary for IκB Phosphorylation and NF-κB Activation. Cell **91:**243-252.

86. **Galani V, Tatsaki E, Bai M, Kitsoulis P, Lekka M, Nakos G, Kanavaros P.** 2010. The role of apoptosis in the pathophysiology of Acute Respiratory Distress Syndrome (ARDS): An up-to-date cell-specific review. Pathology - Research and Practice **206:**145-150.

87. **Kurt-Jones EA, Popova L, Kwinn L, Haynes LM, Jones LP, Tripp RA, Walsh EE, Freeman MW, Golenbock DT, Anderson LJ, Finberg RW.** 2000. Pattern recognition receptors TLR4 and CD14 mediate response to respiratory syncytial virus. Nature Immunology **1:**398-401.

88. **Marchant D, Singhera GK, Utokaparch S, Hackett TL, Boyd JH, Luo Z, Si X, Dorscheid DR, McManus BM, Hegele RG.** 2010. Toll-Like Receptor 4-Mediated Activation of p38 Mitogen-Activated Protein Kinase Is a Determinant of Respiratory Virus Entry and Tropism. Journal of Virology **84:**11359-11373.

89. **Khanolkar A, Hartwig SM, Haag BA, Meyerholz DK, Harty JT, Varga SM.** 2009. Toll-Like Receptor 4 Deficiency Increases Disease and Mortality after Mouse Hepatitis Virus Type 1 Infection of Susceptible C3H Mice. Journal of Virology **83:**8946-8956.

90. **Murawski MR, Bowen GN, Cerny AM, Anderson LJ, Haynes LM, Tripp RA, Kurt-Jones EA, Finberg RW.** 2009. Respiratory Syncytial Virus Activates Innate Immunity through Toll-Like Receptor 2. Journal of Virology **83:**1492-1500.

91. **Boehme KW, Guerrero M, Compton T.** 2006. Human Cytomegalovirus Envelope Glycoproteins B and H Are Necessary for TLR2 Activation in Permissive Cells. The Journal of Immunology **177:**7094-7102.

92. **Zornetzer GA, Frieman MB, Rosenzweig E, Korth MJ, Page C, Baric RS, Katze MG.** 2010. Transcriptomic Analysis Reveals a Mechanism for a Prefibrotic Phenotype in STAT1 Knockout Mice during Severe Acute Respiratory Syndrome Coronavirus Infection. Journal of Virology **84:**11297-11309.

93. **Law H, Cheung C, Sia S, Chan Y, Peiris JM, Lau Y.** 2009. Toll-like receptors, chemokine receptors and death receptor ligands responses in SARS coronavirus infected human monocyte derived dendritic cells. BMC Immunology **10:**35.

94. **Zhao J, Zhao J, Van Rooijen N, Perlman S.** 2009. Evasion by Stealth: Inefficient Immune Activation Underlies Poor T Cell Response and Severe Disease in SARS-CoV-Infected Mice. PLoS Pathog **5:**e1000636.

95. **Sheahan T, Morrison TE, Funkhouser W, Uematsu S, Akira S, Baric RS, Heise MT.** 2008. MyD88 Is Required for Protection from Lethal Infection with a Mouse-Adapted SARS-CoV. PLoS Pathog **4:**e1000240.

96. **Dahl H, Linde A, Strannegard O.** 2004. In vitro inhibition of SARS virus replication by human interferons. Scandinavian Journal of Infectious Diseases **36:**829-831.

97. **StrÃ¶her U, DiCaro A, Li Y, Strong JE, Aoki F, Plummer F, Jones SM, Feldmann H.** 2004. Severe Acute Respiratory Syndrome-Related Coronavirus Is Inhibited by Interferon-Î±. Journal of Infectious Diseases **189:**1164-1167.

98. **Sainz Jr B, Mossel EC, Peters CJ, Garry RF.** 2004. Interferon-beta and interferon-gamma synergistically inhibit the replication of severe acute respiratory syndrome-associated coronavirus (SARS-CoV). Virology **329:**11-17.

99. **Barnard DL, Day CW, Bailey K, Heiner M, Montgomery R, Lauridsen L, Chan PK, Sidwell RW.** 2006. Evaluation of immunomodulators, interferons and known in vitro SARS-coV inhibitors for inhibition of SARS-coV replication in BALB/c mice. Antiviral Chemistry & Chemotherapy **17:**275-284.

100. **Kumaki Y, Ennis J, Rahbar R, Turner JD, Wandersee MK, Smith AJ, Bailey KW, Vest ZG, Madsen JR, Li JKK, Barnard DL.** 2011. Single-dose intranasal administration with mDEF201 (adenovirus vectored mouse interferon-alpha) confers protection from mortality in a lethal SARS-CoV BALB/c mouse model. Antiviral Research **89:**75-82.

101. **Frieman MB, Chen J, Morrison TE, Whitmore A, Funkhouser W, Ward JM, Lamirande EW, Roberts A, Heise M, Subbarao K, Baric RS.** 2010. SARS-CoV Pathogenesis Is Regulated by a STAT1 Dependent but a Type I, II and III Interferon Receptor Independent Mechanism. PLoS Pathog **6:**e1000849.

102. **Mordstein M, Neugebauer E, Ditt V, Jessen B, Rieger T, Falcone V, Sorgeloos F, Ehl S, Mayer D, Kochs G, Schwemmle M, GÃ¼nther S, Drosten C, Michiels T, Staeheli P.** 2010. Lambda Interferon Renders Epithelial Cells of the Respiratory and Gastrointestinal Tracts Resistant to Viral Infections. Journal of Virology **84:**5670-5677.

103. **Hogan RJ, Gao G, Rowe T, Bell P, Flieder D, Paragas J, Kobinger GP, Wivel NA, Crystal RG, Boyer J, Feldmann H, Voss TG, Wilson JM.** 2004. Resolution of Primary Severe Acute Respiratory Syndrome-Associated Coronavirus Infection Requires Stat1. Journal of Virology **78:**11416-11421.

104. **Kopecky-Bromberg SA, Martinez-Sobrido L, Frieman M, Baric RA, Palese P.** 2007. Severe Acute Respiratory Syndrome Coronavirus Open Reading Frame (ORF) 3b, ORF 6, and Nucleocapsid Proteins Function as Interferon Antagonists. Journal of Virology **81:**548-557.

105. **Pugin J, Ricou B, Steinberg KP, Suter PM, Martin TR.** 1996. Proinflammatory activity in bronchoalveolar lavage fluids from patients with ARDS, a prominent role for interleukin-1. American Journal of Respiratory and Critical Care Medicine **153:**1850-1856.

106. **Schoggins JW, Rice CM.** 2011. Interferon-stimulated genes and their antiviral effector functions. Current Opinion in Virology **1:**519-525.

107. **Huang IC, Bailey CC, Weyer JL, Radoshitzky SR, Becker MM, Chiang JJ, Brass AL, Ahmed AA, Chi X, Dong L, Longobardi LE, Boltz D, Kuhn JH, Elledge SJ, Bavari S, Denison MR, Choe H, Farzan M.** 2011. Distinct Patterns of IFITM-Mediated Restriction of Filoviruses, SARS Coronavirus, and Influenza A Virus. PLoS Pathog **7:**e1001258.

108. **Schoggins JW, Wilson SJ, Panis M, Murphy MY, Jones CT, Bieniasz P, Rice CM.** 2011. A diverse range of gene products are effectors of the type I interferon antiviral response. Nature **472:**481-485.

109. **Snijder EJ, van der Meer Y, Zevenhoven-Dobbe J, Onderwater JJM, van der Meulen J, Koerten HK, Mommaas AM.** 2006. Ultrastructure and Origin of Membrane Vesicles Associated with the Severe Acute Respiratory Syndrome Coronavirus Replication Complex. Journal of Virology **80:**5927-5940.

110. **Knoops K, Kikkert M, van den Worm SHE, Zevenhoven-Dobbe JC, van der Meer Y, Koster AJ, Mommaas AM, Snijder EJ.** 2008. SARS-Coronavirus Replication Is Supported by a Reticulovesicular Network of Modified Endoplasmic Reticulum. PLoS Biol **6:**e226.

111. **Chen Y, Cai H, Pan Ja, Xiang N, Tien P, Ahola T, Guo D.** 2009. Functional screen reveals SARS coronavirus nonstructural protein nsp14 as a novel cap N7 methyltransferase. Proceedings of the National Academy of Sciences **106:**3484-3489.

112. **Bouvet Ml, Debarnot C, Imbert I, Selisko B, Snijder EJ, Canard B, Decroly E.** 2010. In Vitro Reconstitution of SARS-Coronavirus mRNA Cap Methylation. PLoS Pathog **6:**e1000863.

113. **Chen Y, Su C, Ke M, Jin X, Xu L, Zhang Z, Wu A, Sun Y, Yang Z, Tien P, Ahola T, Liang Y, Liu X, Guo D.** 2011. Biochemical and Structural Insights into the Mechanisms of SARS Coronavirus RNA Ribose 2'-O-Methylation by nsp16/nsp10 Protein Complex. PLoS Pathog **7:**e1002294.

114. **Zust R, Cervantes-Barragan L, Habjan M, Maier R, Neuman BW, Ziebuhr J, Szretter KJ, Baker SC, Barchet W, Diamond MS, Siddell SG, Ludewig B, Thiel V.** 2011. Ribose 2[prime]-O-methylation provides a molecular signature for the distinction of self and non-self mRNA dependent on the RNA sensor Mda5. Nature Immunology **12:**137-143.

115. **Daffis S, Szretter KJ, Schriewer J, Li J, Youn S, Errett J, Lin T-Y, Schneller S, Zust R, Dong H, Thiel V, Sen GC, Fensterl V, Klimstra WB, Pierson TC, Buller RM, Gale Jr M, Shi P-Y, Diamond MS.** 2010. 2[prime]-O methylation of the viral mRNA cap evades host restriction by IFIT family members. Nature **468:**452-456.

116. **Frieman M, Ratia K, Johnston RE, Mesecar AD, Baric RS.** 2009. Severe Acute Respiratory Syndrome Coronavirus Papain-Like Protease Ubiquitin-Like Domain and Catalytic Domain Regulate Antagonism of IRF3 and NF-κB Signaling. Journal of Virology **83:**6689-6705.

117. **Yount B, Roberts RS, Sims AC, Deming D, Frieman MB, Sparks J, Denison MR, Davis N, Baric RS.** 2005. Severe Acute Respiratory Syndrome Coronavirus Group-Specific Open Reading Frames Encode Nonessential Functions for Replication in Cell Cultures and Mice. Journal of Virology **79:**14909-14922.

118. **Wathelet MG, Orr M, Frieman MB, Baric RS.** 2007. Severe Acute Respiratory Syndrome Coronavirus Evades Antiviral Signaling: Role of nsp1 and Rational Design of an Attenuated Strain. J. Virol. **81:**11620-11633.

119. **Kamitani W, Huang C, Narayanan K, Lokugamage KG, Makino S.** 2009. A two-pronged strategy to suppress host protein synthesis by SARS coronavirus Nsp1 protein. Nature Structural & Molecular Biology **16:**1134-1140.

120. **Huang C, Lokugamage KG, Rozovics JM, Narayanan K, Semler BL, Makino S.** 2011. SARS Coronavirus nsp1 Protein Induces Template-Dependent Endonucleolytic Cleavage of mRNAs: Viral mRNAs Are Resistant to nsp1-Induced RNA Cleavage. PLoS Pathog **7:**e1002433.

121. **Kamitani W, Narayanan K, Huang C, Lokugamage K, Ikegami T, Ito N, Kubo H, Makino S.** 2006. Severe acute respiratory syndrome coronavirus nsp1 protein suppresses

host gene expression by promoting host mRNA degradation. Proceedings of the National Academy of Sciences **103:**12885-12890.

122. **Tohya Y, Narayanan K, Kamitani W, Huang C, Lokugamage K, Makino S.** 2009. Suppression of Host Gene Expression by nsp1 Proteins of Group 2 Bat Coronaviruses. Journal of Virology **83:**5282-5288.

123. **Wang Y, Shi H, Rigolet P, Wu N, Zhu L, Xi X-G, Vabret A, Wang X, Wang T.** 2010. Nsp1 proteins of group I and SARS coronaviruses share structural and functional similarities. Infection, Genetics and Evolution **10:**919-924.

124. **Devaraj SG, Wang N, Chen Z, Chen Z, Tseng M, Barretto N, Lin R, Peters CJ, Tseng C-TK, Baker SC, Li K.** 2007. Regulation of IRF-3-dependent Innate Immunity by the Papain-like Protease Domain of the Severe Acute Respiratory Syndrome Coronavirus. Journal of Biological Chemistry **282:**32208-32221.

125. **Lei Y, Moore CB, Liesman RM, O'Connor BP, Bergstralh DT, Chen ZJ, Pickles RJ, Ting JPY.** 2009. MAVS-Mediated Apoptosis and Its Inhibition by Viral Proteins. PLoS ONE **4:**e5466.

126. **Chen C-Y, Chang C-k, Chang Y-W, Sue S-C, Bai H-I, Riang L, Hsiao C-D, Huang T-h.** 2007. Structure of the SARS Coronavirus Nucleocapsid Protein RNA-binding Dimerization Domain Suggests a Mechanism for Helical Packaging of Viral RNA. Journal of Molecular Biology **368:**1075-1086.

127. **Lu X, Pan Ja, Tao J, Guo D.** 2011. SARS-CoV nucleocapsid protein antagonizes IFN-β response by targeting initial step of IFN-β induction pathway, and its C-terminal region is critical for the antagonism. Virus Genes **42:**37-45.

128. **Lu X, Pan Ja, Tao J, Guo D.** SARS-CoV nucleocapsid protein antagonizes IFN-β response by targeting initial step of IFN-β induction pathway, and its C-terminal region is critical for the antagonism. Virus Genes **42:**37-45.

129. **Grossoehme NE, Li L, Keane SC, Liu P, Dann Iii CE, Leibowitz JL, Giedroc DP.** 2009. Coronavirus N Protein N-Terminal Domain (NTD) Specifically Binds the Transcriptional Regulatory Sequence (TRS) and Melts TRS-cTRS RNA Duplexes. Journal of Molecular Biology **394:**544-557.

130. **Ye Y, Hauns K, Langland JO, Jacobs BL, Hogue BG.** 2007. Mouse Hepatitis Coronavirus A59 Nucleocapsid Protein Is a Type I Interferon Antagonist. Journal of Virology **81:**2554-2563.

131. **Siu K-L, Kok K-H, Ng M-HJ, Poon VKM, Yuen K-Y, Zheng B-J, Jin D-Y.** 2009. Severe Acute Respiratory Syndrome Coronavirus M Protein Inhibits Type I Interferon Production by Impeding the Formation of TRAF3.TANK.TBK1/IKKε Complex. Journal of Biological Chemistry **284:**16202-16209.

132. **Frieman M, Ratia K, Johnston RE, Mesecar AD, Baric RS.** 2009. Severe Acute Respiratory Syndrome Coronavirus Papain-Like Protease Ubiquitin-Like Domain and Catalytic Domain Regulate Antagonism of IRF3 and NF-{kappa}B Signaling. J. Virol. **83:**6689-6705.

133. **Narayanan K, Huang C, Makino S.** 2008. SARS coronavirus accessory proteins. Virus Research **133:**113-121.

134. **Freundt EC, Yu L, Park E, Lenardo MJ, Xu X-N.** 2009. Molecular Determinants for Subcellular Localization of the Severe Acute Respiratory Syndrome Coronavirus Open Reading Frame 3b Protein. Journal of Virology **83:**6631-6640.

135. **Yuan X, Shan Y, Zhao Z, Chen J, Cong Y.** 2005. G0/G1 arrest and apoptosis induced by SARS-CoV 3b protein in transfected cells. Virology Journal **2:**66.

136. **Khan S, Fielding BC, Tan THP, Chou C-F, Shen S, Lim SG, Hong W, Tan Y-J.** 2006. Over-expression of severe acute respiratory syndrome coronavirus 3b protein induces both apoptosis and necrosis in Vero E6 cells. Virus Research **122:**20-27.

137. **Drexler JF, Gloza-Rausch F, Glende Jr, Corman VM, Muth D, Goettsche M, Seebens A, Niedrig M, Pfefferle S, Yordanov S, Zhelyazkov L, Hermanns U, Vallo P, Lukashev A, MÃ¼ller MA, Deng H, Herrler G, Drosten C.** 2010. Genomic Characterization of Severe Acute Respiratory Syndrome-Related Coronavirus in European Bats and Classification of Coronaviruses Based on Partial RNA-Dependent RNA Polymerase Gene Sequences. Journal of Virology **84:**11336-11349.

138. **Zhou P, Li H, Wang H, Wang L-F, Shi Z.** 2012. Bat severe acute respiratory syndrome-like coronavirus ORF3b homologues display different interferon antagonist activities. Journal of General Virology **93:**275-281.

139. **Tangudu C, Olivares H, Netland J, Perlman S, Gallagher T.** 2007. Severe Acute Respiratory Syndrome Coronavirus Protein 6 Accelerates Murine Coronavirus Infections. Journal of Virology **81:**1220-1229.

140. **Pewe L, Zhou H, Netland J, Tangudu C, Olivares H, Shi L, Look D, Gallagher T, Perlman S.** 2005. A Severe Acute Respiratory Syndrome-Associated Coronavirus-

Specific Protein Enhances Virulence of an Attenuated Murine Coronavirus. Journal of Virology **79:**11335-11342.

141. **Netland J, Ferraro D, Pewe L, Olivares H, Gallagher T, Perlman S.** 2007. Enhancement of Murine Coronavirus Replication by Severe Acute Respiratory Syndrome Coronavirus Protein 6 Requires the N-Terminal Hydrophobic Region but Not C-Terminal Sorting Motifs. Journal of Virology **81:**11520-11525.

142. **Zhou H, Ferraro D, Zhao J, Hussain S, Shao J, Trujillo J, Netland J, Gallagher T, Perlman S.** 2010. The N-Terminal Region of Severe Acute Respiratory Syndrome Coronavirus Protein 6 Induces Membrane Rearrangement and Enhances Virus Replication. Journal of Virology **84:**3542-3551.

143. **Kumar P, Gunalan V, Liu B, Chow VTK, Druce J, Birch C, Catton M, Fielding BC, Tan Y-J, Lal SK.** 2007. The nonstructural protein 8 (nsp8) of the SARS coronavirus interacts with its ORF6 accessory protein. Virology **366:**293-303.

144. **te Velthuis AJW, van den Worm SHE, Snijder EJ.** 2011. The SARS-coronavirus nsp7+nsp8 complex is a unique multimeric RNA polymerase capable of both de novo initiation and primer extension. Nucleic Acids Research.

145. **Zhai Y, Sun F, Li X, Pang H, Xu X, Bartlam M, Rao Z.** 2005. Insights into SARS-CoV transcription and replication from the structure of the nsp7-nsp8 hexadecamer. Nat Struct Mol Biol **12:**980-986.

146. **Frieman M, Yount B, Heise M, Kopecky-Bromberg SA, Palese P, Baric RS.** 2007. Severe Acute Respiratory Syndrome Coronavirus ORF6 Antagonizes STAT1 Function by Sequestering Nuclear Import Factors on the Rough Endoplasmic Reticulum/Golgi Membrane. J. Virol. **81:**9812-9824.

147. **Hussain S, Perlman S, Gallagher TM.** 2008. Severe Acute Respiratory Syndrome Coronavirus Protein 6 Accelerates Murine Hepatitis Virus Infections by More than One Mechanism. Journal of Virology **82:**7212-7222.

148. **Hussain S, Gallagher T.** 2010. SARS-coronavirus protein 6 conformations required to impede protein import into the nucleus. Virus Research **153:**299-304.

149. **Perlman S, Netland J.** 2009. Coronaviruses post-SARS: update on replication and pathogenesis. Nature Reviews Microbiology **7:**439-450.

150. 2014. World Health Organization: Middle East respiratory syndrome coronavirus (MERS-CoV) summary and literature update–as of 11 June 2014.

151. **Falzarano D, de Wit E, Martellaro C, Callison J, Munster VJ, Feldmann H.** 2013. Inhibition of novel β coronavirus replication by a combination of interferon-α2b and ribavirin. Sci. Rep. **3**.

152. **Deming D, Sheahan T, Heise M, Yount B, Davis N, Sims A, Suthar M, Harkema J, Whitmore A, Pickles R, West A, Donaldson E, Curtis K, Johnston R, Baric R.** 2006. Vaccine Efficacy in Senescent Mice Challenged with Recombinant SARS-CoV Bearing Epidemic and Zoonotic Spike Variants. PLoS Med **3:**e525.

153. **Short KR, Kroeze EJBV, Fouchier RAM, Kuiken T.** 2014. Pathogenesis of influenza-induced acute respiratory distress syndrome. The Lancet Infectious Diseases **14:**57-69.

154. **Yoo J-K, Kim TS, Hufford MM, Braciale TJ.** 2013. Viral infection of the lung: Host response and sequelae. Journal of Allergy and Clinical Immunology **132:**1263-1276.

155. **Goffic RL, Balloy V, Lagranderie M, Alexopoulou L, Escriou N, Flavell R, Chignard M, Si-Tahar M.** 2006. Detrimental Contribution of the Toll-Like Receptor (TLR)3 to Influenza A Virus–Induced Acute Pneumonia. PLoS Pathog **2:**e53.

156. **Rudd BD, Smit JJ, Flavell RA, Alexopoulou L, Schaller MA, Gruber A, Berlin AA, Lukacs NW.** 2006. Deletion of TLR3 Alters the Pulmonary Immune Environment and Mucus Production during Respiratory Syncytial Virus Infection. The Journal of Immunology **176:**1937-1942.

157. **Wang Q, Miller DJ, Bowman ER, Nagarkar DR, Schneider D, Zhao Y, Linn MJ, Goldsmith AM, Bentley JK, Sajjan US, Hershenson MB.** 2011. MDA5 and TLR3 Initiate Pro-Inflammatory Signaling Pathways Leading to Rhinovirus-Induced Airways Inflammation and Hyperresponsiveness. PLoS Pathog **7:**e1002070.

158. **Guillot L, Le Goffic R, Bloch S, Escriou N, Akira S, Chignard M, Si-Tahar M.** 2005. Involvement of Toll-like Receptor 3 in the Immune Response of Lung Epithelial Cells to Double-stranded RNA and Influenza A Virus. Journal of Biological Chemistry **280:**5571-5580.

159. **Alexopoulou L, Holt AC, Medzhitov R, Flavell RA.** 2001. Recognition of double-stranded RNA and activation of NF-[kappa]B by Toll-like receptor 3. Nature **413:**732-738.

160. **Oshiumi H, Matsumoto M, Funami K, Akazawa T, Seya T.** 2003. TICAM-1, an adaptor molecule that participates in Toll-like receptor 3-mediated interferon-[beta] induction. Nat Immunol **4:**161-167.

161. **Yamamoto M, Sato S, Hemmi H, Hoshino K, Kaisho T, Sanjo H, Takeuchi O, Sugiyama M, Okabe M, Takeda K, Akira S.** 2003. Role of Adaptor TRIF in the MyD88-Independent Toll-Like Receptor Signaling Pathway. Science **301:**640-643.

162. **Yamamoto M, Sato S, Mori K, Hoshino K, Takeuchi O, Takeda K, Akira S.** 2002. Cutting Edge: A Novel Toll/IL-1 Receptor Domain-Containing Adapter That Preferentially Activates the IFN-β Promoter in the Toll-Like Receptor Signaling. The Journal of Immunology **169:**6668-6672.

163. **Zhang Z, Kim T, Bao M, Facchinetti V, Jung Sung Y, Ghaffari Amir A, Qin J, Cheng G, Liu Y-J.** 2011. DDX1, DDX21, and DHX36 Helicases Form a Complex with the Adaptor Molecule TRIF to Sense dsRNA in Dendritic Cells. Immunity **34:**866-878.

164. **Ichikawa A, Kuba K, Morita M, Chida S, Tezuka H, Hara H, Sasaki T, Ohteki T, Ranieri VM, dos Santos CC, Kawaoka Y, Akira S, Luster AD, Lu B, Penninger JM, Uhlig S, Slutsky AS, Imai Y.** 2013. CXCL10-CXCR3 Enhances the Development of Neutrophil-mediated Fulminant Lung Injury of Viral and Nonviral Origin. American Journal of Respiratory and Critical Care Medicine **187:**65-77.

165. **Shirey KA, Lai W, Scott AJ, Lipsky M, Mistry P, Pletneva LM, Karp CL, McAlees J, Gioannini TL, Weiss J, Chen WH, Ernst RK, Rossignol DP, Gusovsky F, Blanco JCG, Vogel SN.** 2013. The TLR4 antagonist Eritoran protects mice from lethal influenza infection. Nature **497:**498-502.

166. **Zhao J, Wohlford-Lenane C, Zhao J, Fleming E, Lane TE, McCray PB, Perlman S.** 2012. Intranasal Treatment with Poly(I·C) Protects Aged Mice from Lethal Respiratory Virus Infections. Journal of Virology **86:**11416-11424.

167. **Iwata-Yoshikawa N, Uda A, Suzuki T, Tsunetsugu-Yokota Y, Sato Y, Morikawa S, Tashiro M, Sata T, Hasegawa H, Nagata N.** 2014. Effects of Toll-Like Receptor Stimulation on Eosinophilic Infiltration in Lungs of BALB/c Mice Immunized with UV-Inactivated Severe Acute Respiratory Syndrome-Related Coronavirus Vaccine. Journal of Virology **88:**8597-8614.

168. **Pérez-Girón JV, Belicha-Villanueva A, Hassan E, Gómez-Medina S, Cruz JLG, Lüdtke A, Ruibal P, Albrecht RA, García-Sastre A, Muñoz-Fontela C.** 2014. Mucosal Polyinosinic-Polycytidylic Acid Improves Protection Elicited by Replicating

Influenza Vaccines via Enhanced Dendritic Cell Function and T Cell Immunity. The Journal of Immunology **193:**1324-1332.

169. **Gralinski LE, Bankhead A, Jeng S, Menachery VD, Proll S, Belisle SE, Matzke M, Webb-Robertson B-JM, Luna ML, Shukla AK, Ferris MT, Bolles M, Chang J, Aicher L, Waters KM, Smith RD, Metz TO, Law GL, Katze MG, McWeeney S, Baric RS.** 2013. Mechanisms of Severe Acute Respiratory Syndrome Coronavirus-Induced Acute Lung Injury. mBio **4**.

170. **Menachery VD, Yount BL, Josset L, Gralinski LE, Scobey T, Agnihothram S, Katze MG, Baric RS.** 2014. Attenuation and Restoration of Severe Acute Respiratory Syndrome Coronavirus Mutant Lacking 2′-O-Methyltransferase Activity. Journal of Virology **88:**4251-4264.

171. **Hamelmann E, Schwarze J, Takeda K, Oshiba A, Larsen GL, Irvin CG, Gelfand EW.** 1997. Noninvasive Measurement of Airway Responsiveness in Allergic Mice Using Barometric Plethysmography. American Journal of Respiratory and Critical Care Medicine **156:**766-775.

172. **Zhang Q, Lai K, Xie J, Chen G, Zhong N.** 2009. Does unrestrained single-chamber plethysmography provide a valid assessment of airway responsiveness in allergic BALB/c mice? Respiratory Research **10:**61.

173. **Julander JG, Kesler K, Van Wettere AJ, Morrey JD, Smee DF.** 2014. The use of plethysmography in determining the severity of lung pathology in a mouse model of minimally lethal influenza virus infection. Antiviral Research **108:**10-13.

174. **Hamelin M-È, Prince GA, Gomez AM, Kinkead R, Boivin G.** 2006. Human Metapneumovirus Infection Induces Long-Term Pulmonary Inflammation Associated with Airway Obstruction and Hyperresponsiveness in Mice. Journal of Infectious Diseases **193:**1634-1642.

175. **Mitchell HD, Eisfeld AJ, Sims AC, McDermott JE, Matzke MM, Webb-Robertson B-JM, Tilton SC, Tchitchek N, Josset L, Li C, Ellis AL, Chang JH, Heegel RA, Luna ML, Schepmoes AA, Shukla AK, Metz TO, Neumann G, Benecke AG, Smith RD, Baric RS, Kawaoka Y, Katze MG, Waters KM.** 2013. A Network Integration Approach to Predict Conserved Regulators Related to Pathogenicity of Influenza and SARS-CoV Respiratory Viruses. PLoS ONE **8:**e69374.

176. **Schwarze J, Hamelmann E, Bradley KL, Takeda K, Gelfand EW.** 1997. Respiratory syncytial virus infection results in airway hyperresponsiveness and enhanced airway sensitization to allergen. The Journal of Clinical Investigation **100:**226-233.

177. **Palmer LA, May WJ, deRonde K, Brown-Steinke K, Gaston B, Lewis SJ.** 2013. Hypoxia-induced ventilatory responses in conscious mice: Gender differences in ventilatory roll-off and facilitation. Respiratory Physiology & Neurobiology **185:**497-505.

178. **Menasria R, Boivin N, Lebel M, Piret J, Gosselin J, Boivin G.** 2013. Both TRIF and IPS-1 Adaptor Proteins Contribute to the Cerebral Innate Immune Response against Herpes Simplex Virus 1 Infection. Journal of Virology **87:**7301-7308.

179. **Seo S-U, Kwon H-J, Song J-H, Byun Y-H, Seong BL, Kawai T, Akira S, Kweon M-N.** 2010. MyD88 Signaling Is Indispensable for Primary Influenza A Virus Infection but Dispensable for Secondary Infection. Journal of Virology **84:**12713-12722.

180. **Menachery VD, Eisfeld AJ, Schäfer A, Josset L, Sims AC, Proll S, Fan S, Li C, Neumann G, Tilton SC, Chang J, Gralinski LE, Long C, Green R, Williams CM, Weiss J, Matzke MM, Webb-Robertson B-J, Schepmoes AA, Shukla AK, Metz TO, Smith RD, Waters KM, Katze MG, Kawaoka Y, Baric RS.** 2014. Pathogenic Influenza Viruses and Coronaviruses Utilize Similar and Contrasting Approaches To Control Interferon-Stimulated Gene Responses. mBio **5**.

181. **Williams AECRC.** 2014. The mercurial nature of neutrophils: still an enigma in ARDS? American Journal of Physiology - Lung Cellular and Molecular Physiology **306:**L217-L230.

182. **Perrone LA, Plowden JK, García-Sastre A, Katz JM, Tumpey TM.** 2008. H5N1 and 1918 Pandemic Influenza Virus Infection Results in Early and Excessive Infiltration of Macrophages and Neutrophils in the Lungs of Mice. PLoS Pathog **4:**e1000115.

183. **Seo S-U, Kwon H-J, Ko H-J, Byun Y-H, Seong BL, Uematsu S, Akira S, Kweon M-N.** 2011. Type I Interferon Signaling Regulates Ly6C^{hi} Monocytes and Neutrophils during Acute Viral Pneumonia in Mice. PLoS Pathog **7:**e1001304.

184. **Shi C, Pamer EG.** 2011. Monocyte recruitment during infection and inflammation. Nat Rev Immunol **11:**762-774.

185. **Leung YHC, Nicholls JM, Ho C-K, Sia S-F, Mok CKP, Valkenburg SA, Cheung P, Hui KPY, Chan RWY, Guan Y, Akira S, Peiris JSM.** 2014. Highly pathogenic avian influenza A H5N1 and pandemic H1N1 virus infections have different phenotypes in Toll-like Receptor (TLR) 3 knock-out mice. Journal of General Virology.

186. **Daffis S, Samuel MA, Suthar MS, Gale M, Diamond MS.** 2008. Toll-Like Receptor 3 Has a Protective Role against West Nile Virus Infection. Journal of Virology **82:**10349-10358.

187. **Wang T, Town T, Alexopoulou L, Anderson JF, Fikrig E, Flavell RA.** 2004. Toll-like receptor 3 mediates West Nile virus entry into the brain causing lethal encephalitis. Nat Med **10:**1366-1373.

188. **Kumar H, Koyama S, Ishii KJ, Kawai T, Akira S.** 2008. Cutting Edge: Cooperation of IPS-1- and TRIF-Dependent Pathways in Poly IC-Enhanced Antibody Production and Cytotoxic T Cell Responses. The Journal of Immunology **180:**683-687.

189. **Mandraju R, Murray S, Forman J, Pasare C.** 2014. Differential Ability of Surface and Endosomal TLRs To Induce CD8 T Cell Responses In Vivo. The Journal of Immunology **192:**4303-4315.

190. **Baric RS.** 2008. SARS-CoV: Lessons for global health. Virus Research **133:**1-3.

191. **Bermingham A CM, Brown CS, Aarons E, Tong C, Langrish C, Hoschler K, Brown K, Galiano M, Myers R, Pebody RG, Green HK, Boddington NL, Gopal R, Price , N NW, Drosten C, Fouchier RA, Zambon M.** 2012. Severe respiratory illness caused by a novel coronavirus, in a patient transferred to the United Kingdom from the Middle East. Euro Surveill **17**.

192. **Gralinski LE, Baric RS.** 2014. Molecular Pathology of Emerging Coronavirus Infections. The Journal of Pathology**:**n/a-n/a.

193. **Nicholls JM, Poon LLM, Lee KC, Ng WF, Lai ST, Leung CY, Chu CM, Hui PK, Mak KL, Lim W, Yan KW, Chan KH, Tsang NC, Guan Y, Yuen KY, Malik Peiris JS.** 2003. Lung pathology of fatal severe acute respiratory syndrome. The Lancet **361:**1773-1778.

194. 2014. World Health Organization: Middle East respiratory syndrome coronavirus (MERS-CoV) summary - as of 16 October 2014

195. **Klouwenberg PK, Tan L, Werkman W, van Bleek GM, Coenjaerts F.** 2009. The Role of Toll-like Receptors in Regulating the Immune Response against Respiratory Syncytial Virus. **29:**531-550.

196. **Guillot L, Medjane S, Le-Barillec K, Balloy V, Danel C, Chignard M, Si-Tahar M.** 2004. Response of Human Pulmonary Epithelial Cells to Lipopolysaccharide Involves Toll-like Receptor 4 (TLR4)-dependent Signaling Pathways: EVIDENCE FOR AN INTRACELLULAR COMPARTMENTALIZATION OF TLR4. Journal of Biological Chemistry **279:**2712-2718.

197. **Monick MM, Yarovinsky TO, Powers LS, Butler NS, Carter AB, Gudmundsson G, Hunninghake GW.** 2003. Respiratory Syncytial Virus Up-regulates TLR4 and Sensitizes Airway Epithelial Cells to Endotoxin. Journal of Biological Chemistry **278:**53035-53044.

198. **O'Neill LAJ, Bowie AG.** 2007. The family of five: TIR-domain-containing adaptors in Toll-like receptor signalling. Nat Rev Immunol **7:**353-364.

199. **Imai Y, Kuba K, Neely GG, Yaghubian-Malhami R, Perkmann T, van Loo G, Ermolaeva M, Veldhuizen R, Leung YHC, Wang H, Liu H, Sun Y, Pasparakis M, Kopf M, Mech C, Bavari S, Peiris JSM, Slutsky AS, Akira S, Hultqvist M, Holmdahl R, Nicholls J, Jiang C, Binder CJ, Penninger JM.** 2008. Identification of Oxidative Stress and Toll-like Receptor 4 Signaling as a Key Pathway of Acute Lung Injury. Cell **133:**235-249.

200. **Drexler JF, Corman VM, Drosten C.** 2014. Ecology, evolution and classification of bat coronaviruses in the aftermath of SARS. Antiviral Research **101:**45-56.

201. **Zhao Z, Zhang F, Xu M, Huang K, Zhong W, Cai W, Yin Z, Huang S, Deng Z, Wei M, Xiong J, Hawkey PM.** 2003. Description and clinical treatment of an early outbreak of severe acute respiratory syndrome (SARS) in Guangzhou, PR China. Journal of Medical Microbiology **52:**715-720.

202. **Donnelly CA, Ghani AC, Leung GM, Hedley AJ, Fraser C, Riley S, Abu-Raddad LJ, Ho L-M, Thach T-Q, Chau P, Chan K-P, Lam T-H, Tse L-Y, Tsang T, Liu S-H, Kong JHB, Lau EMC, Ferguson NM, Anderson RM.** 2003. Epidemiological determinants of spread of causal agent of severe acute respiratory syndrome in Hong Kong. The Lancet **361:**1761-1766.

203. **Peiris JSM, Lai ST, Poon LLM, Guan Y, Yam LYC, Lim W, Nicholls J, Yee WKS, Yan WW, Cheung MT, Cheng VCC, Chan KH, Tsang DNC, Yung RWH, Ng TK, Yuen KY.** 2003. Coronavirus as a possible cause of severe acute respiratory syndrome. The Lancet **361:**1319-1325.

204. **Lee N, Hui D, Wu A, Chan P, Cameron P, Joynt GM, Ahuja A, Yung MY, Leung CB, To KF, Lui SF, Szeto CC, Chung S, Sung JJY.** 2003. A Major Outbreak of Severe

Acute Respiratory Syndrome in Hong Kong. New England Journal of Medicine **348:**1986-1994.

205. **Woo PCY, Lau SKP, Li KSM, Tsang AKL, Yuen K-Y.** 2012. Genetic relatedness of the novel human group C betacoronavirus to Tylonycteris bat coronavirus HKU4 and Pipistrellus bat coronavirus HKU5. Emerg Microbes Infect **1:**e35.

206. **Anthony SJ, Ojeda-Flores R, Rico-Chávez O, Navarrete-Macias I, Zambrana-Torrelio CM, Rostal MK, Epstein JH, Tipps T, Liang E, Sanchez-Leon M, Sotomayor-Bonilla J, Aguirre AA, Ávila-Flores R, Medellín RA, Goldstein T, Suzán G, Daszak P, Lipkin WI.** 2013. Coronaviruses in bats from Mexico. Journal of General Virology **94:**1028-1038.

207. **Geller C, Varbanov M, Duval R.** 2012. Human Coronaviruses: Insights into Environmental Resistance and Its Influence on the Development of New Antiseptic Strategies. Viruses **4:**3044-3068.

208. **Cinatl Jr J, Hoever G, Morgenstern B, Preiser W, Vogel JU, Hofmann WK, Bauer G, Michaelis M, Rabenau HF, Doerr HW.** 2004. Infection of cultured intestinal epithelial cells with severe acute respiratory syndrome coronavirus. Cellular and Molecular Life Sciences **61:**2100-2112.

209. **Cinatl J, Morgenstern B, Bauer G, Chandra P, Rabenau H, Doerr HW.** 2003. Treatment of SARS with human interferons. The Lancet **362:**293-294.

210. **Hart BJ, Dyall J, Postnikova E, Zhou H, Kindrachuk J, Johnson RF, Olinger GG, Frieman MB, Holbrook MR, Jahrling PB, Hensley L.** 2014. Interferon-β and mycophenolic acid are potent inhibitors of Middle East respiratory syndrome coronavirus in cell-based assays. Journal of General Virology **95:**571-577.

211. **Roth-Cross JK, Martínez-Sobrido L, Scott EP, García-Sastre A, Weiss SR.** 2007. Inhibition of the Alpha/Beta Interferon Response by Mouse Hepatitis Virus at Multiple Levels. Journal of Virology **81:**7189-7199.

212. **Zhao X, Guo F, Liu F, Cuconati A, Chang J, Block TM, Guo J-T.** 2014. Interferon induction of IFITM proteins promotes infection by human coronavirus OC43. Proceedings of the National Academy of Sciences **111:**6756-6761.

213. **Rand U, Rinas M, Schwerk J, Nöhren G, Linnes M, Kröger A, Flossdorf M, Kály-Kullai K, Hauser H, Höfer T, Köster M.** 2012. Multi-layered stochasticity and paracrine signal propagation shape the type-I interferon response, vol. 8.

214. **Schlee M.** 2013. Master sensors of pathogenic RNA – RIG-I like receptors. Immunobiology **218:**1322-1335.

215. **Schnell G, Loo Y-M, Marcotrigiano J, Gale M, Jr.** 2012. Uridine Composition of the Poly-U/UC Tract of HCV RNA Defines Non-Self Recognition by RIG-I. PLoS Pathog **8:**e1002839.

216. **Jacobs JL, Coyne CB.** 2013. Mechanisms of MAVS Regulation at the Mitochondrial Membrane. Journal of Molecular Biology **425:**5009-5019.

217. **Li J, Liu Y, Zhang X.** 2010. Murine Coronavirus Induces Type I Interferon in Oligodendrocytes through Recognition by RIG-I and MDA5. Journal of Virology **84:**6472-6482.

218. **Koetzner CA, Kuo L, Goebel SJ, Dean AB, Parker MM, Masters PS.** Accessory Protein 5a Is a Major Antagonist of the Antiviral Action of Interferon against Murine Coronavirus. Journal of Virology **84:**8262-8274.

219. **Zhao L, Rose KM, Elliott R, Van Rooijen N, Weiss SR.** Cell-Type-Specific Type I Interferon Antagonism Influences Organ Tropism of Murine Coronavirus. Journal of Virology **85:**10058-10068.

220. **Cruz JLG, Sola I, Becares M, Alberca B, Plana J, Enjuanes L, Zuñiga S.** Coronavirus Gene 7 Counteracts Host Defenses and Modulates Virus Virulence. PLoS Pathog **7:**e1002090.

221. **Sun L, Xing Y, Chen X, Zheng Y, Yang Y, Nichols DB, Clementz MA, Banach BS, Li K, Baker SC, Chen Z.** Coronavirus Papain-like Proteases Negatively Regulate Antiviral Innate Immune Response through Disruption of STING-Mediated Signaling. PLoS ONE **7:**e30802.

222. **Clementz MA, Chen Z, Banach BS, Wang Y, Sun L, Ratia K, Baez-Santos YM, Wang J, Takayama J, Ghosh AK, Li K, Mesecar AD, Baker SC.** Deubiquitinating and Interferon Antagonism Activities of Coronavirus Papain-Like Proteases. Journal of Virology **84:**4619-4629.

223. **te Velthuis AJW, van den Worm SHE, Snijder EJ.** 2012. The SARS-coronavirus nsp7+nsp8 complex is a unique multimeric RNA polymerase capable of both de novo initiation and primer extension. Nucleic Acids Research **40:**1737-1747.

224. **Hagemeijer MC, Vonk AM, Monastyrska I, Rottier PJM, de Haan CAM.** 2012. Visualizing Coronavirus RNA Synthesis in Time by Using Click Chemistry. Journal of Virology **86:**5808-5816.

225. **Neuman BW, Chamberlain P, Bowden F, Joseph J.** Atlas of coronavirus replicase structure. Virus Research.

226. **Yoneyama M, Kikuchi M, Natsukawa T, Shinobu N, Imaizumi T, Miyagishi M, Taira K, Akira S, Fujita T.** 2004. The RNA helicase RIG-I has an essential function in double-stranded RNA-induced innate antiviral responses. Nat Immunol **5:**730-737.

227. **Zinzula L, Tramontano E.** 2013. Strategies of highly pathogenic RNA viruses to block dsRNA detection by RIG-I-like receptors: Hide, mask, hit. Antiviral Research **100:**615-635.

228. **Ling Z, Tran KC, Teng MN.** 2009. Human Respiratory Syncytial Virus Nonstructural Protein NS2 Antagonizes the Activation of Beta Interferon Transcription by Interacting with RIG-I. Journal of Virology **83:**3734-3742.

229. **Gack MU, Albrecht RA, Urano T, Inn K-S, Huang IC, Carnero E, Farzan M, Inoue S, Jung JU, García-Sastre A.** 2009. Influenza A Virus NS1 Targets the Ubiquitin Ligase TRIM25 to Evade Recognition by the Host Viral RNA Sensor RIG-I. Cell Host & Microbe **5:**439-449.

230. **Cowled C, Baker ML, Zhou P, Tachedjian M, Wang L-F.** 2012. Molecular characterisation of RIG-I-like helicases in the black flying fox, Pteropus alecto. Developmental & Comparative Immunology **36:**657-664.

231. **Matthews KL, Coleman CM, van der Meer Y, Snijder EJ, Frieman MB.** 2014. The ORF4b-encoded accessory proteins of Middle East respiratory syndrome coronavirus and two related bat coronaviruses localize to the nucleus and inhibit innate immune signalling. Journal of General Virology **95:**874-882.

232. **Mielech AM, Chen Y, Mesecar AD, Baker SC.** Nidovirus papain-like proteases: Multifunctional enzymes with protease, deubiquitinating and deISGylating activities. Virus Research.

233. **Sun L, Xing Y, Chen X, Zheng Y, Yang Y, Nichols DB, Clementz MA, Banach BS, Li K, Baker SC, Chen Z.** 2012. Coronavirus Papain-like Proteases Negatively Regulate Antiviral Innate Immune Response through Disruption of STING-Mediated Signaling. PLoS ONE **7:**e30802.

234. **Deming DJ, Graham RL, Denison MR, Baric RS.** 2007. Processing of Open Reading Frame 1a Replicase Proteins nsp7 to nsp10 in Murine Hepatitis Virus Strain A59 Replication. Journal of Virology **81:**10280-10291.

235. **van Lieshout MHP, Blok DC, Wieland CW, de Vos AF, van 't Veer C, van der Poll T.** 2012. Differential Roles of MyD88 and TRIF in Hematopoietic and Resident Cells During Murine Gram-Negative Pneumonia. Journal of Infectious Diseases **206:**1415-1423.

236. **Ting Tan RS, Lin B, Liu Q, Tucker-Kellogg L, Ho B, Leung BPL, Ding JL.** 2013. The synergy in cytokine production through MyD88-TRIF pathways is co-ordinated with ERK phosphorylation in macrophages. Immunol Cell Biol **91:**377-387.

237. **Ferris MT, Aylor DL, Bottomly D, Whitmore AC, Aicher LD, Bell TA, Bradel-Tretheway B, Bryan JT, Buus RJ, Gralinski LE, Haagmans BL, McMillan L, Miller DR, Rosenzweig E, Valdar W, Wang J, Churchill GA, Threadgill DW, McWeeney SK, Katze MG, Pardo-Manuel de Villena F, Baric RS, Heise MT.** 2013. Modeling Host Genetic Regulation of Influenza Pathogenesis in the Collaborative Cross. PLoS Pathog **9:**e1003196.

238. **Sancho-Shimizu V, xE, rez de Diego R, Lorenzo L, Halwani R, Alangari A, Israelsson E, Fabrega S, Cardon A, Maluenda J, Tatematsu M, Mahvelati F, Herman M, Ciancanelli M, Guo Y, AlSum Z, Alkhamis N, Al-Makadma AS, Ghadiri A, Boucherit S, Plancoulaine S, Picard C, Rozenberg F, Tardieu M, Lebon P, Jouanguy E, Rezaei N, Seya T, Matsumoto M, Chaussabel D, Puel A, Zhang S-Y, Abel L, Al-Muhsen S, Casanova J-L.** 2011. Herpes simplex encephalitis in children with autosomal recessive and dominant TRIF deficiency. The Journal of Clinical Investigation **121:**4889-4902.

239. **Graham RL, Becker MM, Eckerle LD, Bolles M, Denison MR, Baric RS.** 2012. A live, impaired-fidelity coronavirus vaccine protects in an aged, immunocompromised mouse model of lethal disease. Nat Med **18:**1820-1826.